4-2024

New Alternative Method Developed for the Measurement of Active and Total Clay in Foundry Green Sands

Piao Jian Tan
Western Michigan University

NEW ALTERNATIVE METHODS DEVELOPED FOR THE MEASUREMENT OF ACTIVE AND TOTAL CLAY IN FOUNDRY GREEN SANDS

Piao Jian Tan, Ph.D.

Western Michigan University, 2024

Precise measurement of active clay content in molding sand is essential in the metal casting foundry to produce high quality end products with no defects. The historical methylene blue (MB) test was considered qualitative, subjective and prone to operator bias in regard to the reading of the halo. A new spectrophotometric or digital clay technique has been developed. The test utilizes the cation exchange capabilities of the Cu(II)-triethylenetetramine dye and the absorbance reading of the sequestered solution through a UV-Vis spectrophotometer. Working with multiple laboratories (Decher, MTI, EJ, and JD) on actual foundry green sand samples, the method was optimized in 3 stages. The finalized method includes cation ion exchange mixing of green sand and Cu(II)-triethylenetetramine dye, separation of the sequestered dye through a syringe filter and CEC measurement via UV-Vis Spectrophotometer. The test data and the GR&R study demonstrated better variability, accuracy and a consistent trend compared to the MB test. The digital clay technique requires minimal training, has a low startup and labor cost, and low run time. This testing method has been submitted to be accepted into the AFS standard test for active clay in green sands and to be featured in the AFS Mold & Core Test Handbook. Additionally, a new optimized method is being optimized to measure total clay in foundry green sands. These methods will improve efficiency and process control in metal casting, helping

propel the industry into Foundry 4.0, a new era in metal casting that will be defined improved process control, by generally transitioning from hands-on labor measurement to utilizing automated CEC or measuring instruments.

Additional work in this study includes elucidation of the pathway by which oxidized lipids affect the monocyte recruitment pathway and ultimately regulate atherosclerosis, an underlying condition that may lead to heart attack or stroke. OxPAPC has been shown to emulate the molecular effects of LDL, including the regulation of more than 1,000 genes in human aortic endothelial cells (HAEC). Isoprostanes, neuroprostanes and neurofurans are derived from polyunsaturated fatty acids though non-enzymatic peroxidation and it is hypothesized that these lipids may act like OxPAPC and regulate monocytes and other genes which cause atherosclerosis. Among these lipids, the results confirm findings from previous studies that 15-F2t-isoprostane induces monocyte binding and regulates inflammatory and oxidative stress. Treatment of 15-F2t-isoprostane with HAECs shows consistent results as previously reported from Leitinger, 2001 upregulating genes MCP-1, IL-8 and HO-1. Treatment of 4-epi-4-F3t-neuroprostane shows downregulation of all genes MCP-1, IL-8 and HO-1, while 4(RS)-ST-Δ5-8-neurofuran treatment shows downregulation of IL-8 and MCP-1, potentially suggesting that they exhibit EC barrier enhancement capabilities. The broader impact of this research will help to develop a novel approach towards understanding atherosclerosis and assist medical professionals in developing novel drug treatments and diagnostic tools to prevent or suppress atherosclerosis lesions or inflammation.

NEW ALTERNATIVE METHODS DEVELOPED FOR THE MEASUREMENT OF ACTIVE AND TOTAL CLAY IN FOUNDRY GREEN SANDS

by

Piao Jian Tan

A dissertation submitted to the Graduate College
in partial fulfillment of the requirements
for the degree of Doctor of Philosophy
Chemical and Paper Engineering
Western Michigan University
April 2024

Doctoral Committee:

James R. Springstead, Ph.D., Chair
Qing Liu Wu, Ph.D.
Mert Atilhan, Ph. D.
John. M. Spitsbergen, Ph. D.

ACKNOWLEDGEMENTS

I would like to express my deepest gratitude to Dr. James R. Springstead for his invaluable guidance, unwavering support and profound dedication throughout my journey in pursuing my Master's and Ph.D. He created a stimulating academic environment that fosters collaboration and critical thinking. I would also like to acknowledge his mentorship, relentless patience, kindness and generosity in sharing his knowledge and expertise with me, a pivotal role model in nurturing and expanding my skill set, fostering both professional and personal growth.

I would like to extend my gratitude to my committee members and the entire faculty and staff from the Chemical and Paper Engineering department from Western Michigan University for their support and encouragement throughout my Ph.D program.

Lastly, I am profoundly grateful to my family and friends for their support, unwavering love and encouragement during this challenging yet rewarding journey. Their belief in me has been the cornerstone to my success, pushing me to pursue greatness.

Piao Jian Tan

TABLE OF CONTENTS

Table of Contents—Continued

Table of Contents—Continued

Table of Contents—Continued

Table of Contents—Continued

Table of Contents—Continued

Table of Contents—Continued

LIST OF TABLES

LIST OF FIGURES

List of Figures—Continued

INTRODUCTION

Purpose of Dissertation

The main objective is to help develop a new method of measurement of active clay content in the metal casting foundry. Active clay content measurement in molding sand is vital in the metal casting foundry to ensure the desired surface finishes with minimal defects that can lead to increased cleaning labor. To date, the methylene blue (MB) test has been used and is technically considered as a semi-qualitative measurement of active clay content due to the call point being a visual inspection of the appearance of a blue halo ring on a filter paper. The newly developed method as presented in this dissertation utilizes a spectrophotometer to measure absorbance reading of the cation exchanged dye and can directly relate to the active clay content of the sand sample. This test was optimized through 3 stages. In the first stage we replaced the methylene blue dye with Cu(II)-triethylenetetramine dye in the protocol. After dosing and mixing the sand sample with an orbital shaker, the used dye is separated via centrifugation and subject to absorbance reading via UV-Vis spectrophotometer. In the second stage we optimize the separation process by replacing centrifugation with a syringe filter in the protocol to separate sand from used dye. Lastly, in the third stage we optimized the mixing process by replacing the orbital shaker with a vortex mixer, as well as integrating other small procedural changes. This newly developed technique that we hereby call the spectrophotometric technique or digital clay test will hopefully supersede the MB test and improve measurement of the active clay content of molding sands in the foundry.

Additionally, a second research project that is presented in this dissertation is related to determining pathways by which oxidized lipids affect the development of atherosclerosis, a

completely different area than our studies in metal casting. The second major aim of this dissertation is to determine the activity of a model isoprostane, neuroprostane and neurofuran in human aortic endothelial cells (HAECs), continuing the work previously started by Cole, 2017 [1]. HAECs have been treated with 15-F_{2t}-isoprostane, 4-epi-4-F_{3t}-neuroprostane and 4(RS)-ST-Δ^5-8-neurofuran, and the regulation of gene expression of IL-8, HO-1 and MCP-1 by each of these lipids were analyzed using PCR.

PAPC is the molecule 1-palmitoyl-2-arachidonoyl-*sn*-glycero-3-phosphocholine that is a phospholipid with a palmitoyl group in the sn-1 position, a phosphocholine headgroup in the sn-3 position, and an arachidonyl group, prone to oxidation, in the sn-3 position. This lipid forms several oxidation products, and the mixture, oxidized PAPC (OxPAPC) has been shown to regulate each of these genes and will be used as a positive control along the treatment with these lipids.

These experiments will give us a new insight on the binding mechanism of oxidized lipids and may eventually lead to new and novel treatment for atherosclerosis and/or other chronic inflammatory diseases.

NEW METHOD DEVELOPMENT FOR METAL CASTING FOUNDRY

Green Sand Active Clay in Metal Casting Foundry

In metal casting, it is essential to have an optimized mold to ensure that the final product of the line comes out perfectly with a smooth surface without defects. These molds need to have enough strength to withstand the metal casting process but also must be able to be shaken out readily after the cast is poured. These molds are usually made of green sand consisting of a heterogeneous mixture of silica sand, bentonite clay, water and other additives [2]. Bentonite is a natural clay that are stimulated by water and acts as a binder to hold sand grains together [2-4]. The two commonly used bentonite clay are sodium bentonite and calcium bentonite, and some foundry used them in combination together to exploit the strength and benefits they provide individually. The most used between the two are sodium or western bentonite, which boast its ability to retain higher amount of water, swell volume, viscosity and hot/dry strength compare to calcium or southern bentonite [5-7]. These advantages help sodium bentonite molds to maintain more accurate mold dimensions; however calcium bentonite has an easier mull and shakeout process due to its lower hot/dry strength, as well as having greater compression strength [8].

In metal casting, hot metals are poured into the molds to take its final product form. During this process, exposure of the elevated temperature of the metal surface deionizes the surface of the green sand in the mold, scalding and reducing the amount of usable bentonite clay [3, 9]. These usable clays are generally called active clay content in green sand. The active clay content composition required for casting varies depending on the metal being cast and differs from foundry to foundry. The composition specifications includes metal type, sand grain size, moisture content, permeability, compressive and compactibility strength [10]. On occasion of a defect, the cast metal will be rejected as a recycled scrap or need to be manually refinished, and

reprocessing increases energy and labor costs in the foundry. Originally developed by Jones, et al in 1964, the methylene blue (MB) test was developed to detect active bentonite in drilling mud. This technique was further optimized by Laboratoire Central des ponts et Chaussees (LCPC) in 1981 and has been used by the foundry since 1967 as the American Foundry Society (AFS) standard control for active clay in green sand [11]. Two types of the MB test method was developed, the turbidimetric method and the spot method [12]. The latter method is more rapid and simpler and does not utilize specialized equipment. As such, the MB test has been a staple technique in the metal casting foundry molding process and other engineering practices [4, 12-15].

The MB spot method is an absorption technique in which MB dye is added to a defined amount of green sand containing active clay. This method is dependent on the cation exchange reaction where active binding anionic sites of the clay are bound to the MB dye which results in sequestration of the dye molecule from the solution. MB is gradually added dropwise to the molding sand sample on a filter paper with a burette until a light blue halo ring appears around the molding sand sample on the filter paper. This light blue halo ring is the indication where the molding sand sample is fully saturated and could no longer absorb any more MB dye, thus ending the test. The active clay content in the sand sample can be determined by the estimated amount of MB dye absorbed by the clay. This method has been catalogued in the AFS handbook (AFS 22100-00-S) and is still currently being used up to this date in the metal casting foundry to calculate its cation exchange capacity (CEC) [4, 12, 13, 15-18]. The active clay content percentage was calculated by comparing the amount of MB titrated for the molding sand sample to a calibration standard sand [15]. Although the method is rapid and simple, the reproducibility and repeatability of the test is subjectively impacted by human expertise and errors. The

technique and execution of reading the blue halo ring is highly dependent on the performance and experience of the operator since the test does not use any digital instrumental reading. Foundries have reported that the major factors of the leading inherent inaccuracies of the test are visual determination expertise, operator discretion and bias on calling the halo points to stay within a certain controlled ranges [19].

An Alternative Method to MB using Spectrophotometry

Due to the nature of the MB dye, higher concentration is required for sufficient binding strength to the active clay. This concentration is an opaque solution, and it is not possible to implement the use of spectrophotometry to determine the CEC as absorbance reading would not be feasible, as we confirmed in preliminary experiments. A tighter binding dye in lower concentration was investigated and a spectrophotometric technique has been developed to replace the MB spot detection method. In this new method, the dye and sand sample will be mixed for cation exchange and be separated through means of centrifugation, and lastly the residual dye will be subjected to absorbance measurement in the spectrophotometer.

Selection of the dye is important in this technique and it has been reported that black or yellow dyes lose potency as much as 25-30% only after a few days due to poor shelf life, whereas an orange dye loses only 10% over the course of month [20]. A spectrophotometer technique outlined in the AFS publication 13-1455, utilizes an orange dye prepared with DI water and hardened by calcium chloride shows significant improvement in test-to-test variability in the range of 2-12% active clay content measurement compare to the traditional MB test method at 5.4% to 40% respectively [20]. It was unclear however which kind of orange dye was used in this technique. In a recent publication, hexamine cobalt (III) chloride, a relatively stable yellow-orange dye has shown better correlation in the measurement of CEC compare to the orange dye

previously reported in Pike et al, 2013 [17, 20]. Although this dye provides more consistent results, the dye is highly toxic and requires the use of extreme precaution when handling. Due to it being highly toxic, proper disposal of the hexamine cobalt (III) chloride is required and can be expensive due to its strict regulation of waste disposal management. Additionally, the dye has shown to be unstable by absorbance reading 1-2 weeks after its creation and only work in limited range of active clay content in green sands [17].

In a recent study, Decher & Ramrattan, 2021 utilized a new dye, Cu(II)-triethylenetetramine with the spectrophotometric technique and demonstrated low test variability when testing prepared bentonite standards with an active clay content from 4-12% [21-23]. Due to stronger binding activity on active clay binding sites, this dye also allows the use of lower dye concentrations in test solutions. The dye is made from mixing copper sulfate, triethylenetetramine and DI water. The cupric ions form a complex with triethylenetetramine and tightly bind to the cation in bentonite with the assistance of the four nitrogen atoms from triethylenetetramine. This dye is excited at an absorbance of 578nm and is more stable and less toxic compared to MB and hexamine cobalt (III) chloride, although proper disposal of the dye would still need to be employed. However, due to the lower toxicity of the dye, disposal of the dye is still less expensive.

In this dissertation, the spectrophotometric procedure using Cu(II)-triethylenetetramine was investigated further and a new standard procedure was developed to replace the use of MB test to determine the CEC and active clay content in green sand. The development of this new standard procedure is separated into 3 stages. The first stage included validation of this procedure with the use of Cu(II)-triethylenetetramine in foundry sand samples instead of just bentonite standard. In this procedure we also used lower amounts of dye and sample sizes, utilizing the

spectrophotometer technique with the use of an orbital shaker and centrifuge. Additionally, multiple laboratories performed this procedure to determine laboratory to laboratory and operator to operator variability of the test. The participating laboratories included the Decher, Hoffman Estates (HE) and WMU laboratories. The second phase included optimization by modification of the first stage separation procedure of replacing separation via centrifuge with syringe filtration. Additionally, in this stage, the tests were performed in three separate foundries, in addition to at WMU on several samples. The three foundries included EJ, John Deere (JD) and Metal Technologies, Inc. (MTI). The third and last stage included optimization through modification of the second stage mixing procedure of replacing orbital shaker with vortex mixing. These samples were also tested at the three foundries and at WMU. This testing method has been submitted to be accepted into the AFS standard test for active clay in green sands and to be featured in the AFS Mold & Core Test Handbook.

Additionally, a main objective of these dissertation studies was to establish that cation exchange capacity (CEC) could be used as an alternative measurement of clay activity as opposed to % active clay, which is the currently used measurement. The percent active clay is based on the activity of the original bentonite standards and thus the measurement of the clay activity of the same sample generally changes from foundry to foundry. The CEC measurement that has been developed generally remains consistent for the same sample when testing the same samples at multiple foundries, as shown in these studies.

Methodology

Material and Reagent

Cu(II)-Triethylenetetramine (SKU: 90460-10ML) and 0.1 mol/L copper sulfate Titripur® (SKU: 1027841000) solutions were purchased from Sigma Aldrich. 2 mL Fisherbrand premium microcentrifuge tubes (CAT: 05-408-138), a bottle top volumetric dispenser (CAT: 13681527), clear polystyrene disposable cuvettes (CAT: 14955129), a Fisher Vortex Genie 2 (CAT: 12-812) and a glass funnel (CAT: 03-865) were purchased from Fisher Scientific. Corning® 384-well clear flat bottom polystyrene NBS microplates (Product No: 3640) were purchased from Corning Life Sciences. Disposable Syringe (Part BH3LS) was purchased from BH supplies. 13 mm 0.45 µm PES syringe filters (CAT: 1470354) were purchased from Sterlitech. A measuring Scoop (42924) was purchased from New Star Foodservice. Deionized (DI) water was available at WMU through a main supply line.

Experimental Procedure

The process of CEC determination requires the preparation of Cu(II)-Triethylenetetramine dye, sample weighing and dosing, mixing/agitation, centrifuging and measurement of absorbance. The procedure/steps were followed and modified as described in Decher & Ramrattan, 2021 [21].

Dye Solution Preparation

3.33 mmol/L Cu(II)-Triethylenetetramine solution was prepared as previously described. 1.05 g of liquid Triethylenetetramine was accurately weighed and dissolved with 50 mL deionized water (DI) in a beaker. 66.67 mL of 0.1 mol/L of copper sulfate solution was measured using a measuring cylinder and an adjustable 1-10 mL pipette. Both solutions were transferred to a 2 L

volumetric flask and the flask was then filled to 2L with DI water. A magnetic stir bar was used to gently stir the solution overnight while covered to allow for sufficient formation of dye complexes. The Cu(II)-Triethylenetetramine solution was then transferred to a large amber container and stored in a cool and dark place. Due to the hygroscopic nature of triethylenetetramine, rapid handling and proper storage of the solution is required.

Sample Weight and Dosing

1st Stage

The previously described technique uses 1.5 g of sample and dosing with 30 mL of Cu(II)-Triethylenetetramine, and these amounts were used in the spectrophotometric technique by the Decher and HE laboratories in these results. At WMU several combinations of sand sample to dye ratio were tested and it was found that 50 mg of sand sample dosed with 1 mL of Cu(II)-Triethylenetetramine produces consistent results while using smaller sample and dye amounts. Henceforth, in this paper, this ratio for sand to dye ratio was used for all experimental trials. In the first phase experiments at WMU 50 mg (± 0.5 mg) of sand sample was weighed with an analytical balance (d= 0.1 mg) and transferred into a 2 mL microcentrifuge tube. 1 mL of Cu(II)-Triethylenetetramine was then added to the tube and capped. To note, amounts of sample and solution transferred should not exceed 50% of vessel capacity to allow sufficient space for proper mixing.

2nd Stage

After the 1st stage testing, various tests were performed to determine the lowest and acceptable green sand sample size and dye volume. A green sand sample size of 0.5 g (± 0.1 g) along with 10 mL (± 0.1 mL) of Cu-T dye was used in the optimized procedure. This was also based on mass balance sensitivity limitations, and so 0.5g of sample size needed to be used. In the first-

round testing, the amount was set to use exactly or close to 0.5 g of green sand sample with weighing paper and 10 mL of dye with a bottle top dispenser with recirculation valve into a 15 mL centrifuge tube.

3rd Stage

Testing and feedback from 2nd stage were used to further optimize the testing procedure, and the weighing and dosing method were changed. A 15 mL centrifuge tube was weighed, recorded, and tared, and 10 mL (± 0.1 mL) was pipetted using a bottle top dispenser with recirculation valve into the centrifuge tube. The dye was then weighed, recorded, and tared again. Using a glass funnel, and a measuring spoon of 1/16 or 1/8 teaspoons, green sand samples were scooped and transferred into the centrifuge tube. Density and properties of the foundry sands may require the use of the different measuring spoon capacity. The green sand sample was weighed and recorded. This green sand sample size generally needed to be 0.5 ± 0.1g.

To note, total volume should not exceed 10.5 mL to provide sufficient space for proper mixing in the tube. The use of weighing paper for measurement of sand that was used in the first-round testing was removed due to the electrostatic forces acting on the green sand which may cause interference in the transference of green sand into the centrifuge tube. The glass funnel technique eliminates the electrostatic forces and saves time. With a 1/16 or a pinch scoop, the green sand can be easily measured to 0.5 g (± 0.1 g) and need not be the exact amount as the weight of the sand sample and dye can be adjusted in the CEC calculation. Additionally, removing the step of using a weighing paper also minimized user error that may occur if sand accidentally is deposited underneath the weighing paper during measurement or electrostatic forces that causes the sand sample to stick to the weighing paper, which was a problem that was identified in feedback from the second phase of testing.

Mixing/ Agitation

1st Stage

The prepared samples were first shaken by hand to ensure that each sample was fully suspended in the Cu(II)-Triethylenetetramine solution and ensure proper mixing. The samples were then vigorously shaken with tubes horizontal on a Barnstead MaxQ 2000 Orbital Shaker at 300-500 RPM for 10 minutes to allow good dispersion of clay minerals into the Cu(II)-Triethylenetetramine solution.

2nd Stage

The 2nd stage of the mixing process has no changes made from the 1st stage.

3rd Stage

In the 3rd stage of process optimization, a major aim was to improve the cation exchange rate of the green sand-dye mixture. The prepared samples were first mixed by vigorously shaking by hand for 5 seconds and then mixed by vortex mixer at speed setting of approximately 2000 rpm for 10 seconds. The samples are then allowed to sit for at least 2 minutes to allow sufficient settling and equilibration of the green sand. Most foundry green sand samples settle to the bottom quickly, but in some cases if it does not, extra time was allocated for settling. Then the samples were vortexed and allowed to settle a second time for 2 minutes. This second mixing and settling step, as well as use of the vortex instead of an orbital shaker were modified in the optimized procedure from the first set of foundry trials.

Separation of Green Sands and Dye

1st Stage

In the first stage high speed centrifugation was used to separate green sands and spent dye for spectrophotometric analysis. Sufficient G-Force and time of at least 4,000 RCF have been found to be required to separate sand particles from residual Cu(II)-Triethylenetetramine solution that is measured by spectrophotometry. If needed, samples should be allowed to sit for some time before spectrophotometric absorbance reading to stabilize the signal. For this study, since a higher RCF speed was used, a lower amount of time was needed for the separation and additional resting time was not needed. After sufficient mixing, samples were allowed to rest, and 1 mL of the supernatant was transferred to a 2 mL microcentrifuge tube and centrifuged in the Eppendorf 5417C Centrifuge equipped with a F45-30-11 rotor and spun at 18,539 RCF (13200 RPM) for 10 minutes in this stage of testing.

2nd Stage

While centrifugation provides a good separation of the green sand and dye mixture, the requirement of a sufficient G-force centrifuge is generally not available in the foundry. Centrifuges are often very costly to purchase, especially ones that operate on a higher RPM, and the costs of maintenance are high as well. An alternative method was used to separate by syringe filtration. Using a 3 mL disposable syringe 3 mL of the supernatant dye was taken and filtered through a 25mm 0.45 µm PTFE syringe filter into a 4.5 mL clear polystyrene disposable cuvette. Square bottom cuvettes were necessary to minimize variance in our tests and trials. Cuvettes that have a tapered bottom proved to be problematic in the spectrophotometer when measuring absorbance in the next step, as these did not sit in a consistent position in the spectrophotometer.

3rd Stage

In the third stage of testing, the 25mm 0.45 µm PTFE syringe filter was replaced by the 13mm 0.45 µm PES syringe filter. The 13mm 0.45 µm syringe filter was preferred by the operators as it was easier to expel the liquid into the full cuvette volume. The PTFE filters required a strong filter drop that often led to leaking of the filter or wrist pain for the operator. This 13mm syringe filters were cheaper to purchase, have less holdup volume and give comparable results to the 25 mm filters. Using a 3 mL disposable syringe 2 mL of the supernatant dye was taken and filtered through a 13mm 0.45 µm syringe filter into a 4.5 mL clear polystyrene disposable cuvette.

UV-Vis Spectrophotometry

A spectrophotometer is used to measure samples in which light is passed through at specific wavelength adjusted by a monochromator. The light that passes through the sample is measured on the other side of the sample and used to calculate absorbance of the light by the measured sample. The measured absorbance in our test is used to quantify Cu(II)-Triethylenetetramine that is not sequestered/absorbed by the samples after mixing and centrifuging. 100 µL from the sample solution was pipetted into a 384 well microplate and absorbency was measured on a SpectraMax 384 Plus UV-Vis Spectrophotometer at 578 nm. The absorbance value obtained was then used to calculate Cu(II)-Triethylenetetramine concentration.

Dye Concentration Calibration

A dye calibration curve was generated to determine the actual Cu(II)-Triethylenetetramine concentration of the prepared solution from the step above and foundry sand samples. A serial dilution of the prepared dye solution was prepared with DI water at the concentration of 3.33, 2.78, 2.08, 1.28 ad 0.57 mmol/L as shown in Table 1 below. The calibration curve was generated (Figure 1) with the absorbance measured through a UV-Vis Spectrometry at the optimal

wavelength of 578 nm. The slope of the generated plot was then used to calculate the actual concentration of the Cu(II)-Triethylenetetramine of the sample. Due to the highly stable nature of Cu(II)-Triethylenetetramine, no change in absorbance of the dye was observed after two months. Therefore, a calibration curve was not needed to be generated daily or weekly unless a new Cu(II)-Triethylenetetramine solution was made.

Table 1: Serial Dilution for Cu(II)-triethylenetetramine dye calibration

Concentration of Dye (mmol/L)	Volume of 3.33 mmol/L Dye (mL)	Volume of DI Water (ml)
0.57	0.208	1
1.28	0.625	1
2.08	1	0.6
2.78	1	0.2
3.33	1	0

A calibration curve was used to establish the relationship of absorbance to dye concentration, as shown in Figure 1.

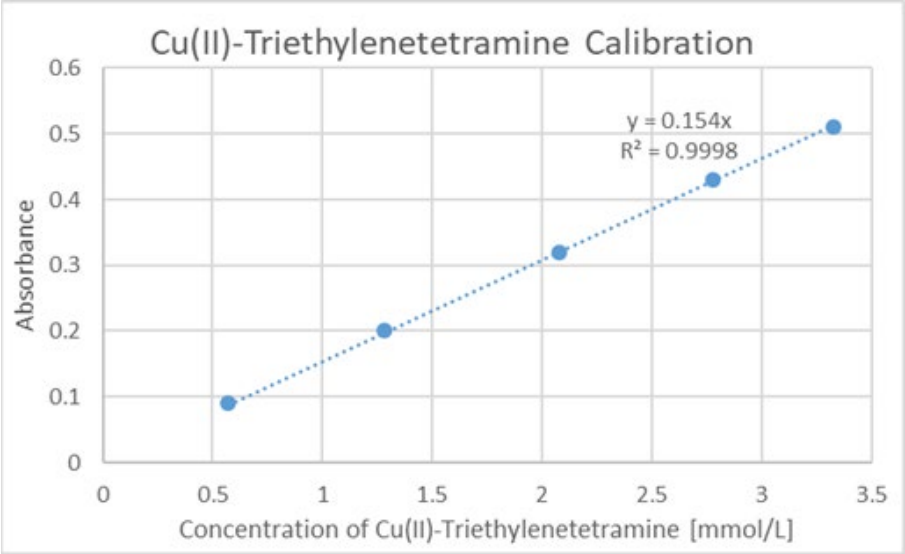

Figure 1: Cu(II)-triethylenetetramine calibration curve

Concentration of Dye Solution

To calculate the concentration of the exchange solution, the actual concentration of the premade Cu(II)-Triethylenetetramine solution was determined. The accuracy of the calibration curve should not drop below 0.997.

The calibration curve in Figure 1 shows sufficient accuracy and the slope of 0.154 was obtained and will be used to calculate Cu(II)-Triethylenetetramine concentration. With an average absorbance of 0.51 (after subtraction of blank (DI water)), the concentration of the premade Cu(II)-Triethylenetetramine solution was calculated by taking the average absorbance, 0.51 divided by the slope, 0.154, as a result showing a concentration of 3.312 mmol/L. The plot was generated several more times on different dates without changing, establishing that the Cu(II)-Triethylenetetramine solution was very stable over a long period of time. We tested stability of the dye over 1 year with minimal absorbance change.

CEC Determination

CEC was determined by the difference in the concentration of Cu(II)-Triethylenetetramine of the sample to a referenced standard, taking into account of the volume of exchange solution and valance of the copper cation, and adjusted by the weight and the moisture content of the sample. Since there is an equivalent exchange of sample and solution, the valance of the Cu(II)-Triethylenetetramine is 2. Concentration of Cu(II)-Triethylenetetramine was calculated by dividing the absorbance obtained through the spectrophotometer by the slope of the calibration curve of Cu(II)-Triethylenetetramine. CEC was calculated using the equation below.

$$CEC=\frac{(x_0-x_i)*V_x*100*z}{m_{sample}*(1-W_{107^o})}\ [\ cmol_c/kg\ ]$$

x_0=concentration of referenced exchange solution [mmol/l]

x_i=concentration of sample exchange solution [mmol/l]

V_x=Volume of exchange solution [mL]

z=valency of index cation

m_{sample}=sample weight [mg]

W_{107^o}=sample moisture measured at 107^oC

Moisture Content

Moisture content was determined by weighing sand sample before and after drying in an oven at 107 ºC. Moisture content was adjusted in the CEC calculation only and not during other methodology. Moisture content for the 1st stage green sand samples were shown in Table 2.

Table 2: Moisture content of 1st stage green sand sample in WMU, Decher HE and EJ

Sample	Moisture %			
	WMU	Decher	HE	EJ
A	2.75	2.9	3.01	3.14
B	3.06	3	3.03	3.2
C	3.66	3	3.07	3.26
D	2.72	3.1	3.16	3.24
E	3.22	3.2	3.24	3.32
F	2.31	3	3.06	3.16
G	2.09	2.1	2.01	2.2
H	2.56	1.8	1.89	2
I	2.20	2.9	3.18	2.24
J	2.88	3.4	3.56	3.52
L	2.91	3.1	2.83	3.48
M	2.15	2.5	2.42	2.68
N	3.18	3	3.09	2.6
O	1.88	2.5	2.73	2.72
P	4.21	3.9	4.2	2.07
Q	3.12	3.6	3.62	3.78
R	2.49	2.6	2.51	2.64
S	2.37	2.1	1.97	2.16
W	2.85	2.9	2.76	2.56
X	3.29	2.6	3.1	3.12

Results and Discussion

Validation of Cu(II)-triethylenetetramine in Foundry Green Sand (1st stage)

In the first stage, 18 molding sand sample from multiple working foundries (sample A-S) and 2 lab sand mixes (sample W and X) was distributed by Hoffman Estate (HE) to three laboratories (Western Michigan University (WMU), HE and Andreas Decher Minerals Services (Decher)) for the measurement of the CEC and to test the variance of the spectrophotometric methodology. Descriptions of the twenty tested sand samples above are listed in Table 3 down below. Some samples were not fully described to maintain anonymity of participating foundries.

Table 3: Molding sand sample description

SAMPLE LETTER DESIGNATION	Notes	Ratio of Sodium to Calcium Clay in bond
A	Received from EJ	63.4
B	Received from EJ	63.4
C	Received from EJ	63.4
D	Received from EJ	63.4
E	Received from EJ	63.4
F	Received from EJ	63.4
G	Received from WMU	NA
H	Received from WMU	NA
I	High FloCarb user/ uses River Water	42.0
J	High coal and FC user / green sand	49.6
L	High overall Active Clay	54.2
M	All Southern (DC-6)	3.2
N	High Core Loading	50.2
O	Blackwater System/ High pH	63.3
P	High conductivity	63.3
Q	Lower Conductivity	63.3
R	Low pH consistently	46.8
S	Very low Active Clay	53.3
W	Lab prepared Western Clay only	63.4
X	Lab Prepared standard mix with	46.8

Table 4: Methodological differences between HE, Decher and WMU

	HE/Decher	WMU
Sand Sample Weigh	1.5 g	50 mg
Dosing Volume	30 mL	1 mL
Centrifuge	4,000 RCF	18,539 RCF
UV-Vis volume	1.5 mL	100 µL

Slightly different methodologies were use between HE, Decher and WMU and were listed in Table 4 above. In this stage, Decher and HE laboratories utilized the previously described technique using 1.5 g of sand sample dosed with 30 mL of Cu(II)-triethylenetetramine, while WMU laboratory scaled down to reduce material consumption and waste disposal by using 50 mg (± 0.5 mg) of sand sample dosed with 1 mL of Cu(II)-triethylenetetramine. The dosed sand sample was then mixed by hand shaking and an orbital shaker, and then sequestered dye was separated through centrifugation. HE and Decher labs used a centrifuge with a centrifugal force of 4,000 RCF while WMU used a centrifuge with a centrifugal force of 18,439 RCF. HE and Decher labs utilized a disposable cuvette with 1.5 mL of exchange solution while WMU utilized 384 well microplates with 100 µL exchange solution in the measurement of absorbency.

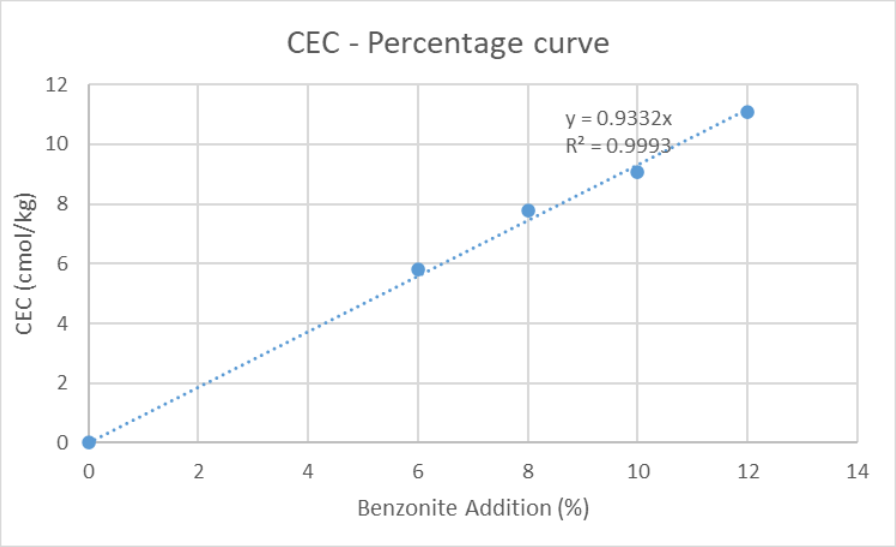

Figure 2: Linearity of percent active clay to dye

Figure 2 calibration curve demonstrated linearity of percent active clay of 6%, 8%, 10% and 12% with absorbance of the Cu(II)-triethylenetetramine dye suggesting scaling of the amount use of sand and dye can be altered linearly. CEC measurements for sand samples at WMU were measured and averaged through at least 4 trials in different days with 3 repetitions each and four different operators (12 data points) while HE and Decher laboratories averaged 2 data points for each CEC sand sample measurement. Figure 3 below shows the CEC trend and measurement of all the sand sample between the three laboratories, sorting from smallest to largest CEC of sand samples tested.

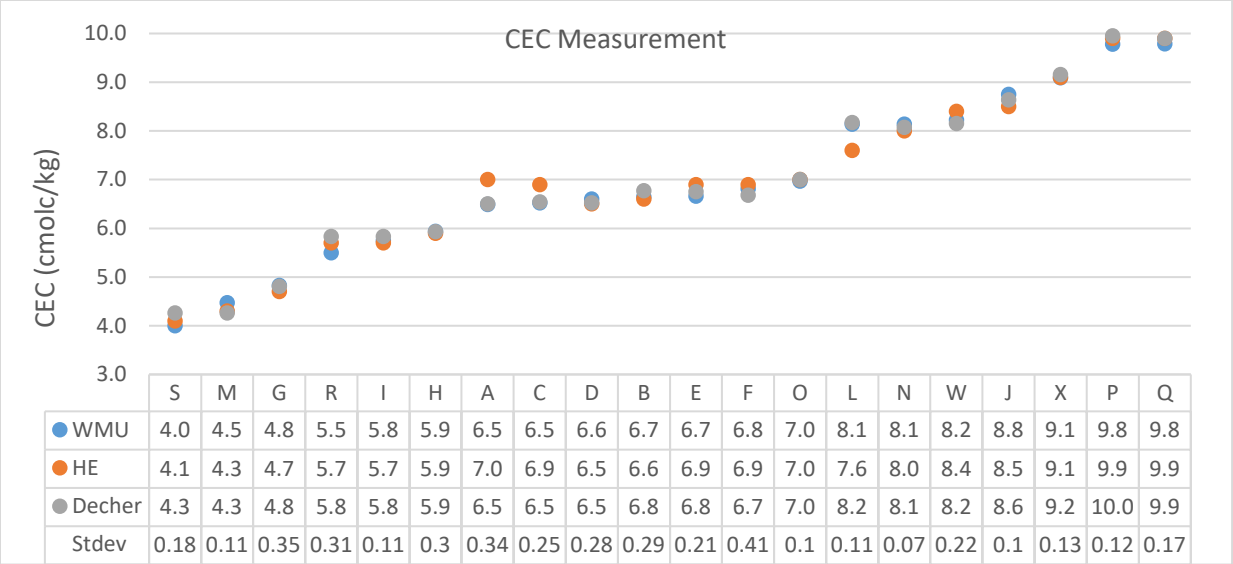

	S	M	G	R	I	H	A	C	D	B	E	F	O	L	N	W	J	X	P	Q
WMU	4.0	4.5	4.8	5.5	5.8	5.9	6.5	6.5	6.6	6.7	6.7	6.8	7.0	8.1	8.1	8.2	8.8	9.1	9.8	9.8
HE	4.1	4.3	4.7	5.7	5.7	5.9	7.0	6.9	6.5	6.6	6.9	6.9	7.0	7.6	8.0	8.4	8.5	9.1	9.9	9.9
Decher	4.3	4.3	4.8	5.8	5.8	5.9	6.5	6.5	6.5	6.8	6.8	6.7	7.0	8.2	8.1	8.2	8.6	9.2	10.0	9.9
Stdev	0.18	0.11	0.35	0.31	0.11	0.3	0.34	0.25	0.28	0.29	0.21	0.41	0.1	0.11	0.07	0.22	0.1	0.13	0.12	0.17

Figure 3: CEC measurement of 20 molding sand samples from WMU, HE and Decher Laboratory

Figure 3 shows that the CEC measurement of the molding sand samples across all three laboratories were consistent. Measurement from WMU demonstrated that the scaled down approach is feasible as the measurement stayed consistent with results from the other laboratories using larger sample size and larger dye volume. The average absolute difference across all data points was only 0.22 cmolc/kg CEC, and with the max difference being 0.57 cmolc/kg CEC for sample L. Standard deviation of the chart indicates stable and reproducible results with slightly higher deviation on sample A-H and R.

To convert measurement of CEC to active clay content, a standard reference calibration curve was generated in Figure 4 below.

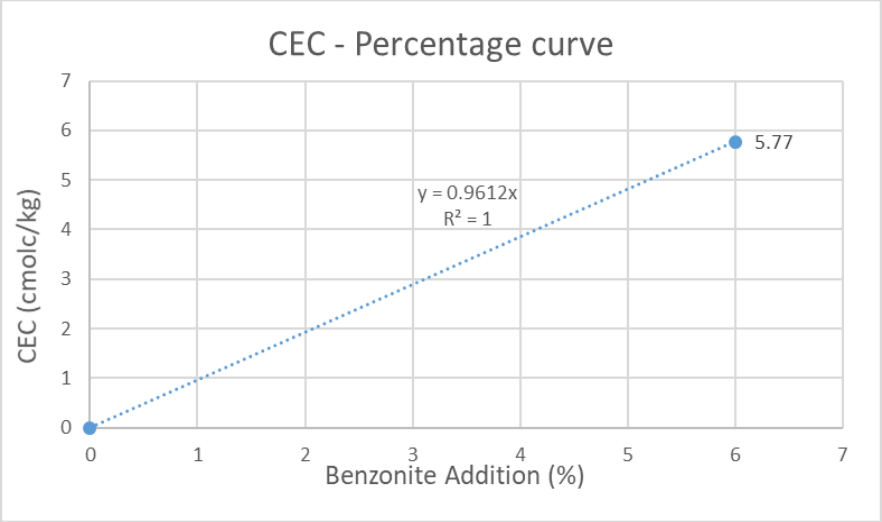

Figure 4: Standard reference calibration curve of 0-6% of western bentonite and silica sand

Standard reference green sand was provided by HE. Using the slop of the standard reference calibration curve, it is possible to directly convert the measurement of CEC to percent active clay content and compare it to the standard AFS MB test. The converted percent active clay content was compared to two other laboratories from HE and East Jordan (EJ) using the MB test on the same 20 sand sample previously mentioned. Active clay content measurement from HE and EJ using the MB test was averaged over two data points, with the exception of sample X to use for variability and accuracy testing. Comparison of the measurement of percent active clay content across three laboratories, sorting form smallest to largest are shown in Figure 5 below.

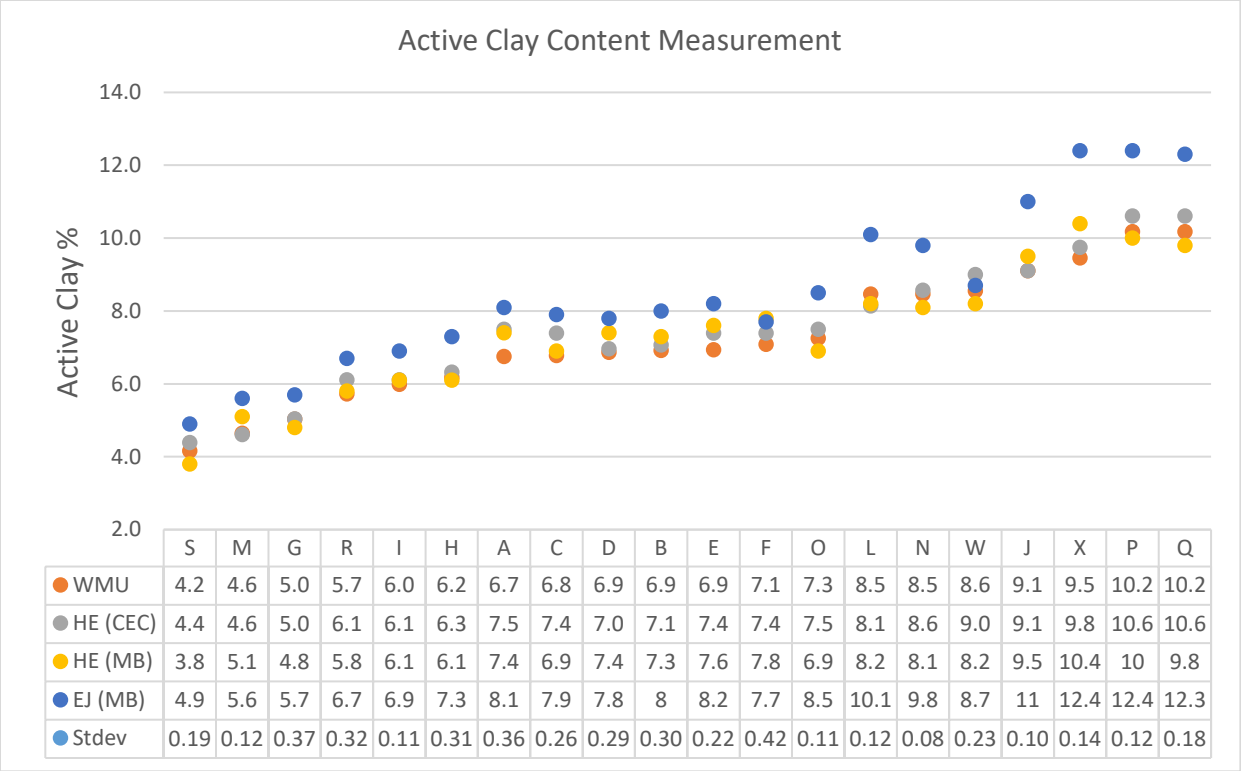

	S	M	G	R	I	H	A	C	D	B	E	F	O	L	N	W	J	X	P	Q
WMU	4.2	4.6	5.0	5.7	6.0	6.2	6.7	6.8	6.9	6.9	6.9	7.1	7.3	8.5	8.5	8.6	9.1	9.5	10.2	10.2
HE (CEC)	4.4	4.6	5.0	6.1	6.1	6.3	7.5	7.4	7.0	7.1	7.4	7.4	7.5	8.1	8.6	9.0	9.1	9.8	10.6	10.6
HE (MB)	3.8	5.1	4.8	5.8	6.1	6.1	7.4	6.9	7.4	7.3	7.6	7.8	6.9	8.2	8.1	8.2	9.5	10.4	10	9.8
EJ (MB)	4.9	5.6	5.7	6.7	6.9	7.3	8.1	7.9	7.8	8	8.2	7.7	8.5	10.1	9.8	8.7	11	12.4	12.4	12.3
Stdev	0.19	0.12	0.37	0.32	0.11	0.31	0.36	0.26	0.29	0.30	0.22	0.42	0.11	0.12	0.08	0.23	0.10	0.14	0.12	0.18

Figure 5: Percent active clay content measurements across three laboratories WMU, HE and EJ

Data from Figure 5 above demonstrated consistent and reliable reproducible results across the three laboratories for the calculation of percent active clay in green sand samples. WMU and HE data show similar average absolute difference of 0.28%, with a max difference of 0.75% for sample L. The differences between these two labs were attributed to the generation of its own standard reference calibration curve. WMU has reported a value of 5.77 CEC in the 6% bentonite standard with a slope of 0.9612 where HE reported a value of 5.6 and 0.9333 respectively. In a MB test comparison, EJ shows slightly higher percent active clay than the others, but the data trends are similar and aligned throughout. Between the MB test of HE and EJ, their average absolute difference is 1.15% with a maximum difference of 2.50% for sample Q in percent active clay content.

It is important to evaluate the stability or the variability and accuracy of the test sample as data demonstrated across the four laboratories across various locations can be seen to be slightly different. Sample A was chosen for this evaluation due to its higher standard deviation and X-bar chart has been plotted in Figure 6 below.

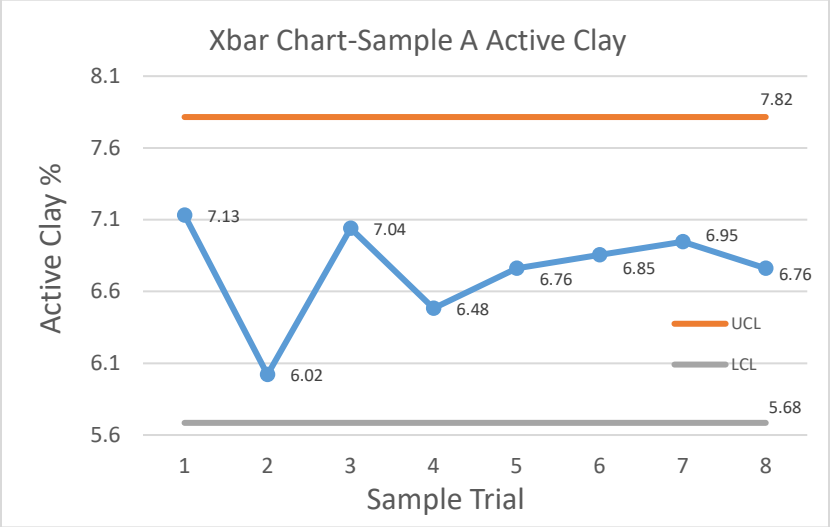

Figure 6: X-bar chart for Sample A active clay measurement

The X-bar chart shows that the upper control limit (ULC) and the lower control limit (LCL) of sample A active clay measurement was found to be 7.82 and 5.68 respectively. The range of the limit was 2.14 with an average measurement of across all trials to be 6.75 and a standard deviation of 0.37. By eliminating the obvious extreme outlier of trial 2, the range of the control limit was reduced to 1.28 with an average measurement of 6.85 and a standard deviation of 0.21. The X-bar chart results demonstrated that this test provides reproducible results.

To test the variability of the test, sample X a laboratory-prepared sand mix by EJ was chosen and compared across the three laboratories. For this test, at least 10 trials with at least three operators were used to run this test. All data were averaged and shown in Table 5 below.

Table 5: Variability test in active clay content of sample X between WMU, HE and EJ

Sample X	WMU	HE	HE (MB)	EJ (MB)
Average (%)	9.46	9.7	10.41	12
Stdev	0.14	0.17	0.22	0.37
UCL (%)	9.88	10.21	11.07	13.11
LCL (%)	9.04	9.19	9.75	10.89
Range (%)	0.84	1.02	1.32	2.22

The test shows that using the spectrophotometric technique has better variance compared to the MB test. WMU and HE tested sample X with the spectrophotometric technique with a standard deviation of 0.14 and 0.17 respectively while HE and EJ tested the MB test with a standard deviation of 0.22 and 0.37 respectively. The spectrophotometric technique has a lower standard deviation and range compared to the MB test. As for the other foundry molding sand sample A to W, the standard deviation is listed in Table 6 below.

Table 6: Standard deviation for active clay measurement in WMU, HE and EJ

Sample	AC Measurement Standard Deviation			
	WMU	HE	HE (MB)	EJ (MB)
A	0.36	0.25	0.4	0.14
B	0.30	0.46	0.27	0.28
C	0.26	0.26	0	0.21
D	0.29	0.36	0.13	0
E	0.22	0.06	0.13	0.14
F	0.42	0.06	0.4	0
G	0.37	0	1.46	0
H	0.31	0.05	0.13	0.14
I	0.11	0.07	0.64	0.28
J	0.10	0.01	0.51	0.35
L	0.12	0.59	0.26	0.35
M	0.12	0.04	0.12	0
N	0.08	0.01	0.12	0.35
O	0.11	0.13	0	0.21
P	0.12	0.08	0.12	0.14
Q	0.18	0.03	0.12	0.78
R	0.32	0.01	0	0.21
S	0.19	0.08	0.12	0.07
W	0.23	0.05	0.3	0
X	0.14	0.15	0.24	0.37
Avg. Std. Dev.	0.24	0.21	0.42	0.27

The average standard deviation across all samples tested was found to be lower for the spectrophotometric technique at 0.24 for WMU and 0.21 for HE than the MB test at 0.42 for HE and 0.27 for EJ. These results demonstrate that the spectrophotometric technique produces more stable and accurate data over the MB test.

To further demonstrate the reliability of this spectrophotometric technique, 6 green sand samples were collected at different times from a working foundry line, were received 1 week after collection and tested. Moisture content was measure, and the spectrophotometric technique was utilized to measure the CEC and percent active clay content as shown in Table 7 below.

Table 7: Time stamp collected foundry green sand sample active clay measurement with spectrophotometric technique

Sample	Time	Moisture %	%AC
1	10.10 am	3.11%	6.16
2	10.40 am	3.31%	6.40
3	11.50 am	3.47%	6.53
4	1.30 pm	3.24%	6.64
5	2.05 pm	3.25%	6.58
6	2.50 pm	3.25%	6.46

The foundry that provided the green sand samples reported the active clay content to be at 7% using the MB test, while WMU using the spectrophotometric technique reports it at 6.16, 6.40, 6.53, 6.64, 6.58 and 6.46 for samples 1-6 respectively.

The reported measurement of active clay content of the spectrophotometric technique has a lower figure when compared to the MB test. This slight variation can be caused by several factors including freshness of sample, water quality, and climate or conditions of the location. Since these sand samples were at least a week old, the moisture content could have changed in the mixture thus altering the measurement. Climate or conditions of the location where testing was performed might also indirectly affect the test as more humidity might change the sands

condition. Another area of improvement that can be worked on is reducing the deviation or variance of sample A-H. All samples were weighed precisely at 50 mg with a given 1% (0.5 mg) error, however sand particles or clumps were observed and may have an impact on the measurement. When a sand clumps together, it is usually an indication of dead clay content, or it could be a wetter green sand mix that just happens to conglomerate. The best way possible is to completely avoid taking said sand clumps into measurement, instead of breaking the sand clumps apart. Other step in improvement that can be taken are to increase mixing time and introducing resting time so more cation exchange can occur.

It can be concluded that the spectrophotometric technique provides a consistent measurement with good repeatability and lower variance across all the data collected. The variation of the scaled down test method tested here in WMU produced acceptable results with comparison to HE and demonstrating lower deviation compared to the MB test. The scaled down version of the spectrophotometric technique used a reduced amount of Cu(II)-triethylenetetramine which reduces the cost of procurement and consumption as well as the cost of hazardous waste removal, also reducing overall environmental impact over an extended period of time. After further discussion with the foundries, due to most working foundry balances not being able to measure to the nearest 0.5 mg and having heavy vibration in the workplace, it was suggested and agreed on for the next round of testing to change the sand sample size to 0.5 g with a dosing volume of 10 mL of Cu(II)-triethylenetetramine.

Optimization of 1st stage Separation through Syringe Filtration (2nd Stage)

In the 2nd stage, the centrifugation process was replaced by syringe filtration for the separation of the sand sample from the Cu(II)-triethylenetetramine dye.

After mixing, dosed samples were allowed to sit for at least 2 minutes to allow sedimentation of the green sand particles and the supernatant was filtered through a 25 mm 0.45 µm PTFE syringe filter. Absorbance for CEC measurement was done in a disposable cuvette.

Table 8: Validation study of separation method change from centrifuge to syringe filter

	CEC	CEC avg	Stdev
Syringe Filter	7.439	7.628	0.196
	7.831		
	7.613		
Centrifuge	7.863	7.748	0.295
	7.968		
	7.412		

A validation study was done as summarized in Table 8. This data demonstrated that the protocol when using the syringe filter for separation has comparable results to protocol when using the centrifuge in the separation process.

In this and the next stage, Metal Technologies Inc (MTI), East Jordan (EJ) and John Deere (JD) participated in this optimization of the spectrophotometric technique. All laboratories used the same inventory and model of equipment sent out from WMU for the test to reduce equipment bias. These item includes the Cu(II)-triethylenetetramine dye, centrifuge tubes, orbital shaker, syringes, syringe filters, disposable cuvettes and the spectrophotometer device. The averaged CEC and standard deviation of each sample across 3 trials reported by MTI, EJ and JD were reported in Table 9 below.

Table 9: CEC measurement with syringe filtration by MTI, EJ and JD

MTI			**EJ**			**JD**		
Sample ID	CEC (cmolc/kg)	SD CEC (cmolc/kg)	Sample ID	CEC (cmolc/kg)	SD CEC (cmolc/kg)	Sample ID	CEC (cmolc/kg)	SD CEC (cmolc/kg)
MTI-1	8.47	0.07	EJ-1	6.58	0.16	JD-1	6.87	0.29
MTI-2	8.41	0.24	EJ-2	6.53	0.09	JD-2	7.85	0.78
MTI-3	8.66	0.17	EJ-3	6.50	0.07	JD-3	7.48	0.15
MTI-4	8.88	0.15	EJ-4	6.30	0.14	JD-4	7.54	0.31
MTI-5	9.28	0.13	EJ-5	6.47	0.26	JD-5	7.37	0.21
MTI-6	8.51	0.15	EJ-6	6.57	0.31	JD-6	7.79	0.06
MTI-7	8.56	0.24	EJ-7	6.49	0.03	JD-7	7.86	0.20
MTI-8	8.42	0.10	EJ-8	6.49	0.33	JD-8	7.77	0.04
MTI-9	8.44	0.03	EJ-9	6.41	0.14	JD-9	7.36	0.09
MTI-10	8.49	0.24	EJ-10	6.60	0.26	JD-10	7.81	0.24
MTI-11	8.31	0.03	EJ-11	6.30	0.06	JD-11	7.66	0.17
MTI-12	8.17	0.10	EJ-12	6.38	0.32	JD-12	7.25	0.16
MTI-13	8.20	0.04	EJ-13	6.29	0.14	JD-13	7.98	0.95
MTI-14	9.03	0.06	EJ-14	6.84	0.10	JD-14	7.16	0.14
MTI-15	9.36	0.14	EJ-15	6.40	0.03	JD-15	7.13	0.07
MTI-16	8.57	0.06	EJ-16	6.38	0.21	JD-16	7.15	0.15
MTI-17	8.78	0.36	EJ-17	6.38	0.12	JD-17	7.85	1.05
MTI-18	7.92	0.04				JD-18	7.35	0.16
MTI-19	8.07	0.13				JD-19	8.33	1.07
MTI-20	8.30	0.10				JD-20	8.00	0.37
Average		0.13	**Average**		0.16	**Average**		0.33

In this 2nd stage testing, all three foundries have reported CEC results with good reproducible data and low standard deviation value for most samples. The average SD values were found to be 0.13 for MTI, 0.16 for EJ and 0.33 for JD. Some of the higher SD value obtained were potentially caused by outliers, operator, test or equipment error. It was reported that tubes were falling off the shaker during mixing, possibly due to improper sitting of the tubes in its holder. Even with this error, the overall SD value was deemed to be in the acceptable range for the test. These tested samples from each foundry were sent to WMU and tested independently. The

averaged CEC and standard deviation of each sample sent from the foundry across 3 trials reported by WMU were reported in Table 10 below.

Table 10: WMU trial on foundries green sand sample

MTI			**EJ**			**JD**		
Sample ID	CEC (cmolc/kg)	SD CEC (cmolc/kg)	Sample ID	CEC (cmolc/kg)	SD CEC (cmolc/kg)	Sample ID	CEC (cmolc/kg)	SD CEC (cmolc/kg)
MTI-1	8.53	0.18	EJ-1	6.68	0.22	JD-1	7.56	0.16
MTI-2	8.19	0.22	EJ-2	6.35	0.05	JD-2	7.70	0.11
MTI-3	8.82	0.06	EJ-3	6.35	0.32	JD-3	7.54	0.23
MTI-4	8.80	0.30	EJ-4	6.39	0.25	JD-4	7.54	0.39
MTI-5	9.01	0.07	EJ-5	6.60	0.22	JD-5	7.75	0.13
MTI-6	8.40	0.36	EJ-6	6.51	0.22	JD-6	7.59	0.11
MTI-7	8.62	0.08	EJ-7	6.52	0.14	JD-7	7.77	0.14
MTI-8	8.63	0.14	EJ-8	6.60	0.09	JD-8	7.83	0.27
MTI-9	8.73	0.23	EJ-9	6.40	0.13	JD-9	7.79	0.12
MTI-10	8.49	0.27	EJ-10	6.25	0.18	JD-10	7.72	0.17
MTI-11	8.45	0.20	EJ-11	6.27	0.08	JD-11	7.76	0.10
MTI-12	8.14	0.16	EJ-12	6.45	0.11	JD-12	7.72	0.03
MTI-13	8.42	0.21	EJ-13	6.34	0.16	JD-13	7.49	0.32
MTI-14	8.80	0.13	EJ-14	6.25	0.04	JD-14	7.15	0.49
MTI-15	9.23	0.03	EJ-15	6.41	0.13	JD-15	7.72	0.04
MTI-16	8.72	0.04	EJ-16	6.52	0.17	JD-16	7.55	0.46
MTI-17	8.87	0.20	EJ-17	6.45	0.14	JD-17	8.15	0.04
MTI-18	8.23	0.23				JD-18	7.91	0.04
MTI-19	8.25	0.07				JD-19	8.09	0.01
MTI-20	8.38	0.16				JD-20	7.99	0.49
Average		0.17	**Average**		0.16	**Average**		0.19

WMU analyzed and measured the same foundry green sand samples sent by the three foundries to evaluate and verify the reproducibility of the test method and data. WMU reported foundry sand sample average SD value of 0.17 for MTI, 0.16 for EJ and 0.19 for JD. Overall, it was shown that the data is reproducible indicating that the separation by switching from the centrifuge to a syringe filtration works reducing the time to complete the test by as much as 10 minutes.

Optimization of 2nd stage Mixing by Vortex Mixer (3rd Stage)

A modification was suggested due to the aforementioned technical problem for the test by replacing the mixing through the orbital shaker with a vortex mixer.

Figure 7: Validation and time study for vortex mixing vs orbital shaker

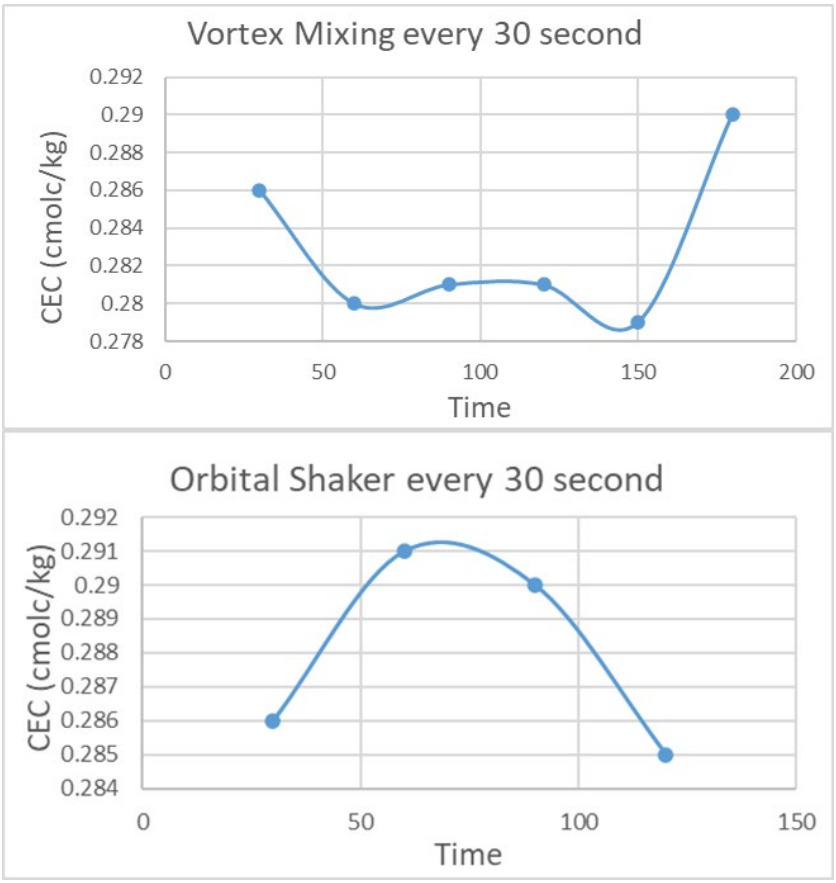

A validation study was done, demonstrating that the change from the orbital shaker to vortex mixing has comparable results. Vortex mixing seems to have shown more consistent data than mixing with the orbital shaker and, after discussion with the AFS steering committee, 10s vortex mixing time was deemed to be sufficient and was used in the method in subsequent testing.

12 green sand samples with the highest standard deviation values between 0.49 to 0.23 were chosen to test this new method of mixing. Sand samples were first added into a centrifuge tube

before dosing previously, but in this stage, Cu(II)-triethylenetetramine was added first. The weight of the Cu(II)-triethylenetetramine was recorded and incorporated into the equation rather than just assuming a flat 10 mL volume used. The sand sample was weighed by means of a 1/16 teaspoon (pinch) scoop added directly into the centrifuge tube instead on a weighing paper. This is to eliminate the electrostatic forces that might cause potential loss of the final amount of sand sample into the centrifuge tube during transference. With this weighing method, the weigh will not need to be measured precisely since the 1/16 scoop measures roughly 0.5 g of green sand samples (still varies from foundry to foundry but does works for MTI, EJ and JD), and the weigh was measured and directly be incorporated into the equation for CEC calculation rather than just a static 0.5 g sample size that was used for calculation in the 1st and 2nd stages. For more efficient mixing and to reduce operator error where tubes were not securely placed, the orbital shaker was replaced by a vortex mixer. Samples were vigorously hand shaken for 5 seconds and subjected to vortex mixing for 10 seconds. Samples were then allowed to rest for 2 minutes before syringe filtration. The variance of the test was greatly reduced for most of the 12 samples using this modified method as reported in Table 11 below.

Table 11: Optimization testing on high SD value green sand samples

Sample ID	Old CEC (cmolc/kg)	Old SD	New CEC (cmolc/kg)	New SD
JD-20	7.99	0.49	7.89	0.14
JD-14	7.15	0.49	7.38	0.07
JD-16	7.55	0.46	7.68	0.12
JD-4	7.54	0.39	7.68	0.08
MT-6	8.40	0.36	7.98	0.07
JD-13	7.49	0.32	7.70	0.06
EJ-3	6.35	0.32	6.14	0.34
MT-4	8.80	0.30	8.30	0.18
MT-10	8.49	0.28	8.26	0.13
JD-8	7.83	0.27	7.89	0.11
EJ-4	6.39	0.26	6.13	0.26
JD-3	7.54	0.23	7.82	0.05

The highest SD value of the sample test was reduced for sample JD-20 at 0.49 to 0.14 and JD-14 at 0.49 to 0.07. Since EJ foundry green sands were generally found to be in the lower active clay content level, remaining dye left after mixing is higher, resulting in higher absorbance values in the test and higher variability. It was also suggested that lower active clay or mixing methods may lead to more aggregation of the green sands at the EJ foundry. To improve the accuracy of the test, the EJ foundry sand sample size was increased from 0.5 g to 0.75 g.

In addition to that, user feedback on the syringe filters on the 2nd stage suggests that the filters have significant backpressure, which resulted in leakage of sample solution and poor user experience which potentially causes an increase in variability of the test. Higher backpressure was determined to be due to syringe filter material, even with a larger diameter, higher surface area filter. The syringe filter was therefore changed to a 13 mm 0.45 µm PES syringe filter in the third stage of testing. Data from Table 12 below demonstrated that when using the protocol with the 13 mm 0.45 µm PES syringe filter for separation has comparable variability to protocol

when using the 25 mm 0.45 µm PTFE syringe filter, with a standard deviations of 0.104 cmolc/kg for the protocol with the PES filter and 0.132 cmolc/kg using the PTFE filter.

Table 12: Validation study for syringe filter change from 25 mm PTFE to 13 mm PES

	CEC	CEC avg	Stdev
PES	8.399	8.310	0.104
	8.196		
	8.335		
PTFE	8.343	8.254	0.132
	8.102		
	8.316		

Testing done at the EJ foundry indicated that some samples have not been fully equilibrated after one cycle of vortex and settling. EJ found that by repeating the cycle of vortex and settling again improved the variability of the test samples. All these modifications stated above were implemented in the 3rd stage of testing for all three foundries, MTI, EJ and JD. To note, absorbance values that were obtained below 0.12 are generally not too reliable and this range of measurement should be avoided by adjusting the sand sample size. CEC measurement and its standard deviation of the foundry green sand sample done by MTI, EJ and JD were summarized in Table 13 below.

Table 13: 3rd stage CEC measurement with final optimized procedure by MTI, EJ and JD

MTI			**EJ**			**JD**		
Sample ID	CEC (cmolc/kg)	SD CEC (cmolc/kg)	Sample ID	CEC (cmolc/kg)	SD CEC (cmolc/kg)	Sample ID	CEC (cmolc/kg)	SD CEC (cmolc/kg)
MTI-1	8.38	0.14	EJ-1	5.82	0.17	JD-1	9.17	0.33
MTI-2	8.01	0.35	EJ-2	5.60	0.38	JD-2	8.68	0.28
MTI-3	8.55	0.15	EJ-3	5.70	0.22	JD-3	6.63	0.29
MTI-4	8.53	0.18	EJ-4	5.90	0.07	JD-4	9.00	0.22
MTI-5	8.57	0.08	EJ-5	6.12	0.20	JD-5	9.45	0.69
MTI-6	7.95	0.24	EJ-6	5.92	0.11	JD-6	9.48	0.11
MTI-7	8.38	0.23	EJ-7	5.74	0.00	JD-7	9.26	0.16
MTI-8	7.76	0.62	EJ-8	5.69	0.15	JD-8	8.73*	0.72*
MTI-9	8.57	0.20	EJ-9	5.97	0.20	JD-9	8.75*	0.73*
MTI-10	8.58	0.11	EJ-10	6.08	0.15	JD-10	9.25	0.13
MTI-11	8.71	0.26	EJ-11	6.00	0.14	JD-11	8.69	0.10
MTI-12	8.46	0.35	EJ-12	5.85*	0.00*	JD-12	8.75	0.13
MTI-13	8.11	0.22	EJ-13	5.59	0.19	JD-13	8.51	0.09
MTI-14	8.41	0.13	EJ-14	5.66	0.07	JD-14	8.67	0.33
MTI-15	8.34	0.24	EJ-15	5.86	0.10	JD-15	8.69*	0.70*
MTI-16	7.78	0.06	EJ-16	5.84	0.27	JD-16	8.53	0.39
MTI-17	7.92	0.10	EJ-17	5.96	0.03	JD-17	8.88	0.34
MTI-18	8.51	0.15	EJ-18	5.79	0.13	JD-18	8.49	0.31
MTI-19	8.40	0.15	EJ-19	5.62	0.02	JD-19	8.67	0.36
MTI-20	8.69	0.26	EJ-20	5.78	0.19	JD-20	9.23	0.31
MTI-21	8.33	0.14	EJ-21	6.05	0.07	JD-21	8.3	0.19
MTI-22	8.79	0.23				JD-22	8.5	0.3
MTI-23	8.08	0.12				JD-23	8.99	0.22
MTI-24	8.29	0.17				JD-24	9.11	0.02
MTI-25	7.66	0.17						
Average		0.21	**Average**		0.12	**Average**		0.22

Data marked with an asterisk above indicates an outlier where the data contains procedural issues or mistakes and therefore will be omitted in the calculation of the average value. The average standard deviation with the optimized method for each foundry was reported to be 0.21 for MTI, 0.12 for EJ and 0.22 for JD. In comparison to the 2nd stage data, it can be concluded that further optimization of the method was effective in reducing testing variation, with the exception of MTI, where it was reported to have a higher average standard deviation value compared to the

2nd stage data. There was a change of operator during the 3rd stage for MTI and the operator was newly and briefly trained on the procedures to complete this testing round. The turnover in operator and less familiarity with the procedure accounts for the slight change in variance off the test, however the results was in satisfactory confined of the test and further shows that this test can easily be trained on and executed compared to the MB test.

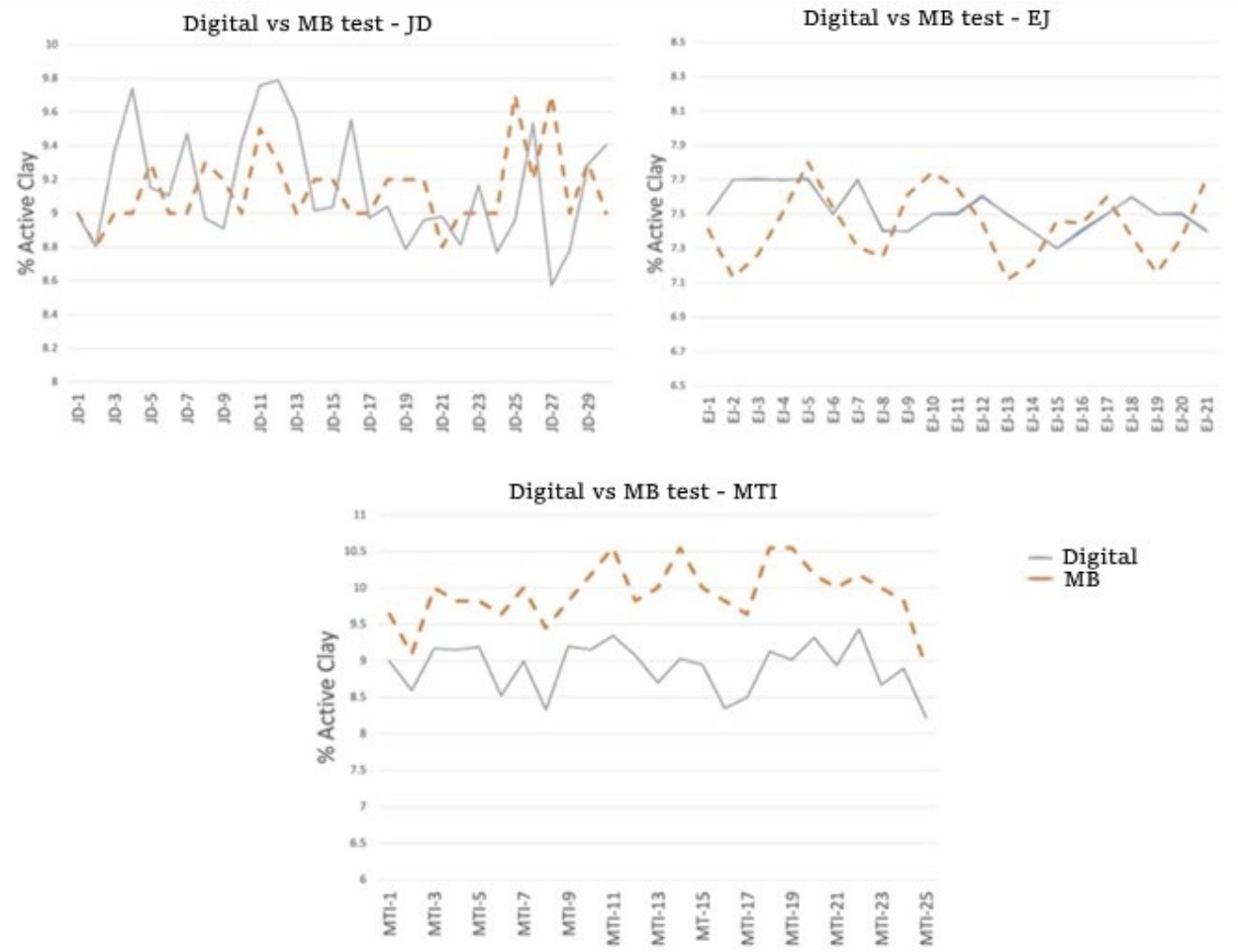

Figure 8: Active clay content comparison between digital (spectrophotometer) and MB test on foundry green sand sample in MTI, EJ and JD

Conversion of the 3rd stage data CEC with a known standard to active clay content was plotted and compared to the MB test data of the same green sand samples from MTI, EJ and JD in

Figure 8 above. In both EJ and JD data, CEC converted active clay content value shows good agreement and consistent trend with the MB test results. For MTI however, an offset of the data was seen, and it was determined that it is most likely due to normalization issue with the change of active clay standard reference. It is more advantageous to normalize the use of CEC value in foundry as a measurement for clay content instead of percent active clay in molding sand to avoid offset issue.

A Gage R&R study (Table 14) was performed to demonstrate the variability of the final optimized spectrophotometric test with different or multiple operators on a random chosen unknown green sand sample conducted by MTI, EJ, JD and WMU individually.

Table 14: Gage R&R comparison between MTI, EJ, JD and WMU for MB vs Digital test

GR&R Comparison Equalized to Same Tolerance Range (1.2%) for All Tests - Xbar/Range Method					
MB Clay Test – Ultrasonic GR&R Results from Various Foundries					
Test By:	Repeatability (EV) % Of Tolerance	Reproducibility (AV) % Of Tolerance	Total R&R % of Tolerance	Standard Deviation	Method
Foundry 1	64%	0%	64%	0.127	10 Samples, 3 tests per sample, 3 operators.
Foundry 2	59%	24%	64%	0.128	10 Samples, 3 tests per sample, 2 operators.
Foundry 3	33%	33%	58%	0.116	2 Samples, 10 tests per sample, 2 operators.
Digital Active Clay Test					
Test By:	Repeatability (EV) % Of Tolerance	Reproducibility (AV) % Of Tolerance	Total R&R % of Tolerance	Standard Deviation	Method
WMU and EJ	64%	0%	64%	0.128	10 Samples, 3 tests per sample, 3 operators.

Between foundry 1, foundry 2 and WMU, the equipment variance or repeatability tolerance was found to be between 59% to 64%. The operator variance or reproducibility tolerance was found to be between 0% to 24%. The total R&R tolerance was found to be 64%. Results of the GR&R study indicate that the digital or the spectrophotometric technique has similar or marginally lower variance when compared to the traditional MB test.

As triethylenetetramine is a moderately toxic compound that can cause severe irritation to the skin and eyes, it is important to understand and study its waste on environmental safety and impact. The original and the spent Cu(II)-triethylenetetramine dye were analyzed with the toxicity characteristic leaching procedure (TLCP). Metal levels, organic including volatile and semi-volatile levels, pesticides, SDS components and concentration were analyzed by qualified environmental personnel. It was determined that the Cu(II)-triethylenetetramine waste, in which the dye is diluted by a factor of 2000, is considered nonhazardous and solution disposal is similar to the MB test, depending on local environmental regulations.

A startup cost analysis was conducted to show that this new spectrophotometric method is economical for any foundry. The equipment required as a one-time cost includes glass and scoop (~$20), vortex mixer (~$300-$500), and UV-Vis spectrophotometer (~$1500) for a total of approximately $2000. Cost of consumable per test was analyzed and shown in Table 15 below.

Table 15:Estimated consumable cost comparison between MB and Digital test

Cost Breakdowns	
Digital Clay Test	**Cost Per Test**
Cu(II) triethylenetetramine Dye	$0.08
Centrifudge Tube	$0.25
Syringe	$0.12
Syringe Filter	$0.20
Cuvette	$0.25
Total Per Test	**$0.90**
MB Clay Test	**Cost Per Test**
Sodium Pryophosphate	$0.15 - $0.65
MB Solution	$0.79 - $0.84
Filter Paper	$0.49 - $1.18
Total Per Test	**$1.44 - $2.66**

The cost breakdown for the digital test is conservative as this is priced out based on the consumable we use in this paper. Cost can potentially be reduced by purchasing different brands or styles of consumables or reusing certain items such as centrifuge tubes, syringes or cuvettes.

Labor costs are not considered in this analysis, but it should be noted that the time to train and run the digital test is less than that of that MB test.

Conclusion

The scaled down method from WMU utilizing only 50 mg of green sand sample with 1 mL of Cu(II)-triethylenetetramine dye demonstrated good consistency and variability in comparison to the other two laboratories from Decher and HE, with 1.5g of green sand sample and 30 mL of Cu(II)-triethylenetetramine dye. Although higher standard deviation was shown in some of the sand samples, this variation is close to that of the MB test showing that that the new spectrophotometric technique is equal to or better than the MB test. Conversion of CEC to active clay content shows agreeable results and the trend were uniform and consistent to the MB test.

To optimize separation (2^{nd} stage), residual dye and sand sample was separated through a 25 mm 0.45 µm PTFE syringe filter instead of a centrifuge. Due to certain limitations in the foundry workplace, sample size of the green sand was modified to 0.5 g in the second stage of testing that was performed at WMU and in foundries, as well as changing dosing volume of Cu(II)-triethylenetetramine to 10 mL. 2^{nd} stage testing reported low variability over a range of clay levels in the foundry, as well as good consistency between all laboratories MTI, EJ, JD and WMU. This demonstrated the feasibility of the use of syringe filters for separating the sand sample from the sequestered dye, eliminating the use of a centrifuge, a high-cost equipment that requires periodic maintenance.

After 2^{nd} stage testing and discussion, in 3^{rd} stage testing we incorporated several changes towards the procedure in mixing and dosing, and separation. Due to lower active clay content level in EJ green sand samples, the sample size for EJ was increased from 0.5 g to 0.75 g to

improve accuracy and variation. It was also found that adding the sand sample after Cu(II)-triethylenetetramine dye improves variation. Furthermore, the sand sample measurement was changed from using weighing paper to measure 0.5g to using a 1/16 (pinch) scoop to measure a variable amount of sand. The weights of the Cu(II)-triethylenetetramine dye and the sand sample were recorded and explicitly implemented into the equation for CEC calculation. Due to user feedback on the back pressure of the syringe, which causes leakage of solution and poor user experience, the 25 mm 0.45 μm PTFE syringe filter was replace by the 13 mm 0.45 μm PES syringe filter. Measurement from this final optimized test and the Gage R&R test shows good variability and correlated well with the MB test measurement.

In conclusion, the new spectrophotometric or digital clay test demonstrated good variability, accuracy and consistency as an enhanced alternative method to the MB test. This test is relatively easy to perform with minimal training or experience required compared to the MB test. This digital clay test has low startup and operational costs, and the test can be performed in 10 minutes or less in contrast to the traditional MB test that generally takes 30-60 minutes by experienced operators. In the broader impact, based on the results in these studies, this new digital clay test will be a standardized test for all metal casting foundry to determine the active clay content level. These data and the simplicity of the test suggest potential conversion from hands-on labor testing to utilizing automated measuring system of CEC and/or active clay for green sand, propelling any foundry system to Foundry 4.0 a new era in metal casting that will be defined improved process control.

Special Acknowledgements are given to the generous support of AFS through contract 21-22#05 and the personnel involved in this project's discussion. We are thankful to all participating laboratories for their data work. The primary WMU research team including James R.

Springstead and Sam Ramrattan, the steering committee and industry partners including Brian Rachwits, Quality and Technical Services Manager from EJ, Michele Ring, Technical Director, Ductile Iron Society and Technical Manager from Norican Group, Steve Nelltner, Technical Service Engineer from REFCOTEC Inc, Thomas Arenholz, Sr. Application Engineer from Simpson. We like to thank Andreas Decher of Andreas Decher Mineral Services in Wenden Germany for his early contributions and directions in the development of this digital clay method, as well as Scott Outman, Manager and Quality from Metal Technologies Inc, Jay Morrison from Carpenter Brothers Inc, and Liam Miller from Mineral Technologies Inc.

POLYUNSATURATED FATTY ACID IN THE REGULATIION OF ATHEROSCLEROSIS IN HAEC

Importance of Atherosclerosis Research

Cardiovascular diseases (CVD) collectively are the number one cause of death worldwide, representing about 31% of all global death with 17.7 million people dying just from CVDs in 2015 (7.4 million death from coronary heart disease (CHD) and 6.7 million from stroke) [24]. According to the World Health Organization, over three quarters of CVDs occur in low- and middle- income countries [25]. In just in the United States alone, approximately 610,000 people die from heart disease every year. In comparison to other death causes, that is 1 in every 4 deaths [26]. Coronary Heart Disease (CHD) which develops due to atherosclerosis, is the most common type of heart disease, taking over 370,000 lives annually (61% of all heart diseases) [26].

Atherosclerosis, the Underlying Condition in CHD

Atherosclerosis, the underlying condition that develops during CHD, occurs when one or more artery vessels that supply blood, oxygen and nutrients to the heart, are occluded from plaques, typically formed from lipid deposits [26-28]. Advanced plaques that lead to blockage of arteries also typically contain dead blood cells, cholesterol, fatty substances, and cellular waste products. The development of this process typically starts with LDL, a lipoprotein, adhering and slowly building up in the artery wall, potentially eventually restricting blood flow to the heart [26-28]. This build up poses an imminent risk to health, as it could cause a clot in the artery or potentially lead to the development of different health problems, depending on where it is blocked [27-29]. The surface of the plaque might rupture and lead to a blood clot on the plaque, thereby blocking the flow of blood [26]. The plaque could also form in the blood circulation which lead to

blockage of a downstream artery [26]. Figure 9 shows the progression of atherosclerosis, the plaque buildup on the inner wall of the artery and eventually causing a blockage of blood flow (from left to right) [26].

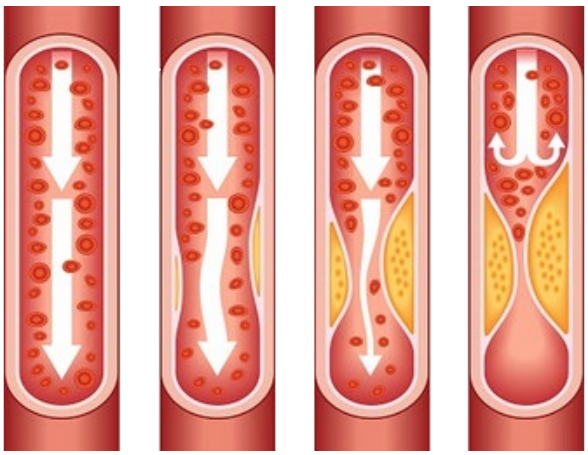

Figure 9: Atherosclerosis progression in the artery

Often after a checkup, physicians may order a "blood panel" which will test levels of several components of the patient blood, including triglycerides, HDL (high density lipoprotein) and LDL (low density lipoprotein) cholesterol levels. These components may be biomarkers for risk of heart disease and are valuable as diagnostic tools to indicate further patient treatment and interventions to prevent CVD. HDL is often regarded as the "good cholesterol", and this lipoprotein acts as a scavenger of pro-atherogenic components of LDL, the "bad" cholesterol which contributes to plaque or fatty build ups in the artery back to the liver to be broken down and recycled or excreted from the body [28, 30, 31]. HDL-C not only has anti-inflammatory effects but also antioxidant, anti-apoptotic and anti-thrombotic effects, making it a good atheroprotective agent [30, 32-37]. The Framingham study back in 1977 led a series of studies demonstrating that HDL-C level is an independent factor against CHD [37-39]. Low levels of HDL-C in patient blood were shown to have a stronger association with CHD than high levels of

LDL-C [37-40]. As little as only 1 mg/dL increment in HDL-C resulted in a 2-3% decrease of CHD mortality with 95% confidence [37, 41]. However, there seems to be no further reduction on CHD risk when HDL-C values are higher than 90 mg/dL in men and 75 mg/dL in women [42]. Based on recent study by Ditah, et al., 2016, HDL particle number (HDL-P) and "medium and small" sized HDL particles (MS-HDL-P) have greater association towards CHD risk than just HDL-C and large HDL particle levels, even after the adjustment of other risk factors [43].

HDL-C alone does not affect CHD risk, but elevated triglyceride and LDL-C in conjunction with low HDL-C give rise to the increased risk of CHD, as much as 6-fold when the LDL-C/HDL-C ratio is greater than 5.0 [31, 44-46]. Elevated triglyceride levels or hypertriglyceridemia usually occur when excess free fatty acids return to the liver, concentrating triglycerides, or when metabolism of triglycerides-rich lipoprotein is inhibited [45, 47]. These excess triglycerides lead to increases in levels of pro-inflammatory cytokines, fibrinogen and coagulation factors, and impairment of fibrinolysis which results in an increase of atherogenicity [45, 47]. An 88 mg/dL increase in triglycerides contributes to a 30% and 75% increase in CVD risk for men and women respectively [44, 48]. Even after adjustment for HDL-C levels, the risk of CHD remains to be statistically significant at 14% and 37% increase for men and women respectively [44, 48]. Triglyceride level has an inverse correlation with LDL particle diameter and HDL-C [49]. Triglycerides level, in concurrence with other risk factors, increases risk of CHD. Additionally, patient CVD risk was correlated with higher LDL particle count, specifically small, dense LDL particles, which are also known as pattern B phenotype patients that are at high risk for CHD [50, 51].

Evidence supporting the contribution of LDL levels to atherogenicity has continued to grow through the decades. LDL is a microscopic globule that is made of a hydrophilic outer shell

made out of lipoprotein, phospholipids, free cholesterol, and other polar lipids and a hydrophobic center made out of esterified cholesterol, triglycerides and other hydrophobic lipids [52]. These particles have a density between 1.006 and 1.063 g/mL [53]. Each LDL particles consists of approximately 700 molecules of PL, 600 molecules of free cholesterol, 1600 molecules of cholesterol ester, 185 molecules of triglycerides, and an apolipoprotein B-100 (apoB-100) protein with 4536 amino acids [54]. LDL can be characterized into four subgroups or subfractions based on its size: large LDL (LDL-I), medium or intermediate LDL (LDL-II), small LDL (LDL-III) and very small LDL (LDL-IV) [53, 55]. Past researchers haves concluded that among the LDL-C subfractions, smaller LDL levels are highly associated with CHD [49, 50, 56-58] and are a better biomarker than total cholesterol or total LDL-C [59]. During physiological mechanisms, LDL subfractions are generated from very low-density lipoprotein (VLDL), which is packaged by the liver, through delipidation by lipoprotein lipase and hepatic lipase. This delipidation results in smaller intermediate density lipoprotein (IDL) and LDL particles [53, 60, 61]. Small, dense LDL-C (sd-LDL-C) particle levels were found to be elevated in myocardial infraction (PMI) survivors [62], as well as patients with dyslipidemia, diabetes mellitus and metabolic syndrome [53, 63] compared to controls. Due to the size of sd-LDL-C, it would more easily diffuse into the subendothelial spacing of the arterial wall [53]. Furthermore, sd-LDL remains in circulation longer due to lower affinity with LDL receptors [64, 65], and is more susceptible to oxidation [66, 67]. Since sd-LDL-C has lower affinity than larger LDL particles with LDL receptors, it is less rapidly removed or cleared by the liver [53, 64, 65]. Intracellular lipoperoxide enzymes including 15-lipoxygenase that is produced endothelial cells (EC) may promote oxidation of LDL (Ox-LDL) [68-70] and plays an important role in atherosclerotic initiation and progression [71]. Ox-LDL is cytotoxic and with concentrations in the

subendothelial space, OxLDL may promote activation of endothelial cells and atherosclerotic development [72-74]. In intermediate stages of atherosclerosis, catalyzed by insufficient OxLDL clearance, this may lead to the differentiation of macrophages to foam cells [75]. Probucol or butylated hydroxytoluene, an antioxidant, has successfully reduced lesion formation in hyperlipidemic and cholesterol-fed rabbits in studies, supporting the hypothesis that oxidative modification of LDL increases atherogenicity [70, 76-78]. Association of CHD with elevated circulating Ox-LDL levels has been demonstrated with patients before [79] and after [80-82] a cardiovascular event. Ox-LDL has been shown in many studies to lead to monocytes recruitment into the arterial wall and turning into macrophages [83-85] which may lead to atherosclerotic lesions. This mechanism will be the focus of this dissertation is and further described later in this proposal.

Current Treatment Therapies and Adverse Effects For CHD

CHD risk increases in patients with several risk factors, including but not limited to, age, genetics, cigarette smoking, dietary consumption, diabetes mellitus, obesity, high blood pressure, and elevated triglycerides and cholesterol levels in blood [26, 28, 29, 86]. Some adverse events that might occur in patients include heart attack, heart failure, ischemic stroke (obstruction of blood to brain) and arrythmia (abnormal heart rhythm) [27, 29].

As atherosclerosis often progresses slowly, it is hard to detect severity of the symptoms before it is too late. Symptoms may include chest pain, upper body discomfort, shortness of breath, nausea or light headedness [26, 27]. If anyone were to experience any of these symptoms, it is recommended that they do not hesitate to call and schedule a checkup with their doctor or physician. CHD survivors will have several options to prevent CHD reoccurrences which may include heart-healthy lifestyle choices, surgery, or one of several medications. Heart-healthy

lifestyle treatments include having a heart-healthy diet, routine physical activity, maintaining a healthy weight, limiting sodium and alcohol intake, and quitting smoking [27, 87]. Occasionally a more aggressive approach is needed. Depending on the severity of the artery blockage, surgery may be necessary. Angioplasty and stent placement or percutaneous coronary intervention allow doctors to compress the plaque with a balloon through insertion of a long and thin catheter, followed by the placement of a stent to hold the artery open, restoring blood flow to the heart [27, 87, 88]. Coronary artery bypass surgery allows surgeon to fashion a graft or a bypass made out of artery or veins from the body, redirect blood flow from the blocked artery to the heart [27, 87].

To maintain a healthy body and reduce the incidence of major cardiovascular events, medications are often advised or mandatory and there are several different medication treatments available depending on the situation. Statins which act as a lipid lowering agents that treat for dyslipidemia or hypercholesteremia in atherosclerosis, are the most common [55, 89, 90]. By inhibiting hydroxy-methyl-glutaryl-coenzyme A (HMG-CoA) reductase, statins lower patient levels of all LDL subclasses [55, 61]. In addition to that, the pleiotropic effects of statins include an anti-inflammatory response, improvement of endothelial function, atherosclerotic plaque stabilization [91] and increased nitric oxide bioavailability, which relaxes vascular smooth muscle cells [91, 92]. Although statins lower all LDL subclasses (large, medium or intermediate, small particles), the net effect is potentially only moderate as the ratio of sd-LDL-C to the large, buoyant LDL-C (lb-LDL-C) may remain unchanged [55, 61, 93]. Since it is a drug, the usage of statin may also lead to mild to severe side effects. These effects may include headache and rash (mild) to muscle pain (myopathy) and neurological degradation (moderate) to liver damage (by liver transaminases) and blood sugar and diabetes mellitus progression (severe)

[90, 94-96]. However, the risk of these side effects does not apply to everyone taking statins but only to those that are inducing high statin dosages or statins with alcohol, and females over the age of 65, have a smaller body frame, or those with kidney or liver disease [94].

Although the overall effect of statins may not be as potent, there are other hypolipidemic or antihyperlipidemic agents available that can be taken together to boost lipid-lowering effects. Ezetimibe, a selective cholesterol absorption inhibitor helps lower LDL-C subfraction levels, and to a lesser degree, sd-LDL-C [97], while reducing triglycerides levels roughly 10.7% with a dosage of 10 mg per day [98]. Ezetimibe side effects include reversible impaired hepatic function, myositis and gastrointestinal issues [98, 99]. Fibrate or niacin help reduce sd-LDL-C levels and shift the LDL-C particle distribution towards lb-LDL-C [55] while reducing triglyceride levels by 36% and 25-40% respectively [98]. Fibrate may elevate serum transaminase and creatinine levels, and niacin may cause cutaneous syndrome [98]. Gemfibrozil helps in lowering sd-LDL-C [55] and triglyceride levels, raises HDL-C levels and moderately inhibits or maintains total cholesterol and LDL-C levels [100, 101]. Gemfibrozil overdosage side effects includes abdominal pain, gastrointestinal symptoms, myositis, dyspepsia, nausea and vomiting [102-104]. Fenofibrate helps in improving lipid profile in patients with some pleiotropic effects like reducing levels of fibrinogen, C-reactive protein and pro-inflammatory markers [55, 105]. Its side effects includes gastrointestinal symptoms and increase in transaminase level [105]. In comparison between gemfibrozil and fenofibrate, fenofibrate produces superior reduction in total cholesterol, LDL-C and triglyceride while also offering increase in HDL-C levels in patients [106]. Other medications not within the lipid correction category includes beta blockers, calcium channel blockers, ranolazine, nitroglycerin,

angiotensin-converting enzyme (ACE) inhibitors, angiotensin II receptor blockers (ARBs) and omega-3 fatty acids [27, 98].

All these therapies are effective in the treatment of atherosclerosis, but all too often these medications are only prescribed following severe cardiovascular events. In several cases, treatments may be too late to effectively reduce atherosclerosis or to avoid permanent effects, so it is important to find a way to prevent severe cardiovascular events from happening. In our lab, we aim to determine the mechanisms of atherosclerosis progression prior to formation of advanced lesions and to develop treatments to further prevent severe events.

Oxidized LDL

Ox-LDL has been proven to have atherogenic properties, and among Ox-LDL, minimally modified LDL (mm-LDL) has proven to stimulate endothelial cells, decreasing the arterial wall permeability and recruits the monocyte into the subendothelial space [107, 108]. Studies found that phospholipid with polyunsaturated fatty acids (PUFA) in the *sn*-2 position of the molecule are oxidized to form several of the more biological active components of mm-LDL, including 1-palmitoyl-2-arachidonoyl-*sn*-glycerol-3-phosphatidylcholine (PAPC). PAPC is comprised of a glycerol backbone, phosphatidylcholine head group and two fatty acid residues of different lengths located at the *sn*-1 and *sn*-2 positions. [75, 109]. Oxidation of PL can occur through several mechanisms, but majority of the studies have focus on oxidation due to reactive oxygen species (ROS), generally oxidation of arachidonate or linoleate in the *sn*-2 position [75]. Some of these oxidized products may contain fragments of arachidonate or linoleate while others have the chain completely reacted from the molecule [75].

Atherosclerotic Lesions and Proposed Mechanisms

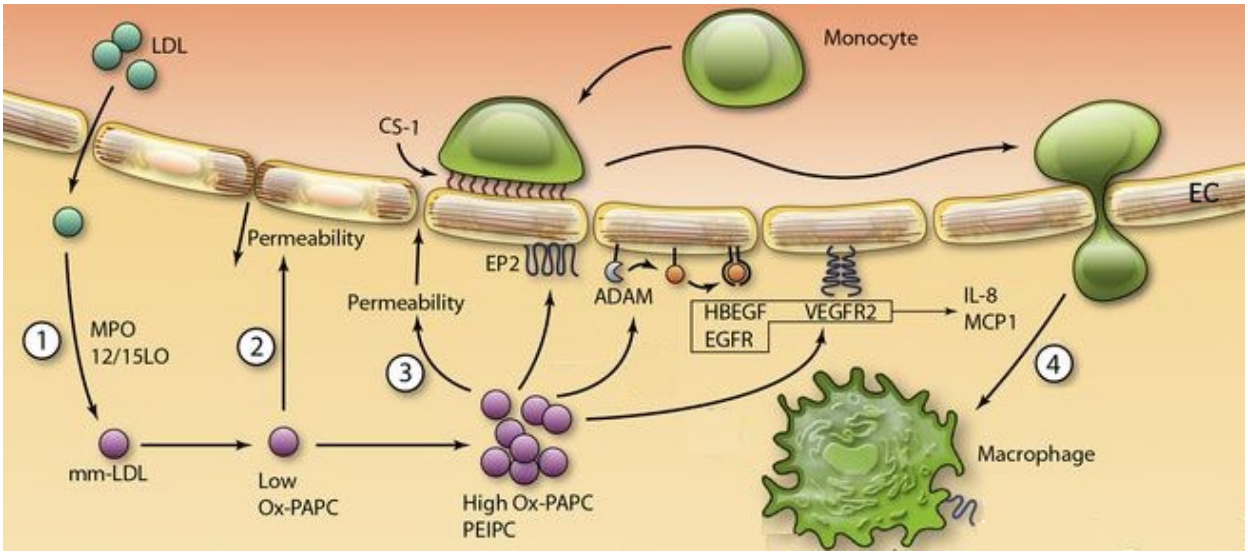

Figure 10: Modified model of early atherosclerosis lesion mechanism.

The model of early atherosclerosis lesion mechanism above (Figure 10) was proposed and modified from Lee et. al., 2012 [75]. 1) LDL enters through the EC into the subendothelial medium and oxidized by myeloperoxidase (MPO) and 12/15-Lipoxygenase (12/15LO) enzyme, along with non-enzymatic oxidation by ROS, forming mm-LDL which is enriched with oxidized phosphatidylcholines [75, 110] including oxidized PAPC (Ox-PAPC). 2) Low concentrations (5-20 µg/mL) of Ox-PAPC enhance barrier protection of EC by forming or tightening adherens junctions, decreasing EC permeability [75, 111]. 3) In contrast, high concentration (25-100 µg/mL) of Ox-PAPC have a reverse effect as at these concentrations, OxPAPC disrupts barrier protection functionality, increasing EC monolayer permeability due to adherens junction breakdown and stress fiber formation [75, 112]. Ox-PAPC binds with prostaglandin E2 receptor (EP2) which promotes expression of connecting segment-1 (CS-1) fibronectin on the apical surface of the endothelial wall [75]. CS-1, which is known to bind monocytes [113], adheres to "rolling" monocytes along the arterial wall, recruiting them to infiltrate the arterial lining instead

of disengaging back into the blood circulation. Ox-PAPC activates various a dysintegrin and metalloproteinases (ADAM) which releases active heparin bind EGF like growth factor (HBEFG), leading to upregulation of epidermal growth factor receptor (EGFR) [75]. Ox-PAPC also stimulates vascular endothelial growth factor receptor 2 (VEGFR2) [75]. These chemokines upregulate the inflammatory pathway (including interleukin-8 (IL-8)) and monocyte recruitment pathway (including monocyte chemotactic protein (MCP-1)), thereby facilitating monocyte entry through the endothelium into the subendothelial space. These monocytes then differentiate into macrophages in order to engulf and clear OxLDL [75, 114, 115]. Figure 11 below depicts the uptake mechanism of OxLDL by macrophages where OxPAPC includes several of the bioactive components in OxLDL. It has also been reported that modified oxidized LDL has lower affinity for LDL-receptor (LDL-R) in the liver, thereby potentially leading to lower clearance than native LDL [54]. Scavenger receptors like scavenger receptor A (SR-A), cluster differentiating 36 lipoprotein (CD36) and lectin-like oxidized LDL receptor-1 (LOX-1) are cell surface receptors expressed in macrophages that recognize OxLDL in order to detect and clear these particles [54]. OxLDL uptake is propagated through the binding of SR-A to lysine of apoB-100 and the binding of CD36 to oxidized phospholipids [54]. Cholesterol may accumulate within the macrophages, as scavenger receptors are not downregulated by intracellular cholesterol transport (maintenance of cholesterol homeostasis) [116] on the macrophage. This accumulation may eventually lead to differentiation of the macrophages to foam cells [54, 75, 117]. These cholesterol-laden foam cells may eventually die in the formation of advanced lesions and are integral in the progression of atherosclerosis [54, 117].

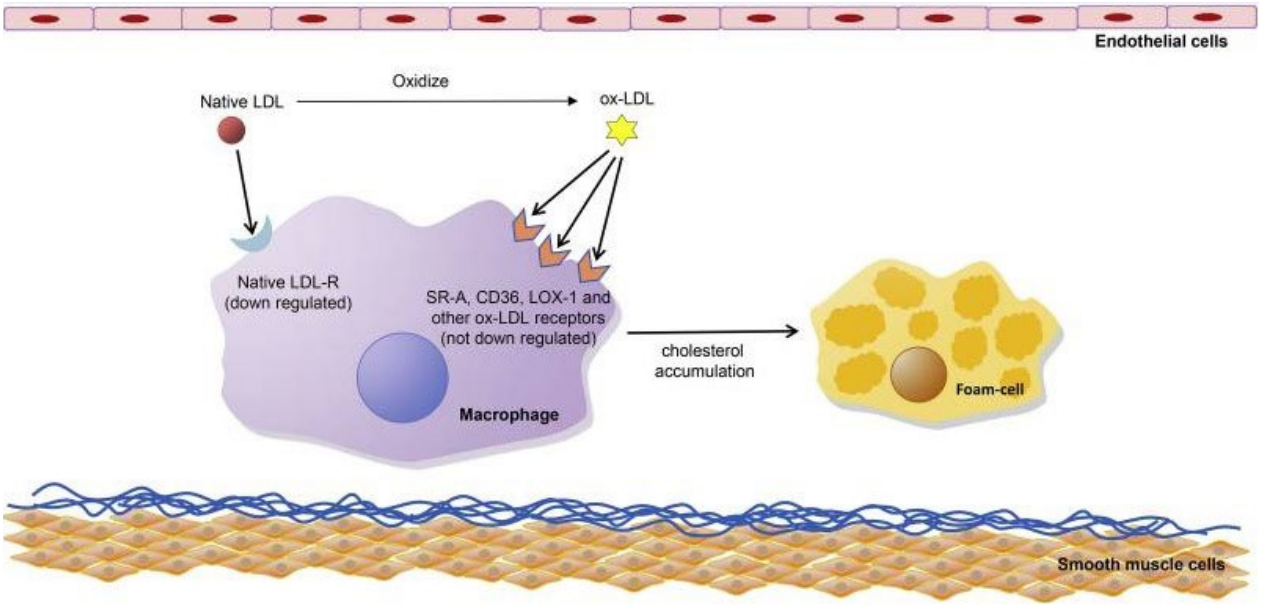

Figure 11: Mechanism of Ox-LDL uptake by macrophages.

Oxidized PAPC Products

Oxidation products of PAPC (mass to charge, m/z 782) (Figure 12) [114], collectively referred to as OxPAPC, have been demonstrated to be the most biological active among all mm-LDL components and have shown to regulate over 1,000 genes in human aortic endothelial cells (HAEC) [118]. As mentioned above, high concentrations of Ox-PAPC induce barrier dysfunction on the EC, increasing the permeability resulting in upregulation of chronic inflammation and monocyte recruitment.

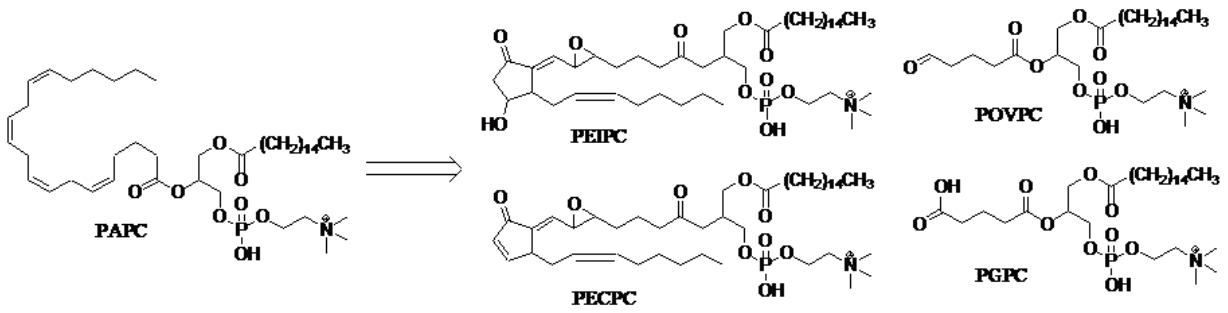

Figure 12: Oxidation products of PAPC

Ox-PAPC contains oxidized fragmentation products of PAPC that are active, among them including 1-palmitoyl-2-(5, 6-epoxyisoprostane E2)-*sn*-glycero-3-phsphocholine (PEIPC) (m/z 828), 1-palmitoyl-2-(epoxyclopentenone)-*sn*-glycero-3-phosphocholine (PECPC) (m/z 810), 1-palmitoyl-2-(5-oxovaleroyl)-*sn*-glycero-phosphatidylcholine (POVPC) (m/z 594) and 1-palmitoyl-2-glutaroyl-*sn*-glycero-phosphatidylcholine (PGPC) (m/z 610). Birukova, et. al., 2013 demonstrated that POVPC and PGPC (20 µg/mL) displayed barrier disruptive effects on EC but was counter balanced by PEIPC, which is generally barrier protective [119]. This is true due to the low concentration (2 µg/mL) PEIPC used for treatment, as they estimated that 1-3 µg/mL of PEIPC was present during Ox-PAPC barrier protective doses [119]. The barrier enhancement effect of PEIPC was reported to decline as higher concentrations were used [119]. Both PEIPC and PECPC were found to be elevated in EC after chemokine stimulation [109, 120]. POVPC increases monocyte binding to EC by activating CS-1 adhesion. PGPC and PEIPC induce both monocyte and neutrophil binding and the increase expression of E-selectin (endothelial-leukocyte adhesion) [121] and vascular cell adhesion molecule 1 (VCAM-1) (cellular junction control and blood vessel formation) [122]. However PEIPC was proven to be more potent [108]. PEIPC is the most active OxPAPC component, as it is active at the lowest concentration relative

to other components. PEIPC is generally considered pro-inflammatory in HAEC, regulating about 80% of Ox-PAPC regulated genes [118, 120, 123].

Phospholipase A2 (PLA_2) catalyzes the hydrolysis of membrane glycerophospholipids at the *sn*-2 position, causing the phospholipids to release the fatty acid in the *sn*-2 position [124]. Arachidonic acid (AA), the *sn*-2 fatty acid in PAPC, subsequently is converted to eicosanoids, including prostaglandins, thromboxane and leukotrienes by the cyclooxygenase (COX) and lipoxygenase (LO) pathways [125], as seen in Figure 16 [126]. Hydrolysis by PLA_2 reduces the inflammatory bioactivities of POVPC, PGPC and PEIPC [30, 127]. Hydrolysis of PEIPC by PLA_2 yields epoxyisoprostane isomers, including 5,6-epoxyisoprostane (EI) (Figure 13) which has been proven to be anti-inflammatory, also inducing angiogenic and endothelial barrier protective properties [123, 128-130]. EI (3μM) inhibits production of IL-1β (inflammatory cytokine) in HAEC, and also inhibits IL-8 at higher concentrations demonstrating EI may be used as an anti-inflammatory agent [131].

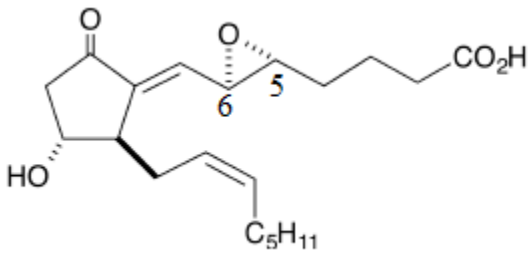

Figure 13: 5,6-Epoxyisoprostane structure

OxPNB, an Analog to OxPAPC

1-palmitoyl-2-arachidonoyl-*sn*-glycero-3-phosphatidyl-(*N*-biotinylethanolamine) (PAPE-*N*-biotin or PNB) (m/z 980 or 964 with negative charge ion) is a biotinylated lipid that we have

synthesized in our lab, with similar structure to PAPC with a biotin-tagged phosphoethanolamine headgroup in the sn-3 position instead of phosphocholine (Figure 14) [132].

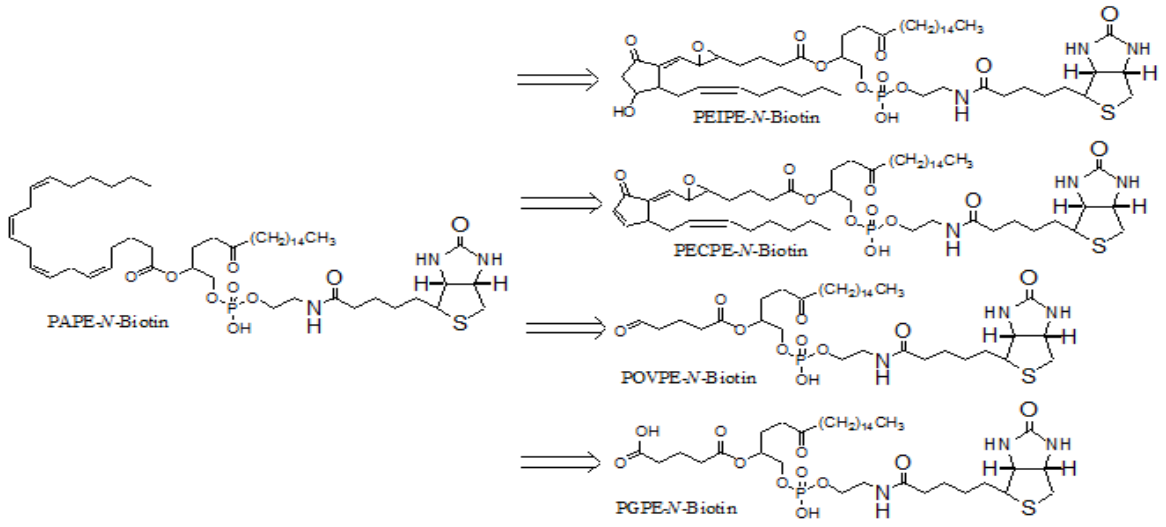

Figure 14: Oxidation products of PAPE-N-Biotin

PNB can be synthesized with 1-palmitoyl-2-arachidonoyl-*sn*-glycero-3-phosphatidylethanolamine (PAPE), *N*-hydroxysuccinimide sulfonate (biotin), dicylohexycarbodiimide (DCC), dimethylaminopyridine (DMAP) and dichloromethane under argon to yield PNB (Figure 15). PNB is then purified with chromatography and oxidized to form oxidized PNB (OxPNB) with exposure to air [132]. A shift of 182 Da was observed due to the biotin tagged onto the lipid. OxPNB has the same structure as OxPAPC, with the noted exception of a biotin-tagged ethanolamine headgroup instead of phosphatidylcholine. Oxidation products include 1-palmitoyl-2-(5,6-epoxyisoprostane E_2)-*sn*-glycero-3-phosphatidyl-(*N*-biotinylethanolamine) (PEIPE-*N*-biotin) (m/z 1010), 1-palmitoyl-2-(5-oxovaleroyl)-*sn*-glycero-phosphatidylethanolamine (PECPE-*N*-biotin) (m/z 992), 1-palmitoyl-2-(5-oxovaleroyl)-*sn*-glycero-3-phosphatidylethanolamine-(*N*-biotinylethanolamine) (POVPE-*N*-biotin) (m/z 776),

and 1-palmitoyl-2-glutaroyl-*sn*-glycero-3-phosphatidylethanolamine-(*N*-biotinylethanolamine) (PGPE-*N*-biotin) (m/z 792), as shown in Figure 15.

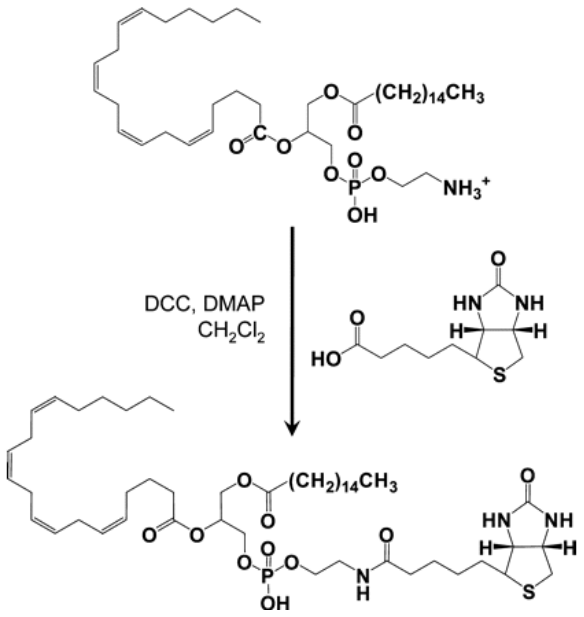

Figure 15: Synthesis of PNB

OxPNB covalently binds to several HAEC proteins and similarly regulates mRNA levels of IL-8, LDL-R, HO-1, and activating transcription factor-3 (ATF-3) to OxPAPC [132]. The interaction of Ox-PAPC and cysteine in HAEC inhibits the binding of OxPNB, showing that the two bind to similar proteins, with similar binding sites [123]. These results demonstrate that OxPNB is an appropriate analog to Ox-PAPC in binding as well as gene expression studies.

Previously, I have confirmed that treatment of HAEC with OxPAPC leads to upregulation of IL-8 (inflammation regulator), hemeoxygenase-1 (HO-1) (cellular oxidative stress) and MCP-1 (monocyte recruitment agent) [114]. I have also demonstrated that small interfering-RNA (si-RNA) knockdown of several proteins in HAEC that may have relevance in inflammatory mechanisms, including glucose regulated 78 protein (GRP78), a chaperon protein inducing

endothelium stress involving the unfolded protein response and prostaglandin E2 Receptor (EP2), a signaling protein for CS-1 for monocyte recruitment, followed by Ox-PAPC treatment and have demonstrated that knockdown of these proteins inhibited regulation of IL-8 and MCP-1 by OxPAPC [114]. These results indicate that these proteins may be involved in regulation of inflammation and monocyte recruitment in HAEC by OxPAPC. In our lab, my colleagues, Abbie Brackman and Gabriel Cole have demonstrated that GRP78 is involved in regulation of the inflammatory pathway in HAEC by PEIPC [133] and EI [1].

Building upon past studies, it would be helpful to screen for new candidate proteins that bind to PEIPC and HAEC using novel methods involving protein digestion, LC/MS/MS, and data base searching to identify PEIPC binding sites in the future. In addition, it would also be helpful to identify the binding site of PEIPE-NB (the biotinylated analog of PEIPC) to human recombinant H-Ras (hr-H-Ras) in HAEC. The binding site of OxPNB was previously identified using transfection and binding studies in HEK 293 [123]. H-Ras will be used as a model protein for method development in determining protein targets of PEIPC as it is a signaling protein in HAEC which was reported to be bound by Ox-PAPC [123]. Initial studies were performed, but preliminary studies did not definitively result in identification of additional proteins or binding sites. However, these studies are included in suggested future studies that build on this dissertation work.

Model Isoprostane, Neuroprostane and Neurofuran that were Studied for Anti-inflammatory Properties in HAEC

Isoprostane

Arachidonic acid is a polyunsaturated fatty acid that is sometimes esterified to phospholipids that are physiologically present in cell membranes [126, 134]. After its release from phospholipid

through hydrolysis by PLA_2, or in esterified form, AA undergoes non-enzymatic peroxidation by reactive oxygen intermediates to produce F_2-isoprostane (Figure 16) [126]. Among this class of fatty acids, we specifically study the effects of 15-F_{2t}-isoprostane (Figure 17). Isoprostanes are stable compounds commonly found in brain cells and could also be quantified in urine, plasma, umbilical cords and other biological fluids to evaluate oxidative stress [134, 135]. Furthermore, they have shown to be prognostic biomarkers via the association of elevated isoprostane levels with lipid peroxidation and vascular disease [136]. It has been shown that F_2-isoprostane levels increase and are correlated with other marks of patient atherosclerotic risk, including smoking, diabetes mellitus, obesity and many more diseases [137, 138].

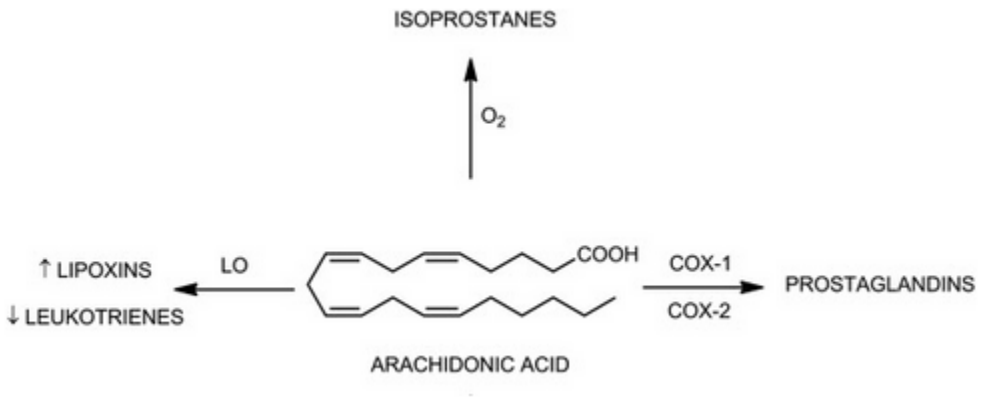

Figure 16: Arachidonic acid metabolism pathways

15-F_{2t}-isoprostane, previously known as 8-iso-$PGF_{2\alpha}$, is a vasoconstrictor in blood vessels [134] and induces monocyte adhesion in HAEC by activating thromboxane receptors (TP, contraction agent of smooth muscle cells). These activities are mediated by protein kinase A (PKA, regulation of lipid metabolism) and Dual specificity mitogen-activated protein kinase 1 (MEK-1, cellular processes like proliferation, differentiation, transcription, regulation and development) pathway, and these activities are independent of inflammatory adhesion molecules like E-selectin

and VCAM-1 [139]. It is reported that 15-F_{2t}-isoprostane concentration was increased in coronary sinus and plasma after a coronary angioplasty but is unlikely to cause vasoconstriction due to its concentration being in the nanomolar range [134, 140, 141]. Then again, large increases in levels of this lipids were found in pathologies of the kidneys [142]. However, many isoprostane isomers exists, with 15-E_{2t}-isoprostane is found to be 10 times more potent as a vasoconstrictor in human internal mammary arteries [143, 144] compared to 15-F_{2t}-isoprostane. 15-E_{2t}-isoprostane was found to constricts chicken ductus arteriosus, pulmonary artery and femoral artery greater than 15-F_{2t}-isoprostane acting through TP receptors more [145].

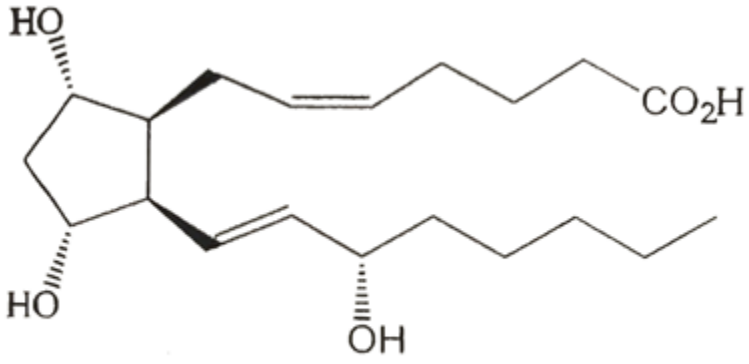

Chemical Formula: $C_{22}H_{34}O_5$
Molecular Weight: 354.5

Figure 17:15-F_{2t}-Isoprostane from AA

Neuroprostane

Isoprostane have been found to upregulate oxidative stress and inflammatory pathways, in contrast to neuroprostanes which are considered be anti-inflammatory mediators [146]. Neuroprostanes are normally derived from non-enzymatic oxygenation of docosahexaenoic acid (DHA) to F_4-neuroprostane and are widely used as specific biomarkers for oxidative stress in neuropathological diseases [147] and to assess renal function [148]. On the other hand, the less

investigated F_3-neuroprostane can be derived similarly from n-6 docosapentanoic acid (DPA). We are studying the specific F_3 neuroprostane, 4-epi-4-F_{3t}-neuroprostane [147, 148]. N-6 DPA (DPA ω6) (omega-6 fatty acid) is found most abundantly in fish oils but is also present at lower levels compared to n-3 DPA (omega-3 fatty acid) [149]. DPA was found to be converted back to AA in rats but only when AA was decreased from high DHA concentration [150].

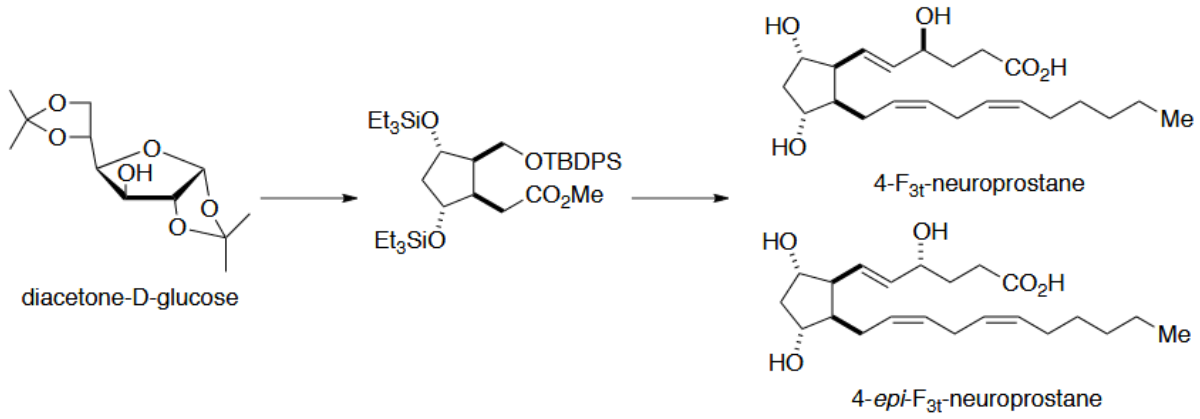

Figure 18: 4-epi-4-F_{3t}-Neuroprostane from diacetone-D-glucose

Alternatively, 4-epi-4-F_{3t}-neuroprostane can also be derived (not in our lab) with diacetone-D-glucose (Figure 18) by accessing its silyl protected cyclopentane [151]. Alkene and the carboxyl group side chain was added through Wittig olefination (Horner-Wadsworth-Emmons modification generated E-alkene) to produce F_{3t}-neuroprostane isomers and were separated with column chromatography to obtain 4-epi-4-F_{3t}-neuroprostane [152, 153].

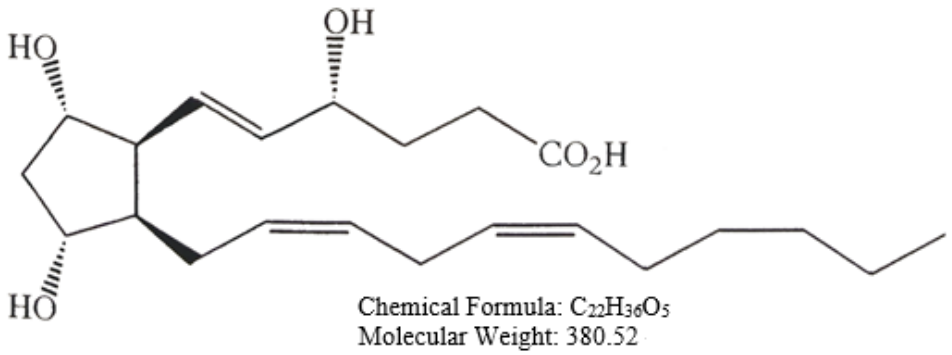

Figure 19: 4-epi-4-F_{3t}-Neuroprostane from DPA ω6

4-epi-4-F_{3t}-neuroprostane (Figure 19) levels were seen to be elevated in renal failure patients and these levels decreased post-kidney transplant after 6 months, as kidney function improved [148]. Up to date, little research has been done on the effects of 4-epi-4-F_{3t}-neuroprostane in endothelial cells and other cell types. Preliminary data from Cole, 2017 suggested that treatment of HAEC with 4-epi-4-F_{3t}-neuroprostane inhibits oxidative stress and inflammatory pathway in HAEC while increasing the monocyte recruitment pathway.

Neurofuran

Similar to isoprostanes and neuroprostanes, neurofurans are chemically stable compounds that can be found abundantly in the places enriched with DHA, like in the grey matter of the brain, in higher concentrations than in the heart, urine or plasma [154, 155]. Neurofurans are considered to be more effective biomarkers oxidative stress than isoprostanes and are used in diagnosis of Alzheimer disease [155]. Neurofurans can be derived from DHA with non-enzymatic free-radical peroxidation [154] such as 2,2'-aZobis (2-amidinopropane) hydrochloride (AAPH) [155]. Interestingly, all omega-polyunsaturated fatty acids and their oxidation products, isoprostanes, isofurans, neuroprostanes and neurofurans can be produced in cooked salmon depending on the cooking method [156].

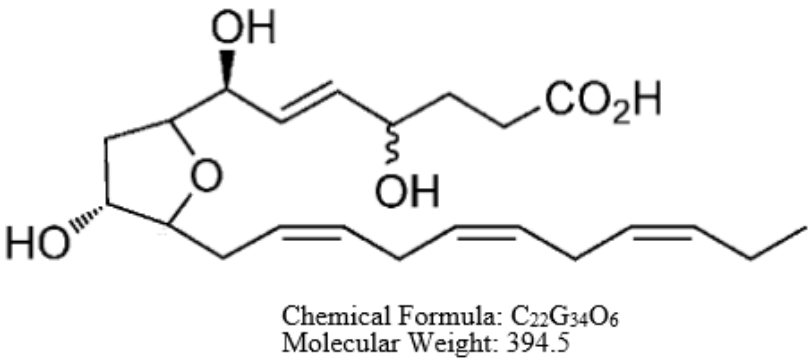

Chemical Formula: $C_{22}G_{34}O_6$
Molecular Weight: 394.5

Figure 20: 4(RS)-ST-Δ5-8-Neurofuran from DHA

4(RS)-ST-Δ^5-8-neurofuran (Figure 20) was found to have higher concentration in both brain and heart tissues which predominates isoprostanes [154]. It was found that there is higher amount of 4(RS)-ST-Δ^5-8-neurofuran in the heart tissue than the brain [154]. Reportedly, higher concentration (1 uM) of 4(RS)-ST-Δ^5-8-neurofuran have been demonstrated to have anti-arrhythmic effects in mice than lower concentration (0.1 uM) [157, 158]. These results suggest that the molecule may potentially be used as a biomarker in the cardiovascular system.

Monocyte binding to 15-F_{2t}-isoprostane [139] in HAEC has been demonstrated, but its gene expression has yet to be tested as well. Previously, aside from oxidative stress and inflammatory pathways, Cole, 2017 has demonstrated that 15-F_{2t}-isoprostane and 4-epi-4-F_{3t}-neuroprostane upregulates the monocyte recruitment pathway (MCP-1) in HAEC but not as much for 15-F_{2t}-isoprostane, although this experiment was conducted using a lower concentration treatment (3 μM instead of 5 μM). Conversely, preliminary results suggested that 4(RS)-ST-Δ^5-8-neurofuran downregulates MCP-1 in HAEC. A re-evaluation of the gene expression of these lipids is needed, as the concentration treatments were not held constant for the two lipids. These fatty acids show enormous potential in regulating monocyte activity and I cotreated HAEC with these

lipids to determine effects of these lipids on monocyte adhesion to HAEC, while using 15-F_{2t}-Isoprostane as a positive control.

Methodology

Materials and Reagents

HAECs were purchased from ATCC, endothelial cell basal medium (ECBM) and growing supplement from Cell Application, and medium 199 (M199) from MediaTech. FBS and solvents (methanol and mass spectrometry grade water) were purchased from Fisher Scientific. Primers for GAPDH, MCP-1, IL-8, HO-1, VEGFR2, GRP78 and EP2 were purchased from Integrated DNA Technologies. PAPC will be obtained from Avanti Polar Lipids. Oxidized fatty acids (isoprostane, neuroprostane and neurofuran) were synthesized by a collaborator and his colleagues at Institut des Biomolecules Max Mousseron (IBMM) (Thierry Durand, Jean-Marie Galano).

Human Aortic Endothelial Cell Culture and Treatment

HAECs were isolated as described previously [107, 159] or purchased from Cell Application. HAECs were grown to complete confluence in ECBM with growth supplements. HAECs were then incubated at 37°C with 5% CO_2 with or without lipid for 2 to 4 hours depending on the lipid used for the experiment in M199 media containing 10% FBS. Cryopreservation of HAECs was done with 62.5% ECBM, 30% FBS and 7.5% DMSO. A step-by-step example for HAEC treatment in 6-well culture plates can be found under HAEC Treatment in Appendices.

Real-Time Polymerase Chain Reaction (RT-PCR)

The model of RT-PCR machine used was the 7900HT Sequence Detector System. Total RNA was isolated from treated cells using the Total RNA extraction kit from Bio-rad. RNA concentrations was measured with NanoDrop 1000 from Thermofisher, and an equal amount of

RNA was withdrawn for cDNA synthesis. cDNA was synthesized using a high-capacity cDNA kit (Applied Biosciences/Life Technologies). SYBR® green master mixture from ThermoFisher was used for PCR quantification and amplification. GAPDH was measured along with the experimental group as a control 'housekeeping' gene that does not change in HAECs with oxidized lipid treatment and is used to normalize mRNA levels and fold changes of other genes between untreated and treated cells [160]. The primer sequences used for RT-PCR were GAPDH: Forward: 5′ -CCT CAA GAT CAT CAG CAA TGC CTC CT-3′, Reverse: 5′ -GGT CAT GAG TCC TTC CAC GAT ACC AA-3′; MCP-1: Forward: 5′ -TGC TCA TAG CAG CCA CCT TCA TTC-3′, Reverse: 5′ -GAC ACT TGC TGC TGG TGA TTC TTC-3′; IL-8: Forward: 5′ -ACC ACA CTG CGC CAA CAC AGA AAT-3′, Reverse: 5′ -TCC AGA CAG AGC TCT CTT CCA TCA GA-3′; HO-1: Forward: 5′ -ATA GAT GTG GTA CAG GGA GGC CAT CA-3′, Reverse: 5′ -GGC AGA GAA TGC TGA GTT CAT GAG GA-3′ [123, 131]. A step by step for RNA Synthesis, cDNA Synthesis and PCR can be found in Appendices.

Synthesis of OxPAPC

PAPC will be diluted with Burdick and Jackson (B&J) chloroform (no other suitable brand of chloroform) and aliquoted into borosilicate glass tube with a chloroform-conditioned pipette tip. Aliquots were dried under argon while creating a thin layer on the wall of the glass tube. Vacuum was used on the glass tube while inverted to rid of additional argon for unhindered oxidation by air. Lipid profile was checked every day on ESI-MS. Once oxidation is done, aliquots were gathered into a single glass tube, transferred into an amber vial, aned concentration was determined with phosphorous assay and kept under argon in -20^{o}C. Step by step Synthesis of Ox-PAPC protocol can be found in Appendices.

Ox-PAPC or Ox-PNB Collection

Add 1mL of B&J chloroform into one aliquot with a "conditioned" pipette tip and vortex it for about 20 seconds. Vortexing produces swirls that allow for the efficient mixing of chloroform and the lipid aliquot without destroying it. Next, with a "conditioned" pipette, pipette chloroform from the current aliquot and add to the next aliquot until 8 aliquots are collected. The last aliquot was used as a stock tube for Ox-PAPC (or Ox-PNB). Add 1mL chloroform into the last aliquot without the stock Ox-PAPC and vortex it for about 10 seconds. Remove the chloroform from the current aliquot and add it to the previous aliquot (reverse direction from the first collection) until all 8 aliquots are collected and add it to the stock Ox-PAPC. Repeat all the steps above for the remaining aliquots and collect all oxidized lipid into the stock Ox-PAPC tube. Sets of 8 tubes are collected for each subsequent collection to maximize the efficiency and yield of lipid recovery. To store the stock Ox-PAPC, argon is added to the top with low argon flow rate. Avoid pointing it directly at the solution to prevent evaporation of the stock and changes in concentration of the stock solution. Shoot the argon at the tube wall and allow the argon to flow down since argon is denser than air. The tube is then capped with a yellow cap and sealed with a parafilm to avoid or reduce argon loss and chloroform evaporation during storage. The Ox-PAPC stock is stored preferably at -40°C or -20°C and must not be stored below the chloroform freezing point (-64.5 °C) as if Ox-PAPC freezes, the lipid components are degraded, and biological activity is modified, generally eliminated or reduced. Ox-PAPC is best stored in -20^{o}C and will remain stable in 4^{o}C for few weeks and at room temperature for less than a week but best practice is to not leave it out more than necessary.

Lipid Concentration Determination with Phosphorous Assay

A phosphorus assay was done to determine lipid concentration. Phosphorus molar concentration is equivalent to phospholipid molar concentration because each phospholipid contains only one phosphorous atom. A calibration standard and two guessed concentrations of the lipid solution will be used. 90 µL of sulfuric acid will be added into all the solution and heated at 220°C for 30 minutes which charring may occur. 30 µL of hydrogen peroxide will then be added to bleach the charred material while heated at 220°C for another 30 minutes. 780 µL water, 100 µL ammonium molybdate and 100 µL ascorbic will be added with vortexing in between each addition. Samples are then submerged into a 50°C water bath to allow for shades of blue color to develop for measurement. Absorbance determining the concentration was performed with 384 SpectraMax Plus Absorbance Reader at 820 nm and 650 nm. A step by step Phosphorous Assay protocol can be found in Appendices.

Statistical Analysis

RT-PCR Ct Value Calculation

Regulations of gene were compared based on fold change performed and analyzed from the RT-PCR. Fold change were calculated by the program based on equations 1-3 below [161] for all replicates.

$$\Delta C_T = Average\ C_{T\ target} - Average\ C_{T\ reference} \quad \textbf{(1)}$$

$$\Delta\Delta C_T = \Delta C_{\mathrm{T\ (test\ sample)}} - \Delta C_{\mathrm{T\ (calibrator\ sample/control)}} \quad \textbf{(2)}$$

$$Fold\ Change = 2^{-\Delta\Delta C_T} \quad \textbf{(3)}$$

$$Average\ Fold\ Change = \frac{\sum Fold\ Change}{Number\ of\ Duplicates} \quad \textbf{(4)}$$

$$Normalized\ Fold\ Change = \frac{Average\ Samples\ Fold\ Change}{Average\ Controls\ Fold\ Change} \quad \textbf{(5)}$$

C_T values are known as cycle threshold which measures the amount of nucleic acid present in the sample. The C_T value was obtained when the RT-PCR detects the first measurable amount signal (threshold) on a specific number of cycles. It has an inverse relationship against the amount of nucleic acid that exists in the sample. Lower C_T values indicate higher the nucleic acid or mRNA levels, but generally, a measurable C_T value would be between 15-30. However, a low C_T value is not necessarily better, e.g. 3-10 C_T, because this may indicate profligacy of resources. On the contrary, a high C_T value between 35 to 40 represents low expression levels and according to Poisson distribution only a single strand of cDNA might be present in the sample. These both will lead to poor precision in C_T values and low fold changes are more problematic to be computed accurately and reliably. To overcome this predicament, run more replicates or run samples in a higher dilution point.

RT-PCR was performed with triplicates for each sample, including the reference housekeeping gene (GAPDH), and the instrument will automatically calculate the average C_T value for all of them. ΔC_T was obtained by subtracting the average C_T values of the sample from the reference in equation 1. The $\Delta\Delta C_T$ was calculated with the ΔC_T value of the sample treated with the fatty acid deducting from the ΔC_T value of the sample treated without the fatty acid (controlled sample) in equation 2. Fold changes were then calculated by taking the value of 2 raised to the power of negative $\Delta\Delta C_T$ value obtained in equation 2 which signifies fold increase or decrease of mRNA level compared to the controls. If duplicates samples were performed, an average fold change for a sample can be obtained with equation 4 and be normalized with the new average control with equation 5.

T-test Paired P-value

To understand the variability of the experiment, a statistical analysis can be conducted commonly known as statistical significance. This answers to the observed differences in an experiment data between two groups usually controls against test samples, whether if they are identical or merely coincidental. This is remedied with a t-test paired p-value analysis as shown in equations 6-12 below [162, 163].

$$Population\ Mean\ Standard\ Deviation\ (sd_p) = \sqrt{\frac{(n_1-1)sd_1^2+(n_2-1)sd_2^2}{n_1+n_2-2}} \quad \textbf{(6)}$$

$$Population\ Mean\ Standard\ Error\ (SE) = sd_p\sqrt{\frac{1}{n_1}+\frac{1}{n_2}} \quad \textbf{(7)}$$

$$T-test\ (t) = \frac{\bar{x}_1-\bar{x}_2}{SE} \quad \textbf{(8)}$$

$$Degree\ of\ Freedom\ (df) = n_1 + n_2 - 2 \quad \textbf{(9)}$$

$$P-value = TDIST(t-test, df, number\ of\ tails) \quad \textbf{(10)}$$

$$Significant = IF(P-value < 0.05, "YES", "NO") \quad \textbf{(11)}$$

Where $n = sample\ size$

$sd = sample's\ standard\ deviation$

$\bar{x} = sample's\ mean\ fold\ change$

$number\ of\ tails = 1\ (one\ side), 2\ (two\ side)\ distribution$

The t-test determines the unlikelihood of two sets of data originating from the same population by looking a t-statistics, t-distribution values and the degree of freedom. This sets up a null hypothesis stating that the two sets of data do indeed originate from the same population and by

the t-test paired p-value analysis, it can be accepted or rejected. The analysis measures the significance level (α) and if p-value obtained was $p < \alpha$, then the null hypothesis is rejected with a slight probability of error, conversely the null hypothesis is accepted if $p > \alpha$. For a result to be significant, the value is set so that $\alpha < 0.05$. This denotes that there would be less than 5% chance that the differences in the two data were not observed. For a result to be highly significant, the value is set so that $\alpha < 0.005$.

For each triplicate sample loaded onto the plate, the RT-PCR analyzed and calculates its fold change with equations 1-5 as well as the $\Delta\Delta C_T$ standard error (SE). Since I have many replicates, it is necessary to first combine the $\Delta\Delta C_T$ SE from controls and test samples separately with equation 12 below.

$$Mean\ Standard\ Error\ = \sqrt{\frac{1}{n-1}\sum SE^2} \tag{12}$$

The calculation for the population mean SE through equations 6-7 has the same values as applying the mean SE calculated with equation 12 into equation 6, substituting the standard deviation value with the mean SE obtained for the calculation. n_1 and n_2 represent the sample size for control replicates and test sample replicates respectively. The t-test was then calculated using equation 8, taking the difference in mean fold change between the control and test sample divided by the population mean SE. The p-value can be calculated in excel with equation 10 with 2 tail distribution to account for both sides of the probability curve.

Results and Discussion

Fatty Acid Binding and Gene Expression to HAECs

Isoprostane, neuroprostane and neurofuran are lipids that have similar structure to PEIPC or EI. These lipids have been tested previously by Gabriel Cole in our lab [1] and they have been

shown to potentially regulate expression of MCP-1 in HAEC. These lipids were re-evaluated again to confirm gene regulation in HAEC. My colleague Cameron Brutsche and I collaborated in these experiments.

HAECs were treated with or without 3 μM of 15-F_{2t}-isoprostane, 4-epi-4-F_{3t}-neuroprostane or 4(RS)-ST-Δ^5-8-neurofuran in 2 mL of M199 media containing 1% FBS for 2 hours in a 6-well cell culture plate. 2 hour treatment was found to have the best signaling among all time points in controlled treatments done by Cole [1]. The treatment was stopped by washing with PBS and lysing with RNA lysis solution. We then proceeded with RNA isolation and cDNA synthesis. Gene expression was then determined with RT-PCR. It was expected that these lipids would have similar gene expression regulation as previously determined. Results from these experiments are summarized below.

Gene regulation of HO-1, IL-8 and MCP-1 with 3 μM 15-F_{2t}-isoprostane lipid treatment in HAEC with OxPAPC are as shown in Figure 21.

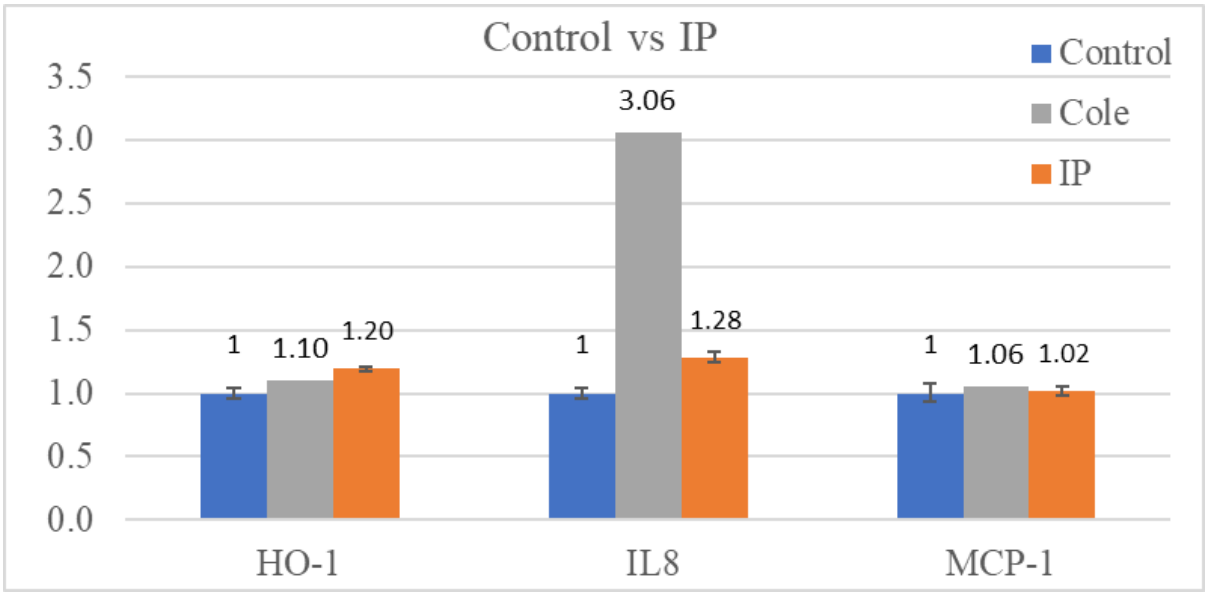

Figure 21: 3 μM 15-F_{2t}-Isoprostane gene regulation in EC

Gene regulation by the isoprostane includes fold changes of 1.2 for HO-1, 1.28 for IL-8 and 1.02 for MCP-1 at the mRNA level in HAEC, where Cole reported her regulation fold change of 1.1 for HO-1, 3.06 for IL-8 and 1.06 for MCP-1. Isoprostane gene regulation that I have obtained shows comparable results to those previously demonstrated by Cole, 2017 with mRNA levels of genes HO-1, IL-8 and MCP-1 were upregulated.

Gene regulation of HO-1, IL-8 and MCP-1 with 3 μM 4-epi-4-F_{3t}-neuroprostane lipid treatment in HAEC with OxPAPC are as shown in Figure 22.

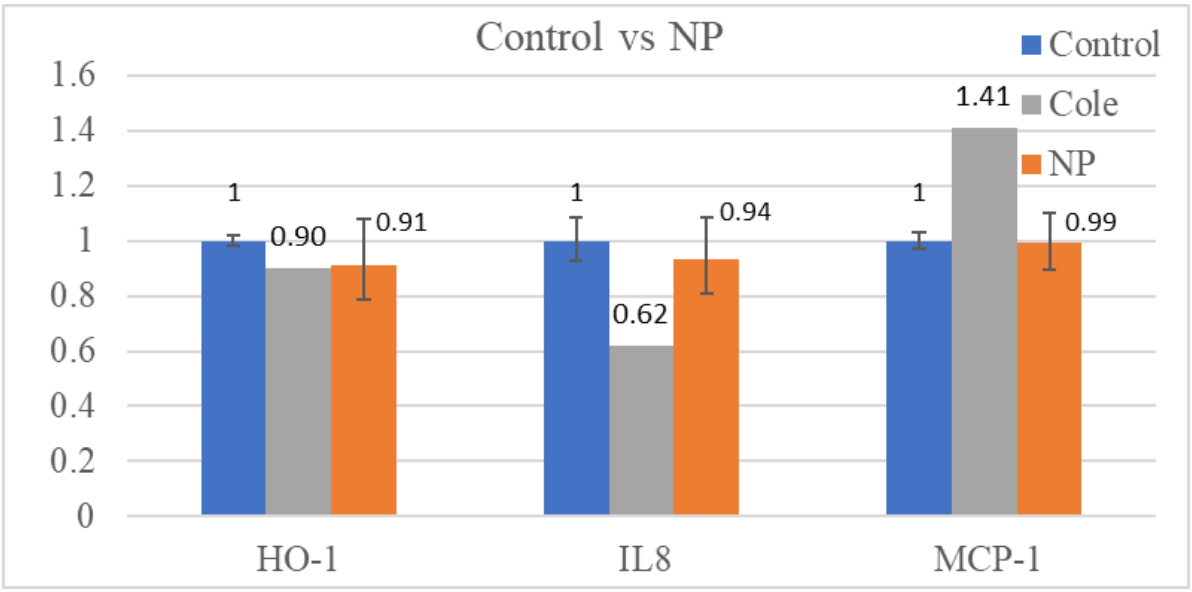

Figure 22: 3 μM 4-epi-4-F_{3t}-Neuroprostane gene regulation in EC

Gene regulation by the neuroprostane shows fold changes of 0.91 for HO-1, 0.94 for IL-8 and 0.99 for MCP-1 in mRNA levels in HAEC, whereas previously Cole reported fold changes of 0.9 for HO-1, 0.62 for IL-8 and 1.41 for MCP-1. Regulation of HO-1 and IL-8 mRNA levels in HAEC show similar trends to Cole, but MCP-1 has slight to no change in our results, and perhaps this regulation needs to be further studied in the future.

Gene regulation of HO-1, IL-8 and MCP-1 with 3 μM 4(RS)-ST-Δ^5-8-neurofuran lipid treatment in HAEC with OxPAPC are as shown in Figure 23.

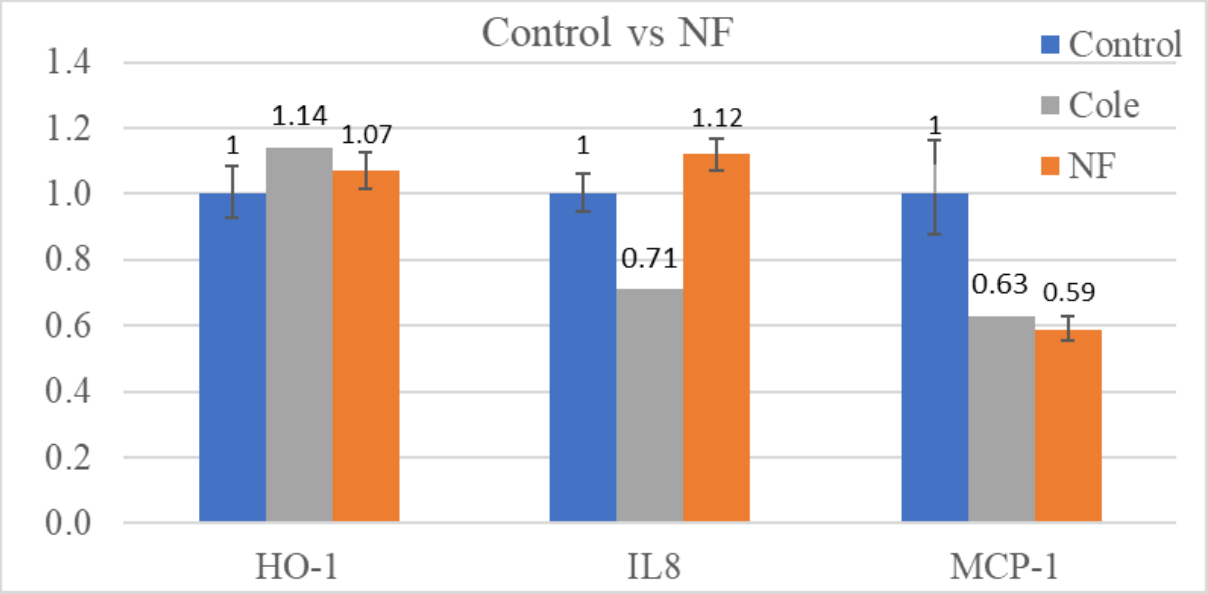

Figure 23: 3 μM 4(RS)-ST-Δ^5-8-Neurofuran gene regulation in EC

Gene regulation of neurofuran shows a fold change of 1.07 for HO-1, 1.12 for IL-8 and 0.59 for MCP-1 in mRNA levels in HAEC, where previously Cole reported fold change of 1.14 for HO-1, 0.71 for IL-8 and 0.63 for MCP-1. Our determined regulation in HAEC by this neurofuran was similar for HO-1 and MCP-1 but our results differed in IL-8 regulation.

MCP-1 was not regulated as much by the isoprostane and the neuroprostane in our experiments, but this result may be due to fact that the concentration used for our treatments was lower than the concentration required for regulation, therefore the experiment was repeated for 5 μM instead of 3 μM (explained below). MCP-1 was reported to be upregulated and downregulated respectively in HAEC by these lipids, signifying that these lipids may play a role in atherosclerotic lesion development by regulating monocyte recruitment. These results may need to be confirmed as they are only preliminary results that need to be replicated, and these

preliminary experiments used a lower concentration than may be necessary for MCP-1 regulation. More replication with higher concentrations may need to be performed before proceeding to monocyte binding.

Based on the low amount of regulation of monocyte recruitment with the isoprostane in HAEC, it appears that the 3 μM concentration used in the experiment was inadequate and this is accurate when comparing to Leitinger, 2001 monocyte binding of 15-F_{2t}-Isoprostane (8-iso-$PGF_{2\alpha}$) to ECs in the Figure 24 below [139].

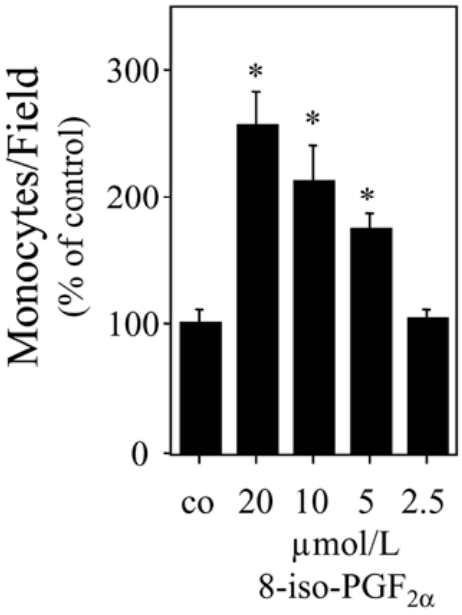

Figure 24: Monocyte binding with 15-F_{2t}-Isoprostane (8-iso-$PGF_{2\alpha}$) to ECs in a concentration-dependent manner

Figure 24 shows that a 2.5 μM concentration of 15-F_{2t}-Isoprostane used demonstrated minimal stimulation of ECs and minimal binding of monocytes to these HAEC. This suggests that the 3 μM concentration used for the experiment might yield similar results to that of the 2.5 μM concentration and the control used in Leitinger, 2001. These experiments were repeated for 5

μM instead of 3 μM in our preliminary experiments. In addition, HAECs were treated with OxPAPC as a positive control for monocyte binding. P-value statistical significance level (α) on the differences between each gene and control will be calculated (refer to values in Table *16* in Appendices).

Gene regulation of HO-1, IL-8 and MCP-1 with 5 μM 15-F_{2t}-isoprostane lipid treatment in HAEC with OxPAPC are as shown in Figure 25.

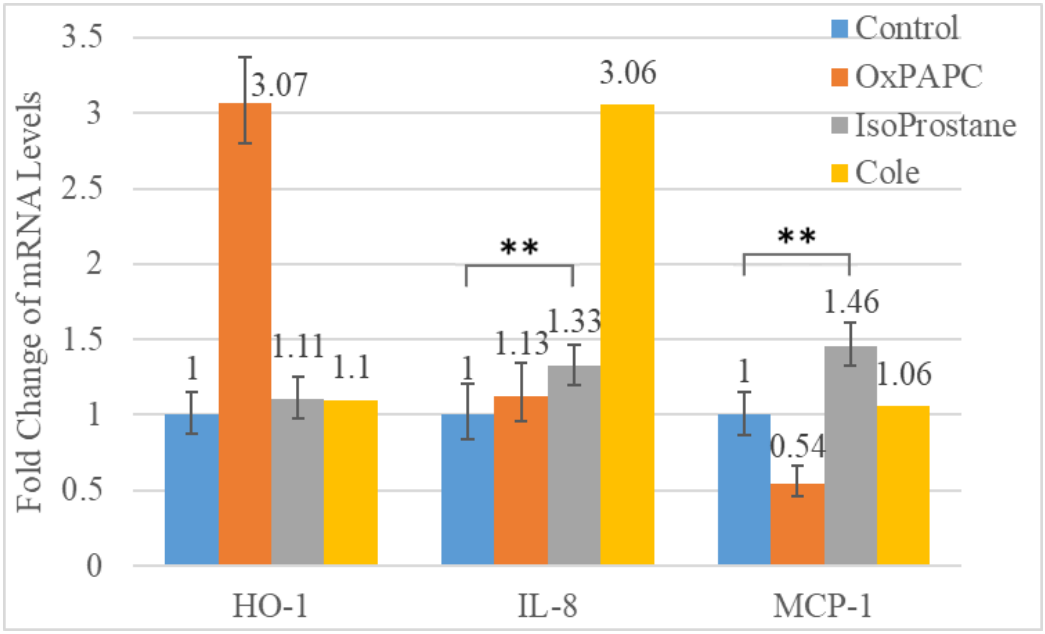

Figure 25: 5 μM 15-F_{2t}-Isoprostane gene regulation in EC

Figure 25 shows that the treatment of HAEC with OxPAPC increases HO-1 and IL-8 mRNA levels with fold changes of 3.07 and 1.13 respectively. However, treatment of HAEC with OxPAPC shows down regulation of MCP-1 with a fold change of 0.54 relative to the control. OxPAPC was shown to increase mRNA levels of MCP-1 with 4 hours treatment [114], but treatment with OxPAPC for 2 hours downregulated MCP-1 in HAEC [111]. With OxPAPC being used as a positive control, it can be concluded that measurement of all gene markers is

working correctly. Treatment of HAEC with the isoprostane increases HO-1, IL-8 and MCP-1 mRNA levels, with fold changes of 1.11, 1.33 and 1.46 respectively. The results show consistent trends and treatment of HAEC with this higher lipid concentration showed more pronounced regulation of MCP-1 in HAEC when compared to the previous 3 µM lipid treatment and Cole's results. This is consistent with prior findings, as higher isoprostane concentration treatment generally increase the amount of monocyte binding to EC [139]. Changes in both IL-8 (*P=0.002)* and MCP-1 (*P<0.001)* mRNA levels were demonstrated to be highly statistically significant.

Gene regulation of HO-1, IL-8 and MCP-1 with 3 µM 4-epi-4-F_{3t}-neuroprostane lipid treatment in HAEC with OxPAPC are as shown in Figure 26.

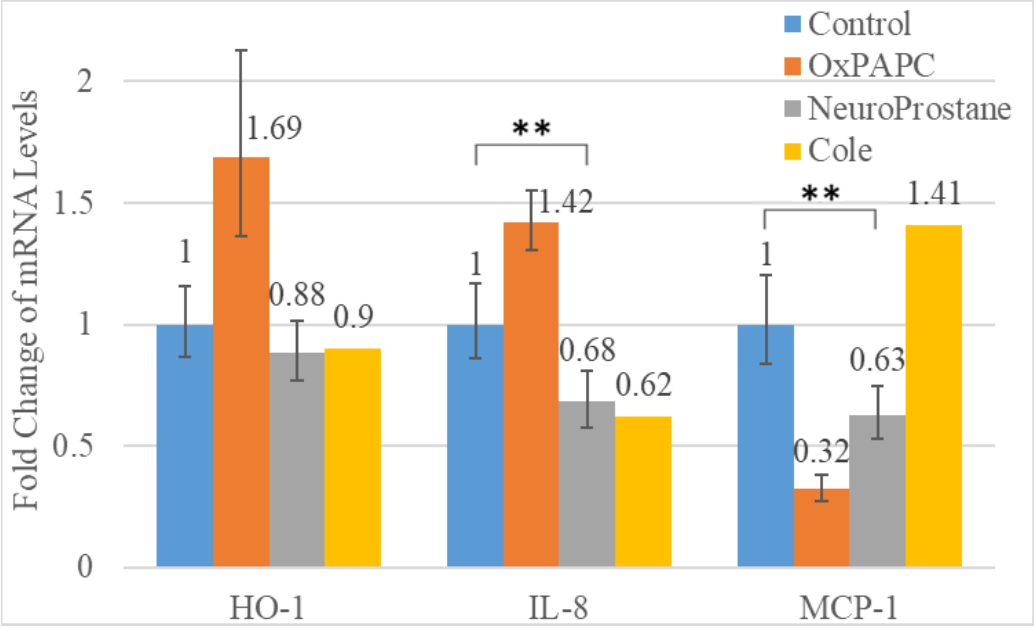

Figure 26: 5 µM 4-epi-4-F_{3t}-Neuroprostane gene regulation in EC

Figure 26 shows that treatment of HAEC with OxPAPC increases mRNA levels of HO-1 and IL-8 with fold changes of 1.69 and 1.42, respectively, and decreases MCP-1 mRNA level with a

fold change of 0.32. OxPAPC regulation is similar to prior results, confirming viability of these results. Treatment of HAEC with the neuroprostane downregulates mRNA levels of all genes with fold change of 0.88 for HO-1, 0.68 for IL-8 and 0.63 for MCP-1 compared to control treatment. These results agree with preliminary results by Cole where HO-1 and IL-8 mRNA levels change with respective fold changes of 0.9 and 0.62 for HO-1 and IL-8 respectively. However, a reverse trend was observed for MCP-1 where Cole shows a regulation with a 1.41-fold change with lipid treatment of HAEC. Our results suggest that with higher amount of neuroprostane present in HAEC, the lower amount of oxidative stress and inflammation are downregulated while also decreasing monocyte recruitment, hypothetically displaying EC barrier enhancement potential. IL-8 (*P=0.004*) and MCP-1 (*P=0.002*) fold changes were both found to be highly statistically significant.

Gene regulation of HO-1, IL-8 and MCP-1 with 5 µM 4(RS)-ST-Δ^5-8-neurofuran lipid treatment in HAEC with OxPAPC are as shown in Figure 27.

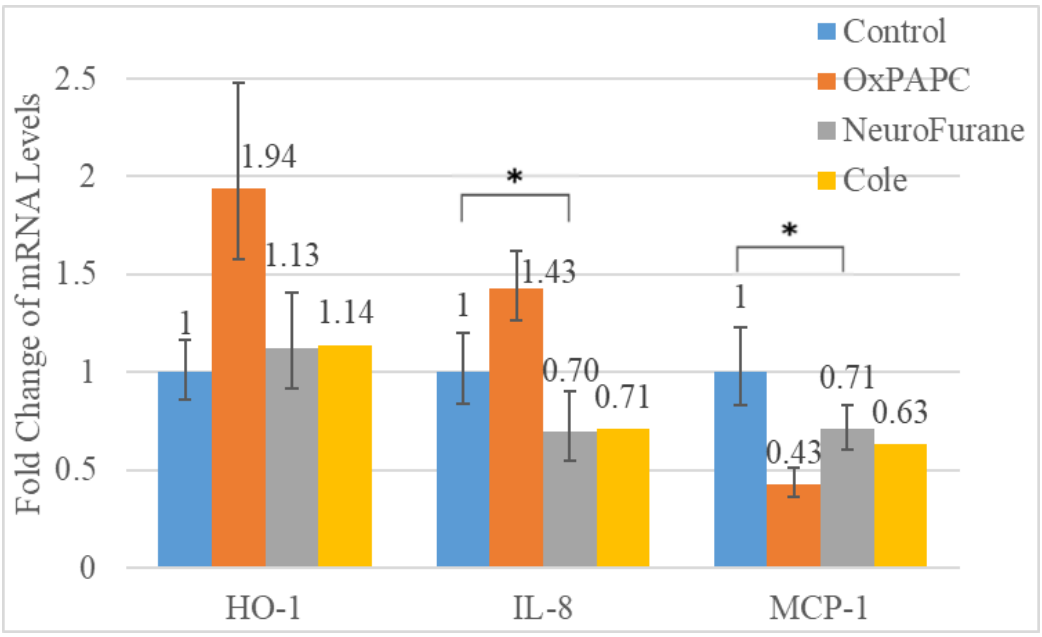

Figure 27: 5 µM 4(RS)-ST-Δ^5-8-neurofuran gene regulation in EC

Results from HAEC treatment with OxPAPC in Figure 19 show consistent trends in regulation of mRNA levels of HO-1, IL-8 and MCP-1, showing fold change of 1.94, 1.46 and 0.43 respectively, thus demonstrating viability of the data. HAEC treatment with the neurofuran results in regulation similar to that of Cole, with HO-1 transcript levels upregulated with a fold change of 1.13 while IL-8 and MCP-1 mRNA levels downregulated with fold changes of 0.70 and 0.71 respectively. This again shows that the neurofuran potentially reduces monocyte recruitment and enhances EC barrier protection. IL-8 (*P=0.035*) and MCP-1 (*P=0.03*) fold change results were both found to be highly statistically significant. The HO-1 fold change results were not found to be statistically significant for all fatty acid (isoprostane (*P*=0.2); neuroprostane (*P*=0.25); neurofurane (*P*=0.26)), but Cole has reportedly concluded all was statistically significant using 3 μM concentration lipid treatments.

Conclusion

In conclusion, results demonstrating 15-F_{2t}-isoprostane regulation of mRNA levels in HAEC were able to be reproduced as previously demonstrated by Cole, 2017. Regulation of the monocyte recruitment pathway (MCP-1) by 15-F_{2t}-isoprostane was substantially lower but this may be due to the fact that a lower concentration (3 μM) of lipid treatment of HAECs was used. Treatment of HAEC with 4-epi-4-F_{3t}-neuroprostane shows similar regulation of oxidative stress and inflammatory pathways at the mRNA levels to the downregulation as demonstrated by Cole, 2017 but MCP-1 levels were not affected in our experiments. Treatment of HAECs with 4(RS)-ST-Δ^5-8-neurofuran did not show similar upregulation of IL-8 (inflammatory pathway) but shows similar upregulation of HO-1 (oxidative stress) and downregulation of MCP-1 (monocyte binding) as demonstrated by Cole, 2017. These results needed to be reproduced as not enough repetitions were done with higher concentration (5 μM) as 3 μM concentration of 15-F_{2t}-

isoprostane may shows similar effects to controls as demonstrated by Leitinger, 2001 (2.5 μM) [139].

With increased lipid concentration treatment in HAECs of 5 μM from 3 μM, gene regulation with 15-F_{2t}-isoprostane were seen to upregulate all mRNA levels of HO-1, IL-8 and MCP-1, consistent with prior findings with Cole's and Leitinger's results. 4-epi-4-F_{3t}-neuroprostane treatment in this concentration in HAECs shows downregulation on all mRNA levels of HO-1, IL-8 and MCP-1. This suggests that a higher amount of neuroprostane present in HAEC reduces oxidative stress, inflammation and monocyte recruitment pathway, exhibiting EC barrier enhancement capability. 4(RS)-ST-Δ^5-8-neurofuran treatment in this concentration in HAECs shows increased regulation in HO-1 but decreased regulation in IL-8 and MCP-1. This result also implies that the neurofuran may play a role in reduction of the monocyte recruitment pathway.

The broader impacts of this research will be to develop a novel approach towards understanding the mechanism of atherosclerosis and to assist medical professionals in developing novel treatments of atherosclerosis or better diagnosis methods to allow for earlier prevention or suppression of atherosclerosis lesions and chronic inflammation.

SUGGESTED FUTURE EXPERIMENTS

Several experiments were planned, but only preliminary data were obtained in several of these experiments, and results need to be further confirmed in order to fully report results. One idea that was explored was to identify specific lipid bound proteins through means of gel electrophoresis, Western Blotting and LC/MS/MS. The lowest effective concentration for specific binding in HAECs treated with or without PEIPE-NB in a dose dependent manner was partially identified. Then using the lowest effective concentration found to treat HAECs with or without PEIPE-NB or PEIPC, protein digest and analyze through the LC/MS/MS. After identifying proteins that bind this lipid, the determined proteins/receptors can be knocked down with siRNA in HAECs prior to treatment with Ox-PAPC or PEIPC determination of the effect of this knockdown on OxPAPC or PEIPC regulation of MCP-1 and other inflammatory genes.

Regulation off Monocyte Binding to Fatty Acids in HAECs

Preliminary monocyte binding experiments were done by treating 1 x 10^5 to 5 x 10^5 cells/mL per well in a 6-well cell culture plate [164]. Treated cells or monocyte were stained in order to ease or facilitate the identification of monocyte adhesion [164] prior to co-incubation with 5 μM BCECF-AM/L (2', 7'-bis-(2-carboxyethyl)-5 (and 6)-carboxy-fluorescent acetoxymethyl ester) EBM for 30 minutes at 37ºC [165].

Assay of the effect of 15-F_{2t}-isoprostane treatment of HAEC on monocyte binding has been done previously [139] as shown in Figure 28 and were used as positive control. The other candidate lipids that would be tested are 4-epi-4-F_{3t}-neuroprostane and 4(RS)-ST-Δ^5-8-neurofuran since MCP-1 levels were downregulated, indicating that these two lipids may reduce monocyte

binding and thereby may have a role in reducing monocyte recruitment, chronic inflammation, and, potentially, atherosclerosis.

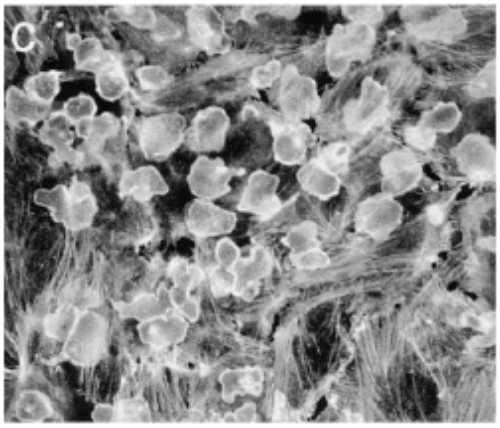

Figure 28:Monocyte attachment under microscope

Figure 28 [164] is an example of what we will most likely observe after co-treatment with one of the lipid to HAEC under an inverted fluorescent microscope. In our preliminary experiments we were only able to test using an inverted non-fluorescent microscope with stained monocytes. More experiments need to be performed to report results.

Affinity Protein Binding of PEIPE-NB in HAECs

PEIPE-NB was demonstrated previously to bind to several HAEC proteins [123]. HAECs were treated with or without 12 μM PEIPE-NB and lysed, followed by gel electrophoresis and Western Blotting to determine lipid binding to proteins as shown below.

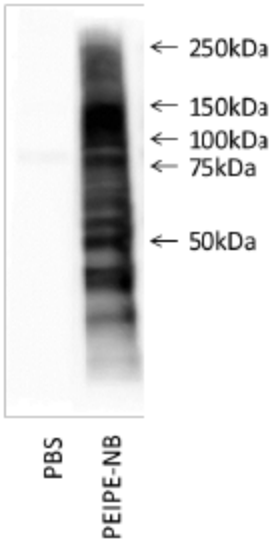

Figure 29:PEIPE-NB binding to HAEC

Figure 29 shows that PEIPE-NB binds strongly to many proteins in HAECs [123]. Previously PEIPE-NB has been demonstrated to be an appropriate biotin-tagged molecular PEIPC analog to be used in binding studies to proteins, and so this biotinylated lipid would be used in future studies. We performed similar preliminary Western blotting experiments, with similar results.

It was hard to tell how many proteins were binding in some of the as thick binding bands that are shown in the Western Blotting results. To remove proteins that may non-specifically bind, an affinity pulldown was attempted with Avidin beads. HAECs were cultured as previously described to full confluency and treated with PEIPE-NB in a dose dependent manner of 12 μM, 10 μM, 7.5 μM and 5 μM at 37ºC for 1 hour. Treated cells were then scraped into a centrifuge tube containing 3mL cold PBS, subsequently washed with 10mL cold PBS and lysed with 1mL of RIPA buffer containing PMSF, phosphate inhibitor and protease inhibitor. Avidin beads were then added, and the samples were incubated while rotating overnight in 4ºC. After incubation, beads were washed with 1 mL cold PBS three times and boiled with 40 μL of Laemmeli sample buffer with 5% β-mercapthoethanol for 10 minutes. Gel Electrophoresis was performed with the

supernatant, taking extra caution to not take up any Avidin Beads. Western Blotting was performed with protein blocking with 5%wt milk in TBST and antibody binding with Streptavidin-HRP. Although these tests were performed, little protein was identified on subsequent Western blots, and it is likely that the bonding of the biotin tagged on the lipid was too strong to allow for elution from the avidin beads or high temperatures led to degradation of the proteins.

Affinity Protein Screening Via MS/MS

Western Blotting results only determine the molecular weight of bound proteins, and not very accurate or definitive results as to protein identity. In order to accurately determine PEIPC-bound proteins, it was also proposed that the protein samples bound specifically to HAEC through PEIPE-NB from the prior experiments would be additionally identified through a MS/MS. The lowest concentration tested for binding through the affinity binding would be used to treat PEIPE-NB or PEIPC in HAEC at 37ºC for 1 hour. Cells will then be scraped and lysed with RIPA containing PMSF, phosphate inhibitor and protease inhibitor. Samples might or might not be acetone-precipitated overnight or ran with gel electrophoresis, but then the samples will be denatured/reduction with Dithiothreitol (DTT), followed by alkylation with Iodoacetamide (IAA) in the dark to cap cysteines, and digest through trypsin at 37ºC overnight. It was proposed that samples will be sent for protein digest analysis using LC/MS/MS. After the data is analyzed, it was proposed to develop new algorithms to search/scan for proteins and lipid binding sites using the LC/MS/MS data and collaboration. Finally, collaborators were then to attempt to characterize lipid protein binding by determining the structure of the lipid protein complex using NMR. It was hypothesized that using NMR we may also be able to characterize non-covalent interactions in addition to covalent interactions of PEIPC and proteins. Techniques

that were developed would potentially also be expanded to using non-biotinylated PEIPC, the endogenous molecule involved in atherosclerosis. This is important as there may be slight binding, transport characteristics, as well as other properties of PEIPC vs. the biotinylated analog PEIPE-NB.

Expression of Lipid-Protein Binding in HAECs

It was also proposed to determine the role of identified lipid-bound proteins in gene regulation, based on mRNA levels of HO-1, IL-8, and MCP-1 in HAECs treated with or without siRNA specific to the lipid bound protein and with or without PEIPC treatment. The levels of mRNA will be measured using the RNA extraction and cDNA methods previously described, in addition to RT-PCR. Gene expression that will be tracked in these experiments will be HO-1 for oxidative stress, IL-8 for inflammatory responses and MCP-1 for monocyte recruitment pathway, as well as GAPDH as a normalization gene.

HAECs would be pretreated with siRNA of the screened protein candidate in lipofectamine 2000 overnight and then washed and treated with or without 50 μg/mL (64 μM) Ox-PAPC or 5 μg/mL (5 μM) PEIPC for 4 hours at 37ºC. RNA and cDNA would be isolated and synthesized and then gene expression would be measured using RT-PCR.

It is expected that the screened protein candidate mRNA levels can be knocked down by 85% or greater, as previously achieved in our lab. With these experiments, we could determine if PEIPC-bound proteins mediate regulation of inflammation by PEIPC in HAECs.

Methodology

Materials and Reagents

HAECs were purchased from ATCC, endothelial cell basal medium (ECBM) and growing supplement from Cell Application, and medium 199 (M199) from MediaTech. FBS and solvents (methanol and mass spectrometry grade water) were purchased from Fisher Scientific. PAPC and PAPE were obtained from Avanti Polar Lipids. Solid phase extraction columns (Strata® C8) were obtained from Phenomenex®. Pierce™ BCA Protein Assay Kit, SDS micropellets, Tris HCl, dithiothreitol, urea, iodoacetamide, ammonium bicarbonate, Promega trypsin gold, Promega sequencing grade modified trypsin, formic acid, microcon-30kDA centrifugal filter unit, GelCode blue safe protein stain and acetonitrile were obtained from Fisher Scientific. 2x Laemmli sample buffer was purchased from Bio-Rad. nUView precast gel tris-glycine 4-20% gels were purchased from NuSep. 2-mercaptoethanol and acetone were purchased from Sigma Aldrich.

THP-1 Monocytic Leukemia Cell Culture

THP-1 monocytic leukemia cell or monocytes were cultured as previously described [132, 166-170]. Monocytes were grown upright in a centrifuge tube with cap not tightened or a T75 Flask with seeding density no less than 300,000 cells/mL (other protocol might state different values) of complete growth media (CGM) consisting of RPMI with 10-20% FBS and 0.05 μM β-mercaptoethanol in 37°C with 5% CO_2. Cell density count was performed every 2-3 days with a hemocytometer to ensure that cell density does not [170] go over 1 x 10^6 cells/mL. Optimal subculturing of monocytes was done at cell density of 800,000 to 900,000 cells/mL. When subculturing is not performed, CGM will be added to lower cell density and left to grow further. Viable cell count will be performed using with a hemocytometer using the dye exclusion method [171]. 50 μL of Trypan Blue Dye will be added along with 50 μL of monocytes and 900 μL of

PBS with Ca^{2+} and Mg^{2+} in a centrifuge tube and let it sit for 3 minutes. Dilution of Trypan Blue Dye with PBS should vary depending on the cell density, it is only required to do this amount if cell density reaches ~1 million, adjust as needed. This allows the dye to traverse into the dead cell's membrane and be stained as live cells with intact cell membrane will not be colored. Cells with blue hues will not be counted and unstained cells will be counted as viable cells. Cryopreservation of monocytes will be done at cell density of 2-5 x 10^6 cells/mL with 75% CGM, 20% FBS and 5% DMSO.

PEIPC Isolation

PEIPC isolation was done as previously described [172]. Ox-PAPC undergoes SPE with C8 columns from Phenomenex, equilibrated at 50:50 methanol-water solution, washed with 70:30, 80:20 and 90:10 methanol-water solution. It is then eluted with an increment of 2% methanol thereafter at 92:8, 94:6, 96:4, 98:2 methanol-water solution. The column was then rinsed with 100% methanol. All fractions were collected and analyzed through ESI-MS, and the fraction with the most and pure PEIPC (usually in the 94:6, 96:4 and 98:2) was collected, stored at -20ºC and used.

Synthesis of PAPE-N-Biotin (PNB) and Oxidized PAPE-N-Biotin (OxPAPE-NB)

PAPE was biotinylated and oxidized as previously described [132]. 50 mg of PAPE in 5 mL of dry dichloromethane solution was added dropwise to a solution of 17 mg biotin, 29 mg of dicyclohexylcarbodiimide and 17 mg of dimethylaminopyridine in 3 ml of dry dichloromethane under argon at room temperature and was mixed with a magnetic stirrer overnight. Solvent was dried under argon, and the residue was purified by solid phase extraction (SPE) to produce PNB. The SPE fractions were dried under argon and tested for PNB with ESI-MS.

Solid Phase Extraction (SPE) of PNB

PAPE-NB and OxPAPE-NB were analyzed by ESI-MS in negative mode on a Thermo Electron LCQ Advantage Mass Spectrometer. Lipids were loaded onto C8 columns from Phenomenex in 50% methanol and 50% H_2O, washed with 70% methanol and 30% H_2O and eluted with 90% methanol and 10% H_2O. Fractions enriched in tagged lipid were then identified using MS as fractions that contain the molecular ion m/z (mass to charge ratio). The mass spectrometer were configured to scan in the range of m/z 500 to 1200 in the negative ion mode and samples peak are averaged over each flow injection.

Purification of PEIPE-N-Biotin (PEIPE-NB)

PEIPE-NB was isolated from Ox-PNB as previously described for PEIPC [172], using an isocratic mobile phase of 77:15:8 acetonitrile:water:methanol through a semipreparative, normal phase LC-MS.

Gel Electrophoresis/Western Blotting

Gel electrophoresis was performed as described previously [114] in a 4-20% gradient gel cassette. Gel electrophoresis runs at 200 volts in a 10% running buffer solution for 40-55 mins or runs near to the bottom or out of the gel. The gel sample was transferred to a membrane in 10% transfer buffer solution with 20% methanol overnight in 4ºC. Protein was blocked from sample with 5%wt milk and bound to specific primary and secondary antibody as necessary. ECL prime solution was used to illuminate the sample bands for imaging. Step by step is provided in Appendices.

Complete Protein Digestion

Protein concentration was determined using Pierce™ BCA Protein Assay Kit. Filter aided sample preparation (FASP) complete protein digestion protocol was provided by Greg Cavey of

WMed and modified to suit experiment. 20 µg of protein samples will be reduced with SDS/Tris HCl/DTT, denatured with urea/Tris HCl and alkalized with IAA/urea/Tris HCl in a 30 kDa Cutoff Microcon Filter. After, protein samples were washed with ammonium bicarbonate (ABC) and digestion with 1:20 (w/w) trypsin:protein sample solution for overnight. Finally, digested samples were acidified with 0.1% formic acid and sent to Greg from WMU Med school for LC/MS/MS analysis. After that, samples may be sent to develop a new algorithm to search for lipid-bound protein in the analyzed LC/MS/MS data, and NMR to determine the lipid-protein bound structure.

Alternatively, in-gel trypsin digestion (protocol provided by Greg Cavey and modified) or single-pot solid-phase-enhanced sample preparation (SP3) [173] can be used and has been modified. For in-gel digestion, protein samples were precipitated with 1:10 (v/v) protein:acetone solution in -20^{o}C. Gel electrophoresis was performed with precipitated samples. Gel was stained with GelCode Blue Safe Protein Stain shaking for 1 hour. Visible bands were carefully cut out. Gel samples were dried with mixture of ABC and acetonitrile, reduced with DTT, alkalized with IAA and digested with 1:1 (w/w) protein:trypsin/ABC/acetonitrile solution overnight. Samples were extracted with 1:2 formic acid:acetonitrile and sent to Greg for LC/MS analysis. For SP3 digestion, SeraMag beads were loaded with protein at 1:10 protein:beads ratio in a PCR tube. Samples are alkalized with IAA, reduced with DTT and digested with 1:25 trypsin/LysC:protein solution. Acetonitrile was to 95% final concentration (v/v), reconstituted with dimethyl sulfoxide (DMSO) and sonicated. Samples were acidified with formic acid and sent to Greg Cavey for LC/MS. Step by step protocol for BCA Assay (Protein Concentration Determination), Complete Protein Digestion, In-Gel Trypsin Digestion for Protein (LC-MS/MS)

and SP3 can be found in Appendices. These protocols were used, and samples were sent out. However, no proteins were identified using gel digestion.

Predicted Conclusions for potential future work

As a predicted conclusion, specific binding of PEIPE-NB to protein in HAECs was demonstrated via gel electrophoresis and Western Blotting. HAECs were treated with or without PEIPE-NB in a dose dependent manner, followed by affinity pull down with avidin beads, gel electrophoresis and Western Blotting. Results similar to prior results, showing lipid-protein bound binding bands. However, preliminary results did not substantially reduce non-specific binding.

Since Western Blotting does not determine the molecular weight of bound protein accurately, it is rather unfeasible to identify the specific lipid-bound protein in HAECs. Therefore, the effective lowest concentration found for the lipid-protein binding should be used in future experiments, treating HAECs with or without PEIPE-NB or PEIPC in HAEC and additionally identified through a MS/MS. Treated cell samples could be protein digested and using MS/MS, bound proteins could be identified through MS/MS database searching. In addition, the analyzed protein data could be used to develop a new algorithm to search/scan for proteins and lipid binding sites with the LC/MS/MS data. Additionally, NMR could be used to identify the lipid-protein complex structure using.

Upon successful completion of these experiments, gene expressions of the protein candidates can be measured through RT-PCR to demonstrate its capability in the regulation of atherosclerotic inflammation.

Appendix A

HAEC Treatment

Lipid Cell Treatment

Concentrations: Control **(no lipid)**

50 ug/uL (OxPAPC)

Lipid Preparation (2ml each well)

1) Pipette **300ug/uL OxPAPC** from the stock solution into a **1mL** borosilicate tube
2) Dry down the lipid with either Nitrogen or Argon
3) Put some Argon into the OxPAPC stock solution, cap, parafilm and store **(-20C)**
4) Make a **10mL** stock solution comprise of M199 media **(10mL)** w/ 10% FBS **(1mL)**
5) Aspirate the media from the 6 well plates
6) Wash cell plates with **2mL** PBS (w/ Ca2+ and Mg2+)
7) Resuspense each well with **1.5mL** of media stock solution
8) Resuspense lipid tube with **1mL** of media stock solution
9) Vortex the tube for **5** seconds
10) Add another **0.5mL** of media stock solution into the lipid tube
11) Do not Vortex, mix it by pipetting up and down
12) Pipette **0.5mL** of lipid from the lipid tube into each well
13) Label each well on the cap
14) Incubate at **37C** for **4** hrs

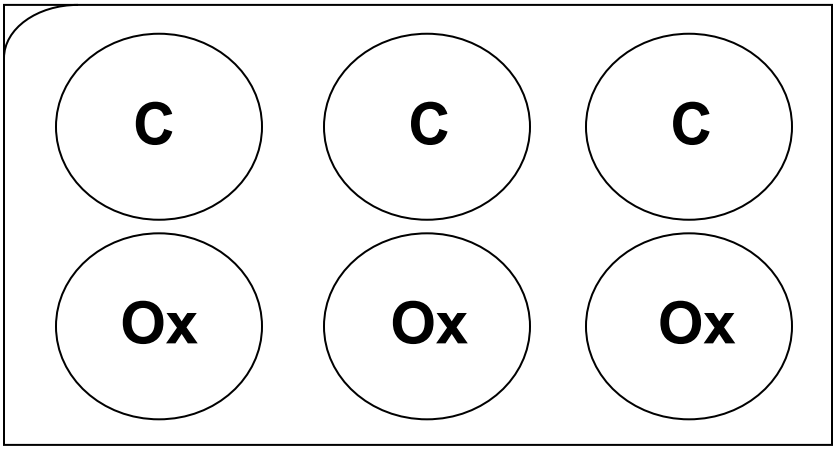

Freezing the treated cell for next day if needed (Better to do RNA/cDNA immediately then freeze it)

15) Aspirate Media

16) Wash each well with **2mL** PBS (w/ Ca2+ and Mg2+), 3 times
17) Pipette **350uL** Total RNase Lysis Solution into each well
18) Parafilm the plate (prevent Oxidation)
19) Freeze cell in **-80C** freezer

Appendix B

RNA Synthesis

1) Unthaw frozen cells in room temperature **(Do not freeze again)**
2) Add **350uL** of Total RNase Lysis solution into each well if you haven't already
3) Add **350uL** of 70% Ethanol (Nuclease-free) into each well
4) Insert **6** labeled RNase-DNase free column in **6** labeled RNase-DNase free capless wash tubes (Should be 2 mL centrifuge tubes)
    a. labeling them with numbers helps e.g. **1**,**2**,**3**-C **4**,**5**,**6**-Ox
    b. It helps to draw circles in your notebook and label them like a plate
5) Pipette all solution in each well several time (to ensure it is solubilized)
6) Pipette all solution from the 6 well plates into corresponding columns
7) Centrifuge the tube for **1** minute at **max speed**
8) Check to make sure most of the column is empty and discard the filtrate
9) Add **700uL** Low Stringency RNa Wash Solution into each column
10) Centrifuge for **1** minute at **max speed**
11) Discard the Filtrate
12) Add **700uL** Low Stringency RNa Wash Solution into each column
13) Centrifuge for **1** minute at **max speed**
    a. **Yes twice**
14) Discard the Filtrate
15) Centrifuge the tube again for **5** minutes to remove residue wash solution
    a. Elution Efficiency depends on amount of ethanol remains
    b. **The less** ethanol **the better** efficiency
16) Transfer column to a new **1.5mL** RNase-DNase free capped microcentrifuge tube
17) Add **40uL** elution solution (Nuclease-free H_20) into the column
18) Allow to **sit for >1 min**
19) Centrifuge for **>2minute** at **max speed** to elute total RNa

Absorbance Test (96 well plate)

Well volume used: 60uL

Dilution Factor: 1:10 (6uL RNa: 54uL nuclease-free H_20)

1) Turn on the switch of the absorbance reader located behind the machine
2) In Settings, set the absorbance wavelength to **260**nm and **280**nm
   (Do not turn PathCheck on)
   (If needed change the reading strip to the one you are using so the reader does not read the whole plate which saves time)

3) Double click the plate grid, customize each grid to your needs (Unknown for Background and sample, Standards for standards)
4) Pipette **6uL** RNA sample into the bottom of each well correspondingly
5) Pipette **54uL** nuclease-free H_20 into the each well (**When pipetting, stick the tip to the wall**)

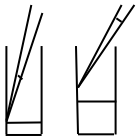

6) Click Read and wait
7) Record the results and calculate the concentration with an online calculator

Absorbance Test Sample

	A260/A280	Corrected A260/A280	Purity	Concentration (ng/uL)
BG	0.135/0.10	-	-	-
1	0.43/0.23	0.295/0.13	2.27	118
2	0.34/0.19	0.205/0.09	2.28	81.9

http://www.kenkyuu.net/js/nacalc.html or just simply

A260 x Dilution Factor x 40 / 1000 = #ng/uL

If using NanoDrop 1000, simply put 2 uL of sample into pedestal. Cleaning after each sample.

Appendix C

cDNA Synthesis

1) Calculate the amount needed for each sample to obtain the same concentration for cDNa

   From Sample, lowest concentration is 819ng

   1 819ng x 1uL / 118ng = **6.94uL sample + 3.06uL H_20**
   2 819ng x 1uL / 819ng = **10uL sample + 0uL H_20**

2) Pipette the amount needed into a PCR tubes, cap for later
3) Thaw Master mix Solution in Ice
4) Make 10x RT Master Mix
   a. Need 10uL in each tube (Total: 60uL)
   b. Make 80uL, to compensate for losses

10x RT Buffer	2.0uL	→	16.0uL
25x DNTP Mix	0.8uL	→	6.4uL
10x RT Random Primer	2.0uL	→	16.0uL
MultiScribe RTranscriptase	1.0uL	→	8.0uL
Nuclease-free H20	4.2uL	→	33.6uL
Total per Reaction	**10uL**	→	**80uL**

5) Transfer 10uL of Master Mix into each tube, cap the tube
6) Set Thermal Cycler

Step	**1**	**2**	**3**	**4**
Temperature	**25C**	**37C**	**85C**	**4C**
Time (min)	**10**	**120**	**5**	∞

7) Store at **-20C** if needed

Appendix D

PCR

Making the primer

1) Dilute into **100uM** primer from primer stock

   Given #nM prim add 10x TE buffer

   E.g. GAPDH_set1_F **86.9nM**

   Add 86.9 x 10 = **869uL** TE buffer

2) Dilute into **5uM** primer from **100uM** primer stock (**1:20** dilution)
   a. Add **50uL** of 100uM primer of forward and reverse into new tube
   b. Add **900uL** TE buffer

Loading 384 well PCR plate

1) Unthaw cDNA PCR tube
2) Add **200uL** of nuclease-free H_20, cap
3) Add **30uL** of each cDNA into standard 1 tube
4) Add **30uL** of standard 1 into standard 2 tube, add **120uL** H_20
   (PCR tube is a set of 8, you used 6, last 2 slot is used as standards so reduce waste)

5) Make SyBr Green Master Mix stock solution for 105 wells (96 wells needed each gene)

	For each Gene		For each Well
SyBr Green	630uL (6uL x 105)	Master Mix	10uL
Primer (F+R)	105uL (1uL x 105)	cDNa	2uL
H_20	315uL (3uL x 105)		
Total	**1050uL**		**12uL**

6) Add **10uL** MM stock solution into each well depending on its gene (24 wells/gene)
   a. Pipette it into the **left side** wall of the well 
   b. Switch tips only in between changing gene
7) Add **2uL** cDNA from the PCR tube into each corresponding well
   a. Pipette it into the **right-side** wall of the well 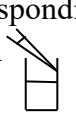
   b. Do all for each cDNa first, this saves tips
8) Apply PCR Adhesive cover on top
   a. Using a Squeegee to seal it better, making sure that it seals all the way
   b. Seal it by using a one direction motion, from IN to OUT
9) Briefly **Centrifuge** the PCR plate 500 RPM for 5 min and check for any bubbles
10) Run PCR

Running the PCR (7900 HT Sequence Detector System)

1) Turn on the PC
2) Turn on the PCR
    a. Turning this on for at least 10 min before running an experiment increases efficiency of PCR
3) Open SDS 2.4 software
4) Click new to open up a wizard
5) Choose **ΔΔRT** (relative quantification), 384 well plates
6) Click on browse to choose template
7) Click OK
8) On the right side of the software, click the real time instrument tab
9) Click Connect to Instrument
10) Click Open/Close
11) Put the PCR plate located on the right side of the PCR machine
    a. It opens slowly and a sliding tray will appear (Do not be afraid)
    b. Make sure A1 well is position at the top left corner
    c. If worry, notice the cut of corner and place it likewise
    d. Do not close the tray
12) Click Run, while the tray is still out
13) Wait, Run Time Approx. 2.5hr to 3.5hr
14) After run is complete, click the Analysis tab from the tool bar and click Analyze
15) Save with desired File Name

16) Look at the base line in triplicates and omit well that does not match or is an outlier
    a. Results would be in the amplification plot located on the right panel
    b. If amplification plot is empty, click and choose desired detector
    c. If after switching wells and its empty, choose All Detectors
    d. If it happens again, Choose the desired detector again and repeat
17) After every well you omit, reanalyze the data, save

18) Open SDS Manager
    a. If password is prompted, just hit ok
19) Choose new study and open the SDS file you just saved
20) Click OK
21) Now you can see a lot of stuff

Figure 30: PCR template example

Treatment Date:
RT-PCR Date:
Lowest RNA concentration:
Data File:

	1	2	3	4	5	6	7	8	9	10	11	12	13	14	15	16	17	18	19	20	21	22	23	24
A	1	1	1	2	2	2	3	3	3	4	4	4	5	5	5	6	6	6	st1	st1	st1	st2	st2	st2
B	7	7	7	8	8	8	9	9	9	10	10	10	11	11	11	12	12	12	st3	st3	st3	st4	st4	st4
C	13	13	13	14	14	14	15	15	15	16	16	16	17	17	17	18	18	18	st5	st5	st5	st6	st6	st6
D	19	19	19	20	20	20	21	21	21	22	22	22	23	23	23	24	24	24	st7	st7	st7	st8	st8	st8
E	1	1	1	2	2	2	3	3	3	4	4	4	5	5	5	6	6	6	st1	st1	st1	st2	st2	st2
F	7	7	7	8	8	8	9	9	9	10	10	10	11	11	11	12	12	12	st3	st3	st3	st4	st4	st4
G	13	13	13	14	14	14	15	15	15	16	16	16	17	17	17	18	18	18	st5	st5	st5	st6	st6	st6
H	19	19	19	20	20	20	21	21	21	22	22	22	23	23	23	24	24	24	st7	st7	st7	st8	st8	st8
I	1	1	1	2	2	2	3	3	3	4	4	4	5	5	5	6	6	6	st1	st1	st1	st2	st2	st2
J	7	7	7	8	8	8	9	9	9	10	10	10	11	11	11	12	12	12	st3	st3	st3	st4	st4	st4
K	13	13	13	14	14	14	15	15	15	16	16	16	17	17	17	18	18	18	st5	st5	st5	st6	st6	st6
L	19	19	19	20	20	20	21	21	21	22	22	22	23	23	23	24	24	24	st7	st7	st7	st8	st8	st8
M	1	1	1	2	2	2	3	3	3	4	4	4	5	5	5	6	6	6	st1	st1	st1	st2	st2	st2
N	7	7	7	8	8	8	9	9	9	10	10	10	11	11	11	12	12	12	st3	st3	st3	st4	st4	st4
O	13	13	13	14	14	14	15	15	15	16	16	16	17	17	17	18	18	18	st5	st5	st5	st6	st6	st6
P	19	19	19	20	20	20	21	21	21	22	22	22	23	23	23	24	24	24	st7	st7	st7	st8	st8	st8

A	Genes	For:	
B	GAPDH	Reference	
C	IL-8	Target	
D	HO-1	Target	
E	MCP-1	Target	

G	For each Genes	24 x 4	well	
H	No. of wells		1	105
I	Constant		uL	uL
J	Master Mix		10	1050
K				
L	cDNA		2	210
M	Primers (F+R), 5 uM		1	105
N	Mol grade H2O		3	315
O	SYBR Green		6	630
P				
	Total Volume:		12	1260

Standard 1:10 Dilution		Vol
Std 1	10 ul of each cDNA sample	180
Std 2	120 ul Mol grade H2O + 30 ul of # 1	150
		150
		150

Samples: 16 x 16 = 256

1	c	7	c	13	c	19	c
2	c	8	c	14	c	20	c
3	o	9	o	15	o	21	o
4	o	10	o	16	o	22	o
5	F2	11	F2	17	F8	23	F8
6	F2	12	F2	18	F8	24	F8
	st1		st3		st5		st7
	st2		st4		st6		st8

Appendix E

Synthesis of Ox-PAPC

Lipid oxidation protocol

Burdick and Jackson (B&J) chloroform is used to dilute stock of PAPC by 2 into 12.5 mg/ml. This specific B&J chloroform is used because chloroform from other suppliers may contain additives or contamination that inhibits PAPC oxidation such as ethanol. Eight aliquots of diluted lipid solution are made by pipetting the lipid stock into borosilicate glass tubes. Two precautionary steps are taken. First, the lipid stock is pipette up and down 3 to 4 times before aliquoting to "condition" the pipette tip; otherwise, chloroform will leak out. Lipid aliquots are then dried with argon by circular swirling pattern using a pipette tip to create as thin a lipid layer as possible on wall of borosilicate tube to increase the oxidation rate. This is important as it is essential to have rapid oxidation since slow oxidation generally results in over-oxidation of desired components such as PEIPC, POVPC and PGPC into less bioactive components such as lysoPC. The second precautionary measure is the drying of aliquots is done in sets of 8 to prevent premature drying of lipid, which results in inefficient oxidation. Since argon is denser than air and will prevent oxidation, it is removed from all tubes via Pasteur pipette connected to a vacuum line prior to oxidation. The Pasteur pipette is lowered near the bottom of each tube to ensure all argon is removed during vacuuming. The aliquots are allowed to sit in the fume hood for approximately 48 hours for oxidation, and the progression of lipid oxidation is monitored with MS flow injection.

MS flow injection

Detection of the oxidized lipid is performed on a Thermo Electron LCQ Advantage Mass Spectrometer. The system is equipped with electrospray and atmospheric chemical ionization interface, which allow for the analysis of a wide range of analytes. Its MS/MS functionality enables extensive structural analysis. The LCQ Advantage Mass Spectrometer is equipped to enable several methods, including chromatographic separation, compound detection, mass analysis, two-stage mass analysis, wideband activation and ZoomScan analysis. Electrospray ionization (ESI) is useful for analyzing polar compounds such as amines, peptides and proteins; Atmospheric pressure chemical ionization (APCI), which is also available, is generally used for non-polar compounds such as steroids, although it is not used in these studies.

Checking lipid oxidation with ESI-MS

The MS must be warmed up for about 2 hours before sample analysis. Nitrogen and helium must be turned on and the MS power is turned on to start warm up. The MS is generally fitted with 20µL injection loop for flow injection. During loading, with the injection loop status on load, flush the injection loop on the MS injection port with 500µL methanol with a 500µL Hamilton syringe. Then flush 25µL Hamilton syringe with 25µL methanol for 5 times to ensure that it is clean from contamination. Removing one aliquot of lipid (0.2-0.5 mg) from oxidation, add 200 µL B&J chloroform and vortex for about 5seconds. Aliquot 25µL into a microcentrifuge tube and dry it with argon. Add 200µL methanol and vortex again for about 5 seconds. Using the 25µL Hamilton

syringe, take up 25µL of the lipid solution and inject it into the MS injection port. In the MS software, open the LCQ tune program and select the most recent tune file for Ox-PAPC (or PNB for negative mode analysis) and click the start button to start data acquisition. If desired, filename/folder can be changed to the preferred filename and location. There is generally the presence of background/noise intensity is usually on the order of 10^2 to 10^5 absorbance unit. Wait around 10 seconds to obtain a good background signal and then change the injection port status to 'inject', to release the oxidized lipid into the MS for data acquisition. To view the MS spectrum for each sample, click the 'View' button and average over the total ion current for the sample peak. (A flat baseline signal followed by an Ox-PAPC peak and then return to the baseline should be seen throughout the period of Ox-PAPC detection.)

Appendix F

Phosphorous Assay

Phosphorous Assay

Why? 1 phospholipid = 1 phosphorous atom

Notes:

- Use Nano-Pure water (high resistance, pulling out extra ions) when making solution
- Set water bath to 50°C
- Set aluminum block heater to 220°C

Sample calculation needed:

$$0.02\ \mu\text{moles} * \frac{1\ \mu\text{L}}{\text{guessed concentration}\ \mu\text{g}} * 782\frac{\mu\text{g}}{\mu\text{mole}}\ for\ papc\ 964\frac{\mu\text{g}}{\mu\text{mole}} for\ PNB = X\ \mu\text{L}$$

$$Sample\ 1\text{: } 0.02\ \mu\text{moles} * \frac{1\ \mu\text{L}}{1.5\ \mu\text{g}} * 782\frac{\mu\text{g}}{\mu\text{mole}}\ for\ papc\ 964\frac{\mu\text{g}}{\mu\text{mole}} for\ PNB = 10.4\ \mu\text{L}$$

$$Sample\ 2\text{: } 0.02\ \mu\text{moles} * \frac{1\ \mu\text{L}}{0.75\ \mu\text{g}} * 782\frac{\mu\text{g}}{\mu\text{mole}}\ for\ papc\ 964\frac{\mu\text{g}}{\mu\text{mole}} for\ PNB = 20.8\ \mu\text{L}$$

Prepare solutions

- Ammonium Molybdate
    1. Weight 0.1g into amber vial
    2. Add 3 mL water
    3. Insert microbar stirrer and stir
- Ascorbic Acid
    1. Weight 0.4g into amber vial
    2. Add 4 mL water
    3. Insert microbar stirrer and stir
- H_2SO_4
    1. Make sure to wear gloves
    2. Pour small amount of concentrated H_2SO_4 into a beaker
    3. Pipette 1.125 mL water into a glass vial
    4. Pipette 375 µL of H_2SO_4 *slowly*

Procedure:

1) Label tubes 1 to 6 (standards) and S1, S2 (samples)
2) Add standard amounts of phosphorous standards as described by manufacturer
    - Tube 1: 0 µL
    - Tube 2: 10 µL
    - Tube 3: 20 µL
    - Tube 4: 35 µL
    - Tube 5: 50 µL
    - Tube 6: 70 µL
3) Add 10.4 µL into Tube S1
4) Add 20.8 µL into Tube S2
5) Dry lipid samples with argon
6) Add 90 µL H_2SO_4 into all tubes
7) Transfer all tubes to the preheated aluminum block at 220ºC for 30 min
    - Charring will occur
8) Add 30 µL H_2O_2 into all tubes
    - Charring will be bleached
9) Transfer all tubes to the preheated aluminum block at 220ºC for 30 min
10) Add 780 µL water into all tubes and vortex
11) Add 100 µL ammonium molybdate into all tubes and vortex
12) Add 100 µL ascorbic acid into all tubes and vortex
13) Submerge all tubes into 50ºC bath for approximately 10 min
    - Not that water flows into tube, just enough to reach level of solution
    - Solution will show shades of blue, gets darker with more phosphorous
14) Pipette 100 µL of each sample in triplicates into a 384 well plate
15) Run absorbance reading with 384 SpectraMax Plus Absorbance Reader at 820 nm and 620 nm
    - 820 nm is the absolute reading for lipid concentration
    - 620 nm is the backup reading incase 820 does not fit trend

Appendix G

Gel Electrophoresis/Western Blotting Protocol

Preparing to run the gel

1300 mL running buffer was made from a solution of 130 mL running buffer solution with 1170 mL Millipore water. The gel plates need to be air bubble free. The gels were placed into the gel apparatus main frame and loaded into the gel running container. Running buffer is poured onto the gel apparatus main frame to check for leakage before pouring the rest to fill up the container. Excess preserve solution of each well in the gel plate is cleaned out carefully with several 200 µL of air and then several 200 µL of running buffer with a gel-loading pipette tip. Samples were boiled for 5-10 minutes before loading into the gel well. 3 µL of magic marker was loaded into the 1st well, 5 µL of benchmark on the 10th well and 10-40 µL samples in between the magic marker and benchmark well. The gel was run at 20 V for 20 minutes and then 200 volts for 45-55 minutes or until the dye from the sample buffer (under 1 kDa molecular weight) runs near to the bottom of the gel.

Preparing membrane to transfer

An appropriate edge (top right) was cut to differentiate or indicate the direction of the membrane will be transferred to. The membrane was wet by soaking in methanol and then rinsed with TBST. The membrane was then immersed in transfer buffer until it is ready to be used.

Transferring the gel

1300 mL Transfer buffer was made by mixing 130 mL transfer buffer solution with 260 mL methanol and 910 mL Millipore water. 2 sponges and 2 filter papers were soaked in the transfer buffer and layered on the transfer cassette, having the sponges to be at the bottom of the filter papers at each side. The gel was separated from its gel case and excess gel such as the well walls is cut off. The gel was placed on top of the filter paper and the prepared membrane on top of the gel slowly to minimize air bubble formation between the gel and the membrane, all the while having the black side of the cassette facing the gel side. The other filter paper was placed on top of the membrane and rolled with a test tube to ensure removal of potential air bubbles. The sponge was then placed on top of the filter and the transfer cassette is closed and locked. The transfer cassette was then placed in the transfer carrier, while ensuring the black part of the transfer cassette faces the black part of the transfer carrier. The transfer was run at 100 mA overnight and then cranked up to 200 mA for around 20 minutes to ensure the transfer of larger proteins to the membrane. To prevent overheating while at 200 mA, an ice pack stored at -80 °C was placed into the transfer carrier and the solution was magnetically stirred throughout the process of transfer to ensure that the gel doesn't melt, and proteins are not damaged during transfer.

Imaging the blot

The membrane was taken out of the transfer cassette and the gel was discarded. The membrane was briefly washed with TBST on a square plate and washed 3 more times for 5 minutes each while swirling. The protein was then blocked with 5wt% milk solution in TBST for an hour swirling. The milk was then removed and is washed with TBST as stated previously. Primary antibody, according to the manufacturer's specifications, was added and swirled in 10 mL of 1wt% BSA or 5wt% milk in TBST at room temperature for 1 hour. The primary antibody solution was then removed and washed in TBST 3 times for five minutes each, as before. Secondary antibody (i.e. 5 μL anti-rabbit or 5μL anti-mouse) was added and swirled in 10 mL of 5wt% milk in TBST for an hour. The secondary antibody solution is then removed, and the membrane was washed in TBST again, as stated previously. ECL solution of 1 mL of solution A and 1 mL of solution B (as purchased from GE Healthcare or Bio-Rad) was dribbled across the membrane to fully wet its surface and the membrane is incubated for 5 minutes before imaging. Imaging was done on a Kodak CF440 Image Station that was set to obtain an average image.

Appendix H

BCA Assay (Protein Concentration Determination)

Solutions & Reagents:
(All pipetting done with RNase, DNase free Barrier Tips)

- H_2O (Molecular Biology Grade)
- SDS/Tris HCl (SDT)
  - 4% w/v SDS in 100 mM Tris HCl pH 7.6
    1. Rinse a clean glass bottle with H_2O and dilute 1 M Tris HCl to 100 mM
    2. Measure 90 mL of H_2O
    3. Pipette 10 mL 1 M Tris HCL
    4. Add 4 g of SDS pellet
       - Pour pellet from stock bottle into a container before taking it for measurement, not taking directly from the stock bottle
    5. Gently swirl to mix

Procedure:
Preparing Standards from Pierce BCA Protein Assay Kit:

1) Prepare and label 16 (2 mL) microcentrifuge tubes
   - Ex. Tube 1: Labeled as A and its concentration 2000 µg/mL
2) Carefully open the top portion of the Albumin Standards Ampule, 2mg/mL
   - Note: some 1 mL pipette tip does not reach the bottom of the ampule
3) Prepare the BSA standards as follow:

Vial	H2O (µL)	Volume and Source of BSA (µL)	Final BSA Concentration (µg/mL)	Final Volume (µL)
A	0	300 of Stock	2000	300
B	125	375 of Stock	1500	325
C	325	325 of Stock	1000	325
D	175	175 from B	750	350
E	325	325 from C	500	325
F	325	325 from E	250	325
G	325	325 from F	125	550
H	400	100 from G	25	500
I	400	0	0	400

- If other standard concentrations are desired, proceed to next page:

Vial	H2O (µL)	Volume and Source of BSA (µL)	Final BSA Concentration (µg/mL)	Final Volume (µL)
A	0	300 of Stock	2000	300
B	125	375 of Stock	1500	325
C	325	325 of Stock	1000	325
D	175	175 from B	750	350
E	325	325 from C	500	325
F	325	325 from E	250	125
	25	100 from F	200	125
	66.7	100 from F	150	166.7
G	325	325 from F	125	250
	25	100 from G	100	125
	66.7	100 from G	75	166.7
	250	100 from G	50	350
H	400	100 from G	25	500
I	400	0	0	400
#	X1	Y1	Z1	
#	X2	Y2	Z2	

— To prepare other standard concentrations, please follow the equation:

$$\frac{Z1}{Z2} = Y2 + X2$$

— Ex. Preparing 200 ug/mL from vial F (250 ug/mL)

$$\frac{250}{200} = 100\ \mu L\ (\text{from F}) + X\ (H_2O)$$

$$X = 25\ \mu L\ H_2O$$

Preparing Working Reagent (WR):

4) Pipette 10 mL BCA Reagent A into a 15 mL centrifuge tube
5) Pipette 200 µL BCA Reagent B into the 15 mL centrifuge tube
   — Mixing 50 parts of Reagent A to 1 part of Reagent B (50:1, Reagent A:B)
   — Prepared amount should depend on how much you need for the assay (number of repetitions, number of standards, number of protein samples)
6) Cap and Vortex
   — Solution should be clear Green color

Preparing Protein Samples:

1) Thaw protein samples from -80 ºC in room temperature
2) Resuspend protein samples by adding 50 µL H_2O into the protein sample container

— Skip this step if already resuspended

3) Add 12.5 µL of SDS/Tris HCl into the protein sample container
   — This makes final volume with 1% SDS (allowable tolerance is 5%)
   — This is Solubilization step
4) Prepare microcentrifuge tubes and label
   — As many as the protein samples you have
5) Pipette 38 µL of H_2O into the microcentrifuge tubes
6) Pipette 2 µL of protein samples into the microcentrifuge tubes
   — **Do not vortex**
   — Mix by pipetting up and down several times
   — This is a 1:20 dilution
7) Return the protein samples to freezing at 80 ºC

Preparing to analyze with UV/VIS Spectrometry (384 well):

8) Briefly vortex WR solution
9) Pipette 88 µL of WR into all the well
   — As much as you need
10) Pipette 11 µL of protein sample into the well
   — Mix by pipetting up and down at least 3 times
   — Switch tips between samples and repetition
11) Cover the 384 well plate with its cover
12) Incubate at 37 ºC for 30 minutes
13) Uncover the 384 well plate and measure the absorbance at 562 nm
14) Repeat step 16 – 18 one more time

Inventory List/Purchase List

- **DNase, RNase, Protease Free**
- **Normal**

- SDS Micropellets ($C_{12}H_{25}NaO_4S$)
   — Fisher Scientific
   — Cat No. BP8200-500
   — Store Room Temperature
- Tris HCl 1 M pH 7.5
   — Fisher Scientific
   — Cat No. BP1757-500
   — Store Room Temperature
- Thermo Scientific Pierce BCA Protein Assay Kit
   — Fisher Scientific
   — Cat No. PI23225 or PI23227
   — Store Room Temperature

Appendix I

Complete Protein Digestion

Total Time required: 6 hrs 30 min + Overnight + 1 hr 20 min

Waiting Time: 4 hrs 30 min (nine 30 min) + Overnight + 1 hr (two 30 min)

Time of actual running: 20 min (solutions) + 20 min (sample prep) + 1 hr 40 min (work)

Materials:

- 20 mL, 200 mL, 1000 mL Pipette
- 2 mL, 15 mL, 50 mL Centrifuge Tube
- 10-30 kDa Cutoff Microcon Filter
- 100 mL Measuring Cylinder (washed with Molecular Biology Grade H_2O)
- Aluminum Foil

Solutions & Reagents:
(All pipetting done with RNase, DNase free Barrier Tips)

- H_2O (Molecular Biology Grade)
- SDS/Tris HCl (SDT)
  - — 4% w/v SDS in 100 mM Tris HCl pH 7.6
    1. Rinse a clean glass bottle with H_2O and dilute 1 M Tris HCl to 100 mM
    2. Measure 90 mL of H_2O
    3. Pipette 10 mL 1 M Tris HCL
    4. Add 4 mg of SDS pellet
       - Pour pellet from stock bottle into a container before taking it for measurement, not taking directly from the stock bottle
    5. Gently swirl to mix
       - Do not vortex
  - — Or
    1. Pipette 1 mL of 1 M Tris HCl into a 15 mL centrifuge tube
    2. Weight 0.4 g SDS and put it in
    3. Dissolve gently by inverting with addition of H_2O made up to 10 mL
- SDS/Dithiothreitol (SDT/DTT) (Each sample needs about 350 µL)
  - — 0.1 M DTT in SDS/Tris HCl
    1. Pipette 1 mL SDS/Tris HCl into a microcentrifuge tube
    2. Weight 15.4 mg of solid DTT
    3. Gently mix by inverting
       - Do not vortex
       - Make new daily
       - Make shortly before use, Store in dark until use

(READ NOTE BELOW)

NOTE: Do not vortex any solutions with SDS, as it is a surfactant that will produce significant bubbles and disturb measurements with the UV/VIS.

- Urea/Tris HCl (UT) (Each sample needs 300 µL)
  - 8 M Urea in pH 8 Tris HCl
    1. Add 1 mL 1 M Tris HCl into a 15 mL centrifuge tube
    2. Weigh 4.8 g Urea and put it in
    3. Gently dissolve with addition of H_2O made up to 10 mL
    4. Vortex
- Iodoacetamide/Urea/Tris HCl (IAA/UT) (Each sample needs 200 µL)
  - 0.05 M IAA in pH 8 UT
    1. Pipette 1 mL UT into a 2 mL microcentrifuge tube
    2. Weigh 9 mg of IAA and put it in
    3. Vortex
       - Make new daily
       - Make shortly before use, Store in dark until use
- Ammonium Bicarbonate (ABC) (Each sample needs 400 µL)
  - 120mM ABC
    1. Weigh 0.20 g Ammonium Bicarbonate into a 50 mL centrifuge tube
    2. Add 50 mL H_2O
    3. Vortex
       - Make new daily
       - Good to keep for 2 days only
- Trypsin (Each sample needs 1:20 Trypsin:Protein)
  - Have 100 µg, dilute to 0.5 µg/µL
    1. Add 200 µL of 50 mM Acetic Acid into the bottle
    2. Gently mix by inversion
    3. Store at -80 ºC
       - Only thaw and use when needed, freeze immediately after
- Formic Acid/Ammonium Bicarbonate (FAB) (Each sample needs 150 µL)
  - 0.1 % Formic Acid in Ammonium Bicarbonate
    1. Pipette 10 mL of ABC into a 15 mL centrifuge tube
    2. Pipette 10 µL of Formic Acid and put it in
    3. Gently mix by inversion

Procedure:

1) Calculate the **LOWEST** amount of protein sample needed to pipette
    - (Ex. 50 µg Protein)
2) Calculate the amount of SDT/DTT buffer needed to fill to a total volume of 350 µL including the protein sample (or to filter's max capacity if less)
3) Insert the Microcon Filter into the given 2 mL microcentrifuge tube
4) Pipette the amount calculated of SDT/DTT buffer into the Microcon Filter
5) Pipette the amount calculated for the protein sample into the Microcon Filters
    - This is Reduction step
    - Pipette up and down to mix and switch tips on every sample
6) Cap and put counterweight on top of the cap
    - to prevent cap from popping or loose
7) Incubate at **56 ºC** for 30 min
8) Cool to **room temperature** (Approx: 10 min)
9) Add 100 µL UT solution into the Micron Filter and gently mix
    - This is Denaturing Step
10) Centrifuge at max 13 kRPM for 30 minutes
    - **** (Note: do not exceed higher RPM) ****
11) Repeat step 9 – 10 two more times
    - (total 3 repetition)
    - Transfer to a cooler holder to improve cooling time
12) Add 200 µL IAA/UT solution into the Microcon Filter
    - This is Alkylation step
13) Cover with Aluminum Foil
    - (to further prevent light or accidental exposure)
14) Incubate at **room temperature** in the **DARK** for 30 minutes
15) Centrifuge at max 13 kRPM for 30 min
16) Add 100 µL ABC
    - This is Washing step
17) Centrifuge at max 13 kRPM for 30 min
18) Repeat step 16 – 17 two more times
    - (total 3 repetition)
19) Remove the Microcon Filter and put it into a new 2mL Low Binding Eppendorf Tube
    - Should have about 50 µL concentrate volume in the bottom of the Microcon Filter
20) Add 100 µL ABC into the Microcon Filter
21) Add 1:20 w/w Trypsin:Protein sample solution
    - (Ex. 2.5 µg trypsin for every 50 µg protein, so add 5 µL of 0.5 µg/µL trypsin)
    - If protein concentration is slow, may adjust trypsin usage in this part (between 1:20 to 1:50)
22) Cap and put counterweight on top of the cap
23) Incubate at **37 ºC** overnight
    - This is Protein Digestion step

24) Centrifuge at max 13 kRPM for 30 min
25) Add 150 µL of 0.1% Formic Acid in ABC buffer
26) Centrifuge at max 13 kRPM for 30 min
    - (Final volume should have 50 µg Protein in 300 µL buffer, 50 µg/300 µL)
    - **<u>Do not throw filter</u>**, can be incubate with Lys-C and Trypsin in case something goes wrong
27) The sample is now ready for LC/MS analysis

Extra Information:

1) DTT is a reducing agent to reduce cysteine by addition of oxygen to the Sulphur group in cysteine to create Thiol (SH)
2) UT is a chaotropic agent to dissociate protein aggregates and completely denature the protein and to eliminate DTT. Endothermic reaction between Urea and Tris HCl which absorbs heat and lowers temperature
3) IAA is an alkylation agent by addition of alkyl group to modify cysteine to prevent Thiol bridges from the addition of Thiol during the DTT reduction step
4) ABC acts as a washing buffer to remove salt/salt crystal from the sample, and acts as a volatile buffer for the Mass Spectrometry

Inventory List/Purchase List

- **DNase, RNase, Protease Free**
- **Normal**

- SDS Micropellets ($C_{12}H_{25}NaO_4S$)
  - Fisher Scientific
  - Cat No. BP8200-500
  - Store Room Temperature
- Tris HCl 1 M pH 7.5
  - Fisher Scientific
  - Cat No. BP1757-500
  - Store Room Temperature
- Dithiothreitol ($C_4H_{10}O_2S_2$) (DTT) (154.24 Mw)
  - Fisher Scientific
  - BP172-5
  - Store -20 ºC
- Urea 99.5% for Molecular Biology (60.06 Mw)
  - Manufacturer: Acros Organics
  - Fisher Scientific
  - Cat No. AC327380010
  - Store Room Temperature
- Iodoacetemide 98% (IAA)
  - Manufacturer: Acros Organics
  - Fisher Scientific
  - Cat No. AC122270050
  - Store 4 ºC
  - Keep away from sunlight
- Ammonium Bicarbonate 99% (CH_5NO_3) (ABC) (79.06 Mw)
  - Manufacturer: Acros Organics
  - Fisher Scientific
  - AC393212500
  - Store Room Temperature
- Promega Trypsin Gold, Mass Spectrometry Grade
  - Fisher Scientific
  - Cat No. PRV5280
  - Store -20 ºC (we store at -80 ºC, which is fine too)
- Formic Acid, Aldehyde Free (Sequencing), Fisher BioReagents™ (46.025 Mw)
  - Fisher Scientific
  - Cat No. BP1215-500
  - Store Room Temperature in Acid Cabinet

- Microcon-10kDa Centrifugal Filter Unit with Ultracel-10 membrane (0.5 mL)
  - Millipore Sigma (emdmillipore.com)
  - Cat No. MRCPRT010
- Microcon-30kDa Centrifugal Filter Unit with Ultracel-10 membrane (0.5 mL)
  - Millipore Sigma (emdmillipore.com)
  - Cat No. MRCPRT030

Appendix J

In-Gel Trypsin Digestion for Protein (LC-MS/MS)

Materials:

- 20 mL, 200 mL, 1000 mL Pipette
- 2 mL, 15 mL, 50 mL Centrifuge Tube
- 2 mL Low Binding Microcentrifuge Tube
- 2 L Measuring Cylinder & Beaker
- Beaker Buddy (Microcentrifuge Tube Holder)
- Ventilation Vial
- Gel Electrophoresis Setup
- Clean Scalpel/Razor
- Orbital Shaker
- Incubators set at 37 ºC and 56 ºC

Solutions & Reagents:
(All pipetting not necessarily done with RNase, DNase free Barrier Tips, depends only when making certain solution and reagent)

- H_2O (Molecular Biology Grade)
- Loading Buffer (20 µL for each sample)
    - 95% Laemmli sample buffer, 5% β-mercapthoethanol
        1. Pipette 95 µL Laemmli into a 2 mL microcentrifuge tube
        2. Add 5 µL β-mercapthoethanol
        3. Mix by pipetting up & down
- Gel Running Solution
        1. Wash a 2 L measuring cylinder with DI
        2. Add 1170 mL Tris/Glycine/SDS buffer
        3. Add 230 mL Methanol
        4. Swirl to mix
- Ammonium Bicarbonate (ABC)
    - 100 mM ABC (20 mL for Solution, 200 µL for each sample)
        1. Weigh 0.3953 g of Ammonium Bicarbonate into a 50 mL tube
        2. Add 50 mL H_2O
        3. Vortex
    - 50 mm ABC with 10% (vol/vol) Acetonitrile (ABC/ACE) (240 µL every 10 samples)
        1. Pipette 225 µL of 100 mM ABC into a 2 mL microcentrifuge tube
        2. Add 225 µL H_2O
        3. Vortex
        4. Add 50 µL Acetonitrile
        5. Vortex

6. Refrigerate to 4 ºC before use
    - Make new daily
    - Good to keep for 2 days only

- Dithiothreitol (DTT)
    - 10 mM DTT in 100 mM ABC (100 µL each sample)
        1. Weigh 15.4 mg DTT into a 15 mL centrifuge tube
        2. Add 10 mL ABC
        3. Vortex
            - Make shortly before use
            - Make new daily
- Iodoacetamide (IAA) (100 µL each sample)
    - 55 mM IAA in 100 mM ABC
        1. Weigh 101.7 mg IAA into a 15 mL centrifuge tube
        2. Add 10 mL ABC
        3. Vortex
            - Make shortly before use, Protect from Light
            - Make new daily
- Trypsin Buffer
    - 20 ng/µL trypsin in 50 mM ABC/ACE (25 µL each sample)
        1. Pipette 240 µL ABC/ACE into a 2mL microcentrifuge tube
        2. Cool to 4 ºC in fridge
        3. Thaw Trypsin stock (20 µg) in RT and use immediately
        4. Pipette in 10 µL of Trypsin stock
        5. Store Trypsin in -80 ºC immediately
            - Make shortly before use, store cold 4 ºC
            - IMPORTANT, Trypsin starts to digest itself above 4 ºC
            - Make new daily
- Extraction Buffer (EB) (100 µL each sample)
    - 1 part 5% Formic Acid in 2 part Acetonitrile
        1. Clean a ventilation vial
        2. Add 2.375 mL of H_2O
        3. Add 125 µL Formic Acid
        4. Mix by pipetting or swirl
        5. Add 5 mL Acetonitrile
        6. Mix by pipetting or swirl

Procedure:

Protein Precipitation:

1) Thaw Protein in Room Temperature (RT)
2) Mix sample Protein by pipetting it up & down gently
3) Pipette 10 µg of sample Protein in a 2 mL microcentrifuge tube
    - Protein concentration can be determined from the BCA Assay

      $$\frac{10\ \mu g}{Protein\ Concentration\ (ng/\mu L)} * 1000 \frac{ng}{\mu g} = \#\ \mu L\ needed$$

    - For Example

      $$\frac{10\ \mu g}{2500\ (ng/\mu L)} * 1000 \frac{ng}{\mu g} = 4\ \mu L\ needed$$

4) Prepare 1:10 part Protein: Acetone Solution by pipetting 10 times the amount of the sample protein for **ICE COLD** Acetone
    - For Example

      $4\ \mu L\ sample\ Protein * 10 = 40\ \mu L\ of\ \boldsymbol{ICE\ COLD}\ Acetone\ needed$

5) Mix sample Protein solution by pipetting it up & down gently, cap
6) Leave sample Protein solution in -20 ºC freezer overnight
    - Acetone will not freeze

Running Gel Electrophoresis:

7) Start Boiling water
8) Take sample Protein solution out of the freezer
9) Centrifuge at Max Speed with the tube hinges facing upwards
10) With a Gel Loading tip, very carefully pipette out the liquid solution while tipping the tube sideways with the hinges facing upwards
    - Protein will appear as a comparatively clear and soft gel-like substance on the top side of the microcentrifuge tube
    - Protein in this stage is very fragile and may move, so try not to use excessive force or movement
11) Pipette 20 Loading Buffer into the tube, mix gently by pipetting up & down, cap
12) Load the protein buffer solution into a microcentrifuge tube clamp holder
13) Boil the protein buffer solution in water for 10 minutes
14) Prepare Gel running solution with 1170 mL Gel Running Solution and 230 mL Methanol, mix by swirling
15) Take Gel cassette out of plastic and lightly jerk it to get excessive solution out of the well
16) Place gel cassette into the Gel Cassette holder
    - Making sure that the gel cassette is placed on the right orientation
    - Do not let the gel cassette to idle as it will dry out, proceed to Step 17

17) Place the Gel Cassette holder into the Gel Cassette holder-box
    - Make sure that the holder's anode and cathode are at the right orientation
    - Black to black, red to red
18) Pour Gel running solution into the holder until it's full then proceed to pour the rest into the holder-mold
    - If gel cassette is on the wrong orientation, the holder will leak
    - If so, re-orient the gel cassette
19) Clean well by pipetting 200 µL of Air into the well 2-3 times using a Gel Loading tip
    - Pipette close to the bottom of the well so that the air barely touches the gel at the bottom
    - This step helps to remove majority of the reserved storing solution in the well of the cassette
20) Clean well by pipetting 200 µL of the Gel running solution into the well slowly 2-4 times using a Gel Loading tip
    - Be careful on this step as pipetting solution has more velocity than air and may damage the well
    - When pipetting, go only ¼ into the well and do it at one end of each well and then the other end, repeat when necessary
    - This step helps to remove the reserved storing solution at the corner of the well
21) Load 10 µL of the protein buffer solution into the well slowly (Well 1-9)
    - Load from ½ in (not inches) from the top of the well, adjust as needed
    - Prevent pipetting air bubbles as it will cause backflow and the protein buffer will flow out of the well
    - Flow of sample will indicate how clean the wells are, the cleaner it is the smoother and faster the flow to the bottom
22) Load 5 µL of BenchMark Prestained Protein Ladder into the well slowly (Well 10)
23) Cap the Gel Cassette holder-mold
    - Make sure that the cap's anode and cathode are at the right orientation as the holder-mold
    - Black to black, red to red
24) Turn on the power of the machine on the side
25) Adjust the Voltage to 200 V
26) Press the running man symbol to run the Gel Electrophoresis
27) Run for 45-50 minutes
28) Press the standing-still man symbol to stop the Gel Electrophoresis
29) Turn off the power

Protein Staining in Gel:

30) Pour about 10 mL of Ultrapure water into a clean 100 cm^2 square tray
31) Take the Gel Cassette out of the holder and holder-box
32) Pry open the Gel Cassette carefully from one of the top ends to the bottom end, then proceed to pry it open throughout
33) Trim the gel barrier between wells with a scalpel/razor and discard
34) Lift the gel off the cassette with a clean thin plastic by inserting the plastic from bottom end below the gel, slowly as to not damage it, slide it to the top end
35) Proceed to slide it throughout the gel to the middle
36) With your fingers lift the half end of the gel slightly and with your thumb put enough pressure to grip the gel
37) Lift the entire gel out of the cassette and transfer to the square tray
38) Pour enough Ultrapure water to cover the gel and then some into the square tray
39) Gently swirl to rinse the gel and discard
40) Repeat the rinse two more times
41) Pour 50 mL of Ultrapure water into the tray and wash for five minutes shaking, then discard water
    — Washing step
    - Cover with lid during washes and incubation
42) Repeat washing two more times
43) Pour 20-25 mL of GelCode Blue Safe Protein Stain into the tray
    - Enough to cover the gel
    - Make sure that Stock bottle has Activator added
44) Incubate covered for 1 hour on a shaker at RT
    — Staining step
45) Discard stain
46) Wash the gel three times with enough Ultrapure water swirling, discard water
47) Add 50 mL Ultrapure water to the tray
48) Fold some Kimwipe™ Tissue or paper towel into the water with the gel
    - Enhances destaining process by absorbing excess stain leaching from gel
49) Wash for 15 minutes on a shaker
    - Destaining step
50) Repeat three more times, while changing the Kimwipe™ Tissue each time
    - May do overnight destaining to reduce background signal and will not reduce band intensity

In Gel Trypsin Digestion:

51) Lay the gel on the tray on top of a white surface so the blue bands are visible
52) Carefully carve out the protein bands with a scalpel/razor
    - Do not lean towards with your face directly on top of the gel, view from a distance
    - Use gloves

- This is to prevent keratin from our face and hand from depositing into the gel, as this will show up on the MS, although newer MS can categorize them it is best to avoid any unnecessary contamination

53) Using a pipette tip, slowly pry out the cut bands one at a time and lay it on top of the scalpel/razor and transfer to a low binding microcentrifuge tube
54) Add 200 µL of 100mM ABC and 200 µL of Acetonitrile
    - 1:1 vol/vol mixture
55) Incubate for 30 minutes at RT, occasionally mix by flicking the tube
56) Add 400 µL Acetonitrile
57) Wait 15 seconds and remove
58) Add 400 µL of Acetonitrile
59) Incubate for 5 minutes at RT, occasionally mix by flicking the tube
    - Gel Pieces will turn white (Shrink and dries)
60) Add 100 µL DTT
61) Incubate for 30 minutes in oven at 56 ^{o}C
    — Reduction Step
    - Intermittent mixing every 5 minutes
    - Put the microcentrifuge tube into the Beaker Buddy and lock it down to prevent cap from popping and potentially losing materials
    - May use heating block
62) Cool tubes to RT
    - Transferring tubes to a new holder will help reduce cooling time
63) Add 400 µL of Acetonitrile
64) Incubate for 2 minutes and remove
    - Gel piece will not completely turn white
65) Add another 400 µL of Acetonitrile
66) Incubate for 3 minutes
    - Gel piece will turn white now
67) Short spin in centrifuge and remove all liquid
68) Add 100 µL IAA
69) Incubate in **DARK** for 30 minutes at RT
    — Alkylation Step
70) Remove all liquid
71) Snip gel piece into 1 mm pieces in the tube with a pipette tip
    - At this point, be careful to not lose gel pieces on pipette tip on each step
72) Wash twice with addition of 200 µL 100 mM ABC, gently flick and remove all liquid in each wash
73) Add 400 µL Acetonitrile
74) Incubate for 2 minutes and remove liquid
75) Add 400 µL Acetonitrile
76) Incubate for 5 minutes and remove liquid

77) Short spin in centrifuge and remove all liquid
    - Samples are now ready for in-gel digestion
    - Alternatively, can be stored in -20 ºC for a few weeks dehydrated with Acetonitrile
78) Add 25 µL of Trypsin buffer and leave it for 2 hours on **ICE** in 4 ºC
79) Transfer tubes to incubation oven at 37 ºC overnight
    - Important to use oven to avoid temperature gradient in tube to prevent condensation of water at the inner surface of the lid and premature dehydrate the gel pieces
80) Add 100 µL EB
    — Extraction Step
    - With samples of larger or smaller volume, use approximate ratio of 1:2 between volumes of the digest
81) Sonicate tubes in water bath for 10 minutes
82) Hand Over to Greg for Analysis

Continuation from Greg for LC-MS/MS Analysis:

83) Cool tubes if warm and transfer supernatant into a new low binding microcentrifuge tube
84) Dry down peptides in vacuum centrifuge for 15 minutes
    - Depending on volume of extraction solution used
    - Do not discard extracted gel pieces
    - Dried extracts can be stored at -20 ºC for few months
85) Add 20-30 µL of 0.1% (vol/vol) Trifluoroacetic acid into the tube containing the dried peptides
    - TFA may contain Waters MassPrep PhosB Hi3 or ClpB Hi3 Peptides at 20-25 fmol/µL if needed
86) Vortex tube briefly and sonicate in water bath for 10 minutes
87) Cool tube and briefly centrifuge
88) Transfer solution to a 1.5 mL glass insert
89) Centrifuge for 10 minutes at 5,000 RPM in a bench-top centrifuge
90) Inject 5-10 µL to the LC-MS/MS and analyze

Inventory List/Purchase List

- **DNase, RNase, Protease Free**
- **Normal**

- Dithiothreitol ($C_4H_{10}O_2S_2$) (DTT) (154.24 Mw)
  - Fisher Scientific
  - Cat No. BP8200-500
  - Store -20 ºC
- 2x Laemmli Sample Buffer
  - Bio-Rad
  - Cat No. 161-0737
  - Store Room Temperature
- 2-Mercaptoethanol (14.3M pure) (C_2H_5SOH) (78.13 Mw) CAS:60-24-2
  - Sigma-Aldrich
  - Cat No. M6250-1L
  - Store 2-8 ºC
- nUView Precast Gel Tris-Glycine 4-20%
  - NuSep
  - Cat No. NG21-420
  - Store 4 ºC
- GelCode Blue Safe Protein Stain
  - Manufacturer: Thermo Scientific
  - Fisher Scientific
  - Cat No. PI24594
  - Store Room Temperature
- Acetone for HPLC, 99.9% (CH_3COCH_3) CAS: 67-64-1
  - Sigma Aldrich
  - Cat No. 270275-1L
  - Store 4 ºC
- Acetonitrile, Optima™ LC/MS Grade, Fisher Chemical (C_2H_3N) (41.053 Mw)
  - Fisher Scientific
  - Cat No. A955-4
  - Store Room Temperature
- Ammonium Bicarbonate99% (CH_5NO_3) (ABC) (79.06 Mw)
  - Manufacturer: Acros Organics
  - Fisher Scientific
  - AC393212500
  - Store Room Temperature

- Iodoacetemide 98% (IAA) (C_2H_4INO) (184.964 Mw)
  - Manufacturer: Acros Organics
  - Fisher Scientific
  - Cat No. AC122270050
  - Store 4 ºC
  - Keep away from sunlight
- Promega™ Sequencing Grade Modified Trypsin, Frozen
  - Fisher Scientific
  - Cat No. PRV5113
  - Store -80 ºC
- Formic Acid, Aldehyde Free (Sequencing), Fisher BioReagents™ (46.025 Mw)
  - Fisher Scientific
  - Cat No. BP1215-500
  - Store Room Temperature in Acid Cabinet

Appendix K

SP3

Solutions & Reagents:
(All pipetting done with RNase, DNase free Barrier Tips???)

- Water, H_2O (Molecular Biology Grade)
- HEPES
  - 50 mM HEPES in water
- Iodoacetamide (IAA)
  - 400 mM iodoacetamide in 50 mM HEPES
    1. Add 36 mg into a microcentrifuge tube
    2. Add 500 µL HEPES
    3. Vortex
       - Sensitive to light
       - Make fresh before use
- Dithiothreitol (DTT)
  - 200 mM DTT in 50 mM HEPES
    - Sensitive to oxygen
    - Make fresh before use
- Acetonitrile
- Ethanol
  - 70% Ethanol (pure grade only) in water
- Digestion Solution
  - 1:25 (w/w) Enzyme to substrate ratio
    1. Add 5 µL HEPES into a microcentrifuge tube
    2. Add 0.8 µg Trypsin/LysC mix (for 20 µg Protein)
    3. Gently vortex
       - Make fresh before use
- Dimethyl sulfoxide (DMSO)
  - 2% DMSO in water (not acidic)
- Formic Acid (FA)
  - 1% FA in water

Procedure:

Beads Preparation:

- 2 SeraMag beads stock concentration provided at 50 mg/mL each
  - Hydrophilic and hydrophobic
- In the preparation below should net 1000 µg of beads resuspended to 20 µg/µL in 50 µL water
- Beads used should be scaled as needed to provide a **1:10** (w/w) Protein to Beads ratio

1) Remove both beads from the fridge and keep at room temperature for 10 min
2) Pipette 10 µL of each bead type into a PCR tube
3) Add 160 µL of water
4) Place PCR tube on magnetic rack and let sit for 2 min to pellet the beads
5) Remove from rack and remove supernatant
6) Rinse beads 3 times with 200 µL of water by pipette mixing and return to rack
   - let sit for 2 min and remove supernatant each time
7) Add 50 µL water
   - Final concentration is now 20 µg/µL
8) Store in 4°C fridge
   - Never freeze
   - Can be store indefinitely

Protein Extraction:

9) Wash Cell thoroughly with PBS
   - Minimize contamination with serum proteins derived from cell culture mediums
10) Lysate cells with either Lysis buffer or commercial lysis buffer from PreOmics iST sample preparation kit
    - Resuspend cell pellet with 10 µL PBS.
    - Then add 200 µL Lysis buffer
      i. Recommended cell density ~500,000 mammalian cells
      ii. Adjust as needed for recommended, more cells more lysis buffer
11) Incubate at 95°C for 10 min **if iST was used**
12) Sonicate at 4°C for 15 min
    - Alternate 30 s of sonication at highest level and 30 s of idle time
    - Lysate can be stored at -80°C until required, avoid freeze-thaw cycles
13) Determine protein concentration with Pierce 660 nm protein assay
    - Recommended reagent-sample ratio 1:15, 150 µL:10 µL in 96 well format

SP3:

14) Pipette 20 µg of protein from the lysate into a PCR tube
15) Add 10 µL of beads mixture (200 µg beads)
16) Add 5 µL of IAA
    - Protein Alkylation
17) Incubate in the **DARK** at RT for 30 min
18) Add 5 µL of DTT
    - Protein Reduction/Quenching of IAA
19) Incubate at 56ºC for 20 min, covered in tin foil in the dark
20) Add acetonitrile to a final concentration of 70% (v/v)
    - Now have 20 µL sample, add 46.7 µL of acetonitrile
    - 0.7*20/0.3=46.7
21) Incubate at room temperature for 18 min
22) Place on magnetic rack at room temperature for 2 min
23) Remove supernatant
    - Careful to not disturb beads
24) Add 200 µL ethanol
25) Incubate at room temperature for 30 s
26) Remove supernatant
27) Add 200 µL ethanol
28) Incubate at room temperature for 30 s
29) Remove supernatant
30) Add 180 µL of acetonitrile
31) Incubate at room temperature for 15 s
32) Remove supernatant
33) Air-dry beads for 30 s
34) Add 5 µL digestion solution, mix by gently pipetting
    - Complete homogenization is not necessary, and to prevent losses (sticky)
    - Beads will be stuck to each other and excessive handling will generate bubbles
    - Cluster will break down as protein is digested
35) Incubate at 37ºC for 14 hours
36) Resuspend beads by pipetting
37) Add acetonitrile to a final concentration of 95% (v/v)
    - Have total 66.7 µL solution with 70% acetonitrile concentration
    - Add 23.8 µL of acetonitrile to reach 95%
    - 0.95*66.7/0.7-66.7=23.8
    - Incubate at room temperature for 8 min
38) Place on magnetic rack at room temperature for 2 min
39) Pipette supernatant into a new PCR tube
    - Keep both beads on old PCR tube and supernatant in new PCR tube
40) Repeat step 15 to 38 for the supernatant
41) Discard supernatant

- Right now, should have 2 tubes with beads in them
- From here onwards, all steps will be done for both tubes

42) Add 180 µL acetonitrile
43) Place on magnetic rack at room temperature for 15 s
44) Remove and discard supernatant
45) Reconstitute beads in desired volume of DMSO (10 µL)
46) Sonicate beads for 1 min
    - Improves peptide recovery
47) Spin tubes in bench-top PCR-tube centrifuge for ~2 s
    - Aiding liquid removal from tube walls
48) Place tubes on magnetic rack at room temperature for 2 min
49) Collect supernatants into a single new PCR tube
    - Careful to not recover any beads
50) Place tubes on magnetic rack at room temperature for 2 min
51) Collect supernatant into a deactivated glass vial containing 1 µL FA
    - Make sure to use new tips
    - This repeated step helps to eliminates any potential beads carryover
52) Mix by pipetting
53) Centrifuge at 5,000g for 30 s
54) Sample are now ready for direct injection to MS
    - Can be stored at -20^{o}C prior to, and after acidification, indefinitely

Appendix L

Gene Regulation P-value

Table 16: 5 μM Fatty Acid Gene Regulation P-value

Fatty Acid	Genes	P-value
IsoProstane	HO-1	0.2018
	IL-8	0.0018
	MCP-1	2.92E-05
NeuroProstane	HO-1	0.2599
	IL-8	0.0352
	MCP-1	0.0300
NeuroFurane	HO-1	0.2476
	IL-8	0.0039
	MCP-1	0.0020

REFERENCES

1. Cole, G.O., *Regulation of chronic inflammation in endothelial cells by oxidized fatty acids.* Master's Theses, 2017: p. 926. https://scholarworks.wmich.edu/masters_theses/926

2. Abdullah, A., et al., *The Effect of Bentonite Clay on Green Compression Strength for Tailing Sands from Old Tin Mines in Perak State, Malaysia for Making Green Sand Casting Mould.* Key Engineering Materials, 2011. **471-472**: p. 769-774.

3. Khan, M.M., S.M. Mahajani, and G.N. Jadhav, *Transformation of bentonite used in green sand molds during metal casting process and its relevance in sand reclamation.* Applied Clay Science, 2021. **206**.

4. Loh, B., *Methylene Blue Clay Test for Molding Sand, Prebelnd and Bentonite.* Metalcasting Congress of the American Foundry Society (AFS), 2005. **109**: p. 419-428.

5. Stawiński, J., *Influence of Calcium and Sodium Concentration on the Microstructure of Bentonite and Kaolin.* Clays and Clay Minerals, 1990. **38**(6): p. 617-622.

6. Muhammad, N. and S. Siddiqua, *Calcium bentonite vs sodium bentonite: The potential of calcium bentonite for soil foundation.* Materials Today: Proceedings, 2022. **48**: p. 822-827.

7. Barbieri, D.M., et al., *Calcium bentonite and sodium bentonite as stabilizers for roads unbound.* Cleaner Engineering and Technology, 2022. **6**.

8. Vingas, G.J., *Thermal Stability of Bentonites in Foundry Molding Sand*.* Clays and Clay Minerals, 1964. **13**(1): p. 367-380.

9. ŻYmankowska-Kumon, S., et al., *Influence of the Changes of the Structure of Foundry Bentonites on Their Binding Properties.* Materials Science, 2012. **18**(1).

10. Campbell, J., *Complete Casting Handbook (Second Edition) Chapter 4- Moulds and Cores.* Metal Casting Processes, Metallurgy, Tehcniques and Design, 2015: p. 135-161.

11. Traners, J.L., *Use of the Methylene Blue Test in Earthworks.* Laboratoire Central des Ponts et Chausees (LCPC), 1981(111): p. 5-16.

12. Turkoz, M. and H. Tosun, *The Use of Methylene Blue Test for Predicting Swell Parameters of Natural Clay Soils.* Scientific Research and essays, 2011. **6**(8): p. 1780-1792.

13. Mandurapperuma, C., *Determination Active Clay Percentage of Moulding Sand by Using Methylene Blue.* Metal Casting, 2011. **1**: p. 1.

14. Boukhemkhem, A. and K. Rida, *Improvement adsorption capacity of methylene blue onto modified Tamazert kaolin.* Adsorption Science & Technology, 2017. **35**(9-10): p. 753-773.

15. Kahr, G. and F.T. Madsen, *Determination of the cation exchange capacity and the surface area of bentonite, illite and kaolinite by methylene blue adsorption.* Applied Clay Science, 1995. **9**(5): p. 327-336.

16. Burrafato, G. and F. Miano, *Determination of the Cation Exchange Capacity of Clays by Surface Tension Measurements.* Clay Minerals, 2018. **28**(3): p. 475-481.

17. Decher, A. and S. Ramrattan, *A New Measure for Active Clay in Green Sand.* AFS Proceedings 2020, Paper 2020-062, 2020.

18. Yukselen, Y. and A. Kaya, *Suitability of the methylene blue test for surface area, cation exchange capacity and swell potential determination of clayey soils.* Engineering Geology, 2008. **102**(1-2): p. 38-45.

19. V, L. and S. Neltner, *Determination of Gaage R&R on Various Methylene Blue Test Procedures.* AFS Transactions, 1990: p. 747-752.

20. Pike, A., et al., *Alternative Approach to Clay Control in Green Sand.* AFS Proceedings 2013, Panel 13-1455, 2013.

21. Decher, A. and S. Ramrattan, *A New Measure for Active Clay in Green Sand.* International Journal of Metalcasting, 2021. **15**(2): p. 373-381.

22. Lévy, L., et al., *Smectite quantification in hydrothermally altered volcanic rocks.* Geothermics, 2020. **85**.

23. Stanjek, H. and D. Künkel, *CEC determination with Cu-triethylenetetramine: recommendations for improving reproducibility and accuracy.* Clay Minerals, 2018. **51**(1): p. 1-17.

24. *World Health Organization. Cardiovasucular disease (CVDs). 2017. Accessed Sept. 17, 2018.*

25. *World Health Organization. Noncummunicable Diseases Progress Monitor 2017. 2017. Accessed Sept. 17, 2018.*

26. CDC, *Heart disease facts. 2017. Accessed Oct. 21, 2018.*

27. *Mayo Clinic. Coronary artery disease. 2018. Accessed Oct. 22, 2018.*

28. *American Heart Association. Atherosclerosis. 2017. Accessed Oct. 21, 2018.*

29. WebMD, *Atherosclerosis and coronary artery disease. 2018. Accessed Oct. 22, 2018.*

30. Navab, M., et al., *HDL and the Inflammatory Response Induced by LDL-Derived Oxidized Phospholipids.* Arterioscler Thromb Vasc Biol, 2001. **21**(4): p. 481-488.

31. *American Heart Association. HDL (Good), LDL (Bad) cholesterol and triglycerides. 2017. Accessed Oct. 25, 2018.*

32. Cockerill, G.W., et al., *High-density lipoproteins inhibit cytokine-induced expression of endothelial cell adhesion molecules.* Arterioscler Thromb Vasc Biol, 1995. **15**(11): p. 1987-94.

33. Baker, P.W., et al., *Ability of reconstituted high density lipoproteins to inhibit cytokine-induced expression of vascular cell adhesion molecule-1 in human umbilical vein endothelial cells.* J Lipid Res, 1999. **40**(2): p. 345-53.

34. Mackness, B., et al., *Paraoxonase-1 inhibits oxidized LDL-induced MCP-1 production by endothelial cells.* Biochem Biophys Res Commun, 2004. **318**(3): p. 680-3.

35. Tölle, M., et al., *HDL-associated lysoshingolipids inhibits NAD(P)H oxidase-dependent monocyte chemoattractant protein-1 production.* Arterioscler Thromb Vasc Biol, 2008. **28**(8): p. 1542-8.

36. Navab, M., et al., *Normal high density lipoprotein inhibits three steps in the formation of mildly oxidized low density lipoprotein: steps 2 and 3.* J Lipid Res, 2000. **41**(9): p. 1495-508.

37. Mahdy Ali, K., et al., *Cardiovascular disease risk reduction by raising HDL cholesterol-current therapies and future opportunities.* Br J Pharmacol, 2012. **167**(6): p. 1177-94.

38. Gordon, T., et al., *High density lipoprotein as a protective factor against coronary heart disease.* The American Journal of Medicine, 1977. **62**(5): p. 707-14.

39. Tan, M.H., *HDL-cholestero: the negative risk factor for coronary heart disease.* Ann Acad Med Sigapore, 1980. **9**(4): p. 491-5.

40. Wilson, P.W., R.D. Abbott, and W.P. Castelli, *High density lipoprotein cholesterol and mortality. The Framingham Heart Study.* Arteriosclerosis, 1988. **8**(6): p. 737-41.

41. Gordon, D.J., et al., *High-density lipoprotein cholesterol and cardiovascular disease. Four prospective American studies.* Circulation, 1989. **79**(1): p. 8-15.

42. Wilkins, J.T., et al., *Coronary heart disease risks associated with high levels of HDL cholesterol.* J Am Heart Assoc, 2014. **3**(2): p. e000519.

43. Ditah, C., et al., *Small and medium sized HDL particles are protectively associated with coronary calcification in a cross-sectional population-based sample.* Atherosclerosis, 2016. **251**: p. 124-131.

44. Cullen, P., *Evidence that triglycerides are an independent coronary heart disease risk factor.* The American Journal of Cardiology, 2000. **86**(9): p. 943-949.

45. Criqui, M.H., et al., *Plasma triglyceride level and mortality from coronary heart disease.* N Engl J Med, 1993. **328**(17): p. 1220-5.

46. Assmann, G., H. Schulte, and A. von Eckardstein, *Hypertriglyceridemia and elevated lipoprotein (a) are risk factors for major coronary events in middle-aged men.* The American Journal of Cardiology, 1996. **77**(14): p. 1179-1184.

47. Tenenbaum, A., R. Klempfner, and E.Z. Fisman, *Hypertriglyceridemia: a too long unfairly neglected major cardiovascular risk factor.* Cardiovasc Diabetol, 2014. **13**: p. 159.

48. Hokanson, J.E. and M.A. Austin, *Plasma Triglyceride Level is a Risk Factor for Cardiovascular Disease Independent of High-Density Lipoprotein Cholesterol Level: A Metaanalysis of Population-Based Prospective Studies.* European Journal of Cardiovascular Prevention & Rehabilitation, 1996. **3**(2): p. 213-219.

49. Stampfer, M.J., R.M. Krauss, and J. Ma, *A Prospective Study of Triglyceride Level, Low-Density Lipoprotein Particle Diameter, and Risk of Myocardial Infarction.* JAMA, 1996. **276**(11): p. 882-888.

50. Austin, M.A., *Low-Density Lipoprotein Subclass Patterns and Risk of Myocardial Infarction.* JAMA: The Journal of the American Medical Association, 1988. **260**(13).

51. Griffin, B.A., et al., *Role of plasma triglyceride in the regulation of plasma low density lipoprotein (LDL) subfractions: relative contribution of small, dense LDL to coronary heart disease risk.* Atherosclerosis, 1994. **106**(2): p. 241-253.

52. *WebMD. LDL: the 'bad' cholesterol. 2017. Accessed Oct. 27, 2018.*

53. Hirayama, S. and T. Miida, *Small dense LDL: An emerging risk factor for cardiovascular disease.* Clin Chim Acta, 2012. **414**: p. 215-24.

54. Gao, S. and J. Liu, *Association between circulating oxidized low-density lipoprotein and atherosclerotic cardiovascular disease.* Chronic Dis Transl Med, 2017. **3**(2): p. 89-94.

55. Ivanova, E.A., et al., *Small Dense Low-Density Lipoprotein as Biomarker for Atherosclerotic Diseases.* Oxid Med Cell Longev, 2017. **2017**: p. 1273042.

56. Hubel, C.A., et al., *Small low-density lipoproteins and vascular cell adhesion molecule-1 are increased in association with hyperlipidemia in preeclampsia.* Metabolism, 1998. **47**(10): p. 1281-1288.

57. Austin, M.A., et al., *Atherogenic lipoprotein phenotype. A proposed genetic marker for coronary heart disease risk.* Circulation, 1990. **82**(2): p. 495-506.

58. Coresh, J., et al., *Association of Plasma Triglyceride Concentration and LDL Particle Diameters, Density, and Chemical Composition with Premature Coronary Artery Disease in Men and Women.* J Lipid Res, 1993. **34**(10): p. 1687-97.

59. Ai, M., et al., *Small dense LDL cholesterol and coronary heart disease: results from the Framingham Offspring Study.* Clin Chem, 2010. **56**(6): p. 967-76.

60. Berneis, K.K. and R.M. Krauss, *Metabolic origins and clinical significance of LDL heterogeneity.* Journal of Lipid Research, 2002. **43**(9): p. 1363-1379.

61. Rizzo, M. and K. Berneis, *The clinical relevance of low-density-lipoproteins size modulation by statins.* Cardiovasc Drugs Ther, 2006. **20**(3): p. 205-17.

62. Gardner, C.D., *Association of Small Low-Density Lipoprotein Particles With the Incidence of Coronary Artery Disease in Men and Women.* JAMA: The Journal of the American Medical Association, 1996. **276**(11).

63. Toledo, F.G., A.D. Sniderman, and D.E. Kelley, *Influence of hepatic steatosis (fatty liver) on severity and composition of dyslipidemia in type 2 diabetes.* Diabetes Care, 2006. **29**(8): p. 1845-50.

64. Packard, C., M. Caslake, and J. Shepherd, *The role of small, dense low density lipoprotein (LDL): a new look.* International Journal of Cardiology, 2000. **74**: p. S17-S22.

65. Rizzo, M. and K. Berneis, *Low-density lipoprotein size and cardiovascular risk assessment.* QJM, 2006. **99**(1): p. 1-14.

66. Tribble, D.L., et al., *Enhanced oxidative susceptibility and reduced antioxidant content of metabolic precursors of small, dense low-density lipoproteins.* The American Journal of Medicine, 2001. **110**(2): p. 103-110.

67. Goulinet, S. and M.J. Chapman, *Plasma LDL and HDL subspecies are heterogenous in particle content of tocopherols and oxygenated and hydrocarbon carotenoids. Relevance to oxidative resistance and atherogenesis.* Arterioscler Thromb Vasc Biol, 1997. **17**(4): p. 786-96.

68. Parthasarathy, S., E. Wieland, and D. Steinberg, *A role for endothelial cell lipoxygenase in the oxidative modification of low density lipoprotein.* Proceedings of the National Academy of Sciences, 1989. **86**(3): p. 1046-1050.

69. Rankin, S.M., S. Parthasarathy, and D. Steinberg, *Evidence for a dominant role of lipoxygenase(s) in the oxidation of LDL by mouse peritoneal macrophages* J Lipid Res, 1991. **32**(3): p. 449-56.

70. Witztum, J.L. and D. Steinberg, *Role of oxidized low density lipoprotein in atherogenesis.* J Clin Invest, 1991. **88**(6): p. 1785-92.

71. Steinberg, D., et al., *Beyond cholesterol: modifications of low-density lipoprotein that increase its atherogenicity.* New England Journal of Medicine, 1989. **320**(14): p. 915-924.

72. Maiolino, G., et al., *The role of oxidized low-density lipoproteins in atherosclerosis: the myths and the facts.* Mediators Inflamm, 2013. **2013**: p. 714653.

73. Schwartz, C.J., et al., *The pathogenesis of atherosclerosis: An overview.* Clinical Cardiology, 1991. **14**(S1): p. 1-16.

74. Cathcart, M.K., D.W. Morel, and G.M. Chisolm, *Monocytes and Neutrophils Oxidize Low Density Lipoprotein Making It Cytotoxic.* Journal of Leukocyte Biology, 1985. **38**(2): p. 341-350.

75. Lee, S., et al., *Role of phospholipid oxidation products in atherosclerosis.* Circ Res, 2012. **111**(6): p. 778-99.

76. Carew, T.E., D.C. Schwenke, and D. Steinberg, *Antiatherogenic effect of probucol unrelated to its hypocholesterolemic effect: evidence that antioxidants in vivo can*

selectively inhibit low density lipoprotein degradation in macrophage-rich fatty streaks and slow the progression of atherosclerosis in the Watanabe heritable hyperlipidemic rabbit. Proceedings of the National Academy of Sciences, 1987. **84**(21): p. 7725-7729.

77. Kita, T., et al., *Probucol prevents the progression of atherosclerosis in Watanabe heritable hyperlipidemic rabbit, an animal model for familial hypercholesterolemia.* Proceedings of the National Academy of Sciences, 1987. **84**(16): p. 5928-5931.

78. Björkhem, I., et al., *The antioxidant butylated hydroxytoluene protects against atherosclerosis.* Arteriosclerosis and Thrombosis: A Journal of Vascular Biology, 1991. **11**(1): p. 15-22.

79. Holvoet, P., et al., *Association of high coronary heart disease risk status with circulating oxidized LDL in the well-functioning elderly: findings from the Health, Aging, and Body Composition study.* Arterioscler Thromb Vasc Biol, 2003. **23**(8): p. 1444-8.

80. Ehara, S., et al., *Elevated Levels of Oxidized Low Density Lipoprotein Show a Positive Relationship With the Severity of Acute Coronary Syndromes.* Circulation, 2001. **103**(15): p. 1955-1960.

81. Holvoet, P., et al., *Oxidized LDL and Malondialdehyde-Modified LDL in Patients With Acute Coronary Syndromes and Stable Coronary Artery Disease.* Circulation, 1998. **98**(15): p. 1487-1494.

82. Toshima, S., et al., *Circulating oxidized low density lipoprotein levels. A biochemical risk marker for coronary heart disease.* Arterioscler Thromb Vasc Biol, 2000. **20**(10): p. 2243-7.

83. Grundy, S.M., *Oxidized LDL and atherogenesis: relation to risk factors for coronary heart disease.* Clin Cardiol, 1993. **16**(4 Suppl 1): p. I3-5.

84. Seo, J.W., et al., *Macrophage Differentiation from Monocytes Is Influenced by the Lipid Oxidation Degree of Low Density Lipoprotein.* Mediators Inflamm, 2015. **2015**: p. 235797.

85. Chen, C. and D.B. Khismatullin, *Oxidized low-density lipoprotein contributes to atherogenesis via co-activation of macrophages and mast cells.* PLoS One, 2015. **10**(3): p. e0123088.

86. Fryar, C.D., T. Chen, and X. Li, *Prevalance of uncontrolled risk factors for cardiovascular disease: United States, 1999-2010. NCHS data brief, no 103. Hyattsville, MD: National Center for Health Statistics.* 2012.

87. *NHLBI. Coronary Heart Disease. 2018. Accessed Oct. 29, 2018.*

88. *MedlinePlus. Angioplasty and stent placement-heart. 2018. Accessed Oct. 29, 2018.*

89. Taylor, F., et al., *Statins for the primary prevention of cardiovascular disease.* Cochrane Database Syst Rev, 2011(1): p. CD004816.

90. Bellosta, S., R. Paoletti, and A. Corsini, *Safety of statins: focus on clinical pharmacokinetics and drug interactions.* Circulation, 2004. **109**(23 Suppl 1): p. III50-7.

91. Davignon, J., *Beneficial cardiovascular pleiotropic effects of statins.* Circulation, 2004. **109**(23 Suppl 1): p. III39-43.

92. Bendall, J.K., et al., *Tetrahydrobiopterin in cardiovascular health and disease.* Antioxid Redox Signal, 2014. **20**(18): p. 3040-77.

93. Fukushima, Y., et al., *Small dense LDL cholesterol is a robust therapeutic marker of statin treatment in patients with acute coronary syndrome and metabolic syndrome.* Clin Chim Acta, 2011. **412**(15-16): p. 1423-7.

94. *Mayo Clinic. Statin side effects: Weigh the benefits and risks. 2016. Accessed Oct. 29, 2018.*

95. Brault, M., et al., *Statin treatment and new-onset diabetes: a review of proposed mechanisms.* Metabolism, 2014. **63**(6): p. 735-45.

96. Casula, M., et al., *Statin use and risk of new-onset diabetes: A meta-analysis of observational studies.* Nutr Metab Cardiovasc Dis, 2017. **27**(5): p. 396-406.

97. Gouni-Berthold, I., D.P. Mikhailidis, and M. Rizzo, *Clinical benefits of ezetimibe use: is absence of proof, proof of absence?* Expert Opin Pharmacother, 2012. **13**(14): p. 1985-8.

98. Scordo, K. and K.A. Pickett, *CE: Triglycerides: Do They Matter?* Am J Nurs, 2017. **117**(1): p. 24-31.

99. Katzung, B.G. and A.J. Trevor, *Basic and clinical pharmacology 2015 13th ed. New York McGraw Hill Education*

100. Rubins, H.B., et al., *Gemfibrozil for the secondary prevention of coronary heart disease in men with low levels of high-density lipoprotein cholesterol. Veterans Affairs High-*

Density Lipoprotein Cholesterol Intervention Trial Study Group. N Engl J Med, 1999. **341**(6): p. 410-8.

101. Athyros, V.G., et al., *Long-term effect of gemfibrozil on coronary heart disease risk profile of patients with primary combined hyperlipidaemia.* Coron Artery Dis, 1995. **6**(3): p. 251-6.

102. Todd, P.A. and A. Ward, *Gemfibrozil. A review of its pharmacodynamic and pharmacokinetic properties, and therapeutic use in dyslipidaemia.* Drugs, 1988. **36**(3): p. 314-39.

103. Heinonen, O.P., et al., *The Helsinki Heart Study: coronary heart disease incidence during an extended follow-up.* Journal of Internal Medicine, 1994. **235**(1): p. 41-49.

104. Shammas, N.W., et al., *Effectiveness of Statin-Gemfibrozil Combination Therapy in Patients With Mixed Hyperlipidemia: Experience of a Community Lipid Clinic and Safety Review From the Literature.* Preventive Cardiology, 2003. **6**(4): p. 189-194.

105. Keating, G.M., *Fenofibrate: a review of its lipid-modifying effects in dyslipidemia and its vascular effects in type 2 diabetes mellitus.* Am J Cardiovasc Drugs, 2011. **11**(4): p. 227-47.

106. Packard, K.A., et al., *Comparison of Gemfibrozil and Fenofibrate in Patients with Dyslipidemic Coronary Heart Disease.* Pharmacotherapy, 2002. **22**(12): p. 1527-1532.

107. Berliner, J.A., et al., *Minimally modified low density lipoprotein stimulates monocyte endothelial interactions.* J Clin Invest, 1990. **85**(4): p. 1260-6.

108. Salomon, R.G., *Structural identification and cardiovascular activities of oxidized phospholipids.* Circ Res, 2012. **111**(7): p. 930-46.

109. Bochkov, V.N., et al., *Generation and biological activities of oxidized phospholipids.* Antioxid Redox Signal, 2010. **12**(8): p. 1009-59.

110. Itabe, H., *Minimally Modified LDL Is an Oxidized LDL Enriched with Oxidized Phosphatidylcholines.* Journal of Biochemistry, 2003. **134**(3): p. 459-465.

111. Starosta, V., et al., *Differential regulation of endothelial cell permeability by high and low doses of oxidized 1-palmitoyl-2-arachidonyl-sn-glycero-3-phosphocholine.* Am J Respir Cell Mol Biol, 2012. **46**(3): p. 331-41.

112. Mehta, D. and A.B. Malik, *Signaling mechanisms regulating endothelial permeability.* Physiol Rev, 2006. **86**(1): p. 279-367.

113. Shih, P.T., et al., *Minimally modified low-density lipoprotein induces monocyte adhesion to endothelial connecting segment-1 by activating beta1 integrin.* J Clin Invest, 1999. **103**(5): p. 613-25.

114. Tan, P.J., *Oxidized phospholipids regulation of the monocyte recruitment pathway in human aortic endothelial cells.* Master's Theses, 2015 p. 634. https://scholarworks.wmich.edu/masters_theses/634.

115. Zimman, A., et al., *Vascular endothelial growth factor receptor 2 plays a role in the activation of aortic endothelial cells by oxidized phospholipids.* Arterioscler Thromb Vasc Biol, 2007. **27**(2): p. 332-8.

116. Soccio, R.E. and J.L. Breslow, *Intracellular cholesterol transport.* Arterioscler Thromb Vasc Biol, 2004. **24**(7): p. 1150-60.

117. Witztum, J., *The oxidative modification hypothesis of atherosclerosis: does it hold for humans?* Trends in Cardiovascular Medicine, 2001. **11**(3-4): p. 93-102.

118. Romanoski, C.E., et al., *Network for activation of human endothelial cells by oxidized phospholipids: a critical role of heme oxygenase 1.* Circ Res, 2011. **109**(5): p. e27-41.

119. Birukova, A.A., et al., *Fragmented oxidation products define barrier disruptive endothelial cell response to OxPAPC.* Transl Res, 2013. **161**(6): p. 495-504.

120. Subbanagounder, G., et al., *Epoxyisoprostane and epoxycyclopentenone phospholipids regulate monocyte chemotactic protein-1 and interleukin-8 synthesis. Formation of these oxidized phospholipids in response to interleukin-1beta.* J Biol Chem, 2002. **277**(9): p. 7271-81.

121. Leeuwenberg, J.F., et al., *E-selectin and intercellular adhesion molecule-1 are released by activated human endothelial cells in vitro.* Immunology, 1992. **77**(4): p. 543-9.

122. Vestweber, D., *VE-cadherin: the major endothelial adhesion molecule controlling cellular junctions and blood vessel formation.* Arterioscler Thromb Vasc Biol, 2008. **28**(2): p. 223-32.

123. Springstead, J.R., et al., *Evidence for the importance of OxPAPC interaction with cysteines in regulating endothelial cell function.* J Lipid Res, 2012. **53**(7): p. 1304-15.

124. Murakami, M. and I. Kudo, *Phospholipase A2.* Journal of Biochemistry, 2002. **131**(3): p. 285-292.

125. Khanapure, S., et al., *Eicosanoids in Inflammation: Biosynthesis, Pharmacology, and Therapeutic Frontiers.* Current Topics in Medicinal Chemistry, 2007. **7**(3): p. 311-340.

126. Weinberger, B., et al., *Chapter 21 - lipid mediators and lung function. Comparative Biology of the Normal Lung (Second Edition).* Academic Press, 2015: p. 403-421.

127. Subbanagounder, G., et al., *Determinants of Bioactivity of Oxidized Phospholipids.* Arteriosclerosis, Thrombosis, and Vascular Biology, 2000. **20**(10): p. 2248-2254.

128. von Schlieffen, E., et al., *Multi-hit inhibition of circulating and cell-associated components of the toll-like receptor 4 pathway by oxidized phospholipids.* Arterioscler Thromb Vasc Biol, 2009. **29**(3): p. 356-62.

129. Bochkov, V.N., et al., *Oxidized phospholipids stimulate angiogenesis via autocrine mechanisms, implicating a novel role for lipid oxidation in the evolution of atherosclerotic lesions.* Circ Res, 2006. **99**(8): p. 900-8.

130. Birukov, K.G., et al., *Signal transduction pathways activated in human pulmonary endothelial cells by OxPAPC, a bioactive component of oxidized lipoproteins.* Microvascular Research, 2004. **67**(1): p. 18-28.

131. Zhong, W., et al., *An epoxyisoprostane is a major regulator of endothelial cell function.* J Med Chem, 2013. **56**(21): p. 8521-32.

132. Gugiu, B.G., et al., *Protein targets of oxidized phospholipids in endothelial cells.* J Lipid Res, 2008. **49**(3): p. 510-20.

133. Brakman A, *Regulation of chronic inflammation of endothelial cells by a pro-inflammatory epoxyisoprostane phospholipid.* Master's Theses, 2017: p. 930. https://scholarworks.wmich.edu/masters_theses/930.

134. Cracowski, J. and O. Ormezzano, *Isoprostanes, emerging biomarkers and potential mediators in cardiovascular diseases.* European Heart Journal, 2004. **25**(19): p. 1675-1678.

135. Obwegeser, R., et al., *Maternal cigarette smoking increases F2-isoprostanes and reduces prostacyclin and nitric oxide in umbilical vessels.* Prostaglandins & Other Lipid Mediators, 1999. **57**(4): p. 269-279.

136. Cracowski, J.L., et al., *Vascular biology of the isoprostanes.* J Vasc Res, 2001. **38**(2): p. 93-103.

137. Morrow, J.D., *Quantification of isoprostanes as indices of oxidant stress and the risk of atherosclerosis in humans.* Arterioscler Thromb Vasc Biol, 2005. **25**(2): p. 279-86.

138. Stojiljkovic, M.P., et al., *Increasing plasma fatty acids elevates F2-isoprostanes in humans: implications for the cardiovascular risk factor cluster.* J Hypertens, 2002. **20**(6): p. 1215-21.

139. Leitinger, N., et al., *The isoprostane 8-iso-PGF2α stimulates endothelial cells to bind monocytes: differences from thromboxane-mediated endothelial activation.* The FASEB Journal, 2001. **15**(7): p. 1254-1256.

140. Greaves, K., et al., *Influence of isoprostane F2alpha-III on reflow after myocardial infarction.* Eur Heart J, 2004. **25**(10): p. 847-53.

141. Kromer, B.M. and J.R. Tippins, *Coronary artery constriction by the isoprostane 8-epi prostaglandin F2α.* British Journal of Pharmacology, 1996. **119**(6): p. 1276-1280.

142. van 't Erve, T.J., et al., *Classifying oxidative stress by F2-isoprostane levels across human diseases: A meta-analysis.* Redox Biol, 2017. **12**: p. 582-599.

143. Janssen, L.J., *Involvement of TP and EP3 Receptors in Vasoconstrictor Responses to Isoprostanes in Pulmonary Vasculature.* Journal of Pharmacology and Experimental Therapeutics, 2002. **301**(3): p. 1060-1066.

144. Cracowski, J.-L., et al., *Isoprostaglandin E2 type-III (8-iso-prostaglandin E2) evoked contractions in the human internal mammary artery.* Life Sciences, 2001. **68**(21): p. 2405-2413.

145. van der Sterren, S. and E. Villamor, *Contractile effects of 15-E2t-isoprostane and 15-F2t-isoprostane on chicken embryo ductus arteriosus.* Comp Biochem Physiol A Mol Integr Physiol, 2011. **159**(4): p. 436-44.

146. Miller, E., et al., *Isoprostanes and neuroprostanes as biomarkers of oxidative stress in neurodegenerative diseases.* Oxid Med Cell Longev, 2014. **2014**: p. 572491.

147. Galano, J.-M., et al., *Isoprostanes, neuroprostanes and phytoprostanes: An overview of 25 years of research in chemistry and biology.* Progress in Lipid Research, 2017. **68**: p. 83-108.

148. De Las Heras-Gomez, I., et al., *Potential applications of lipid peroxidation products - F4-neuroprostanes, F3-neuroprostanesn-6 DPA, F2-dihomo-isoprostanes and F2-isoprostanes - in the evaluation of the allograft function in renal transplantation.* Free Radic Biol Med, 2017. **104**: p. 178-184.

149. Gunstone, F.D., J.L. Harwood, and A.J. Dijkstra, *The lipid handbook with CD-ROM.* CRC press, 2007.

150. Tam, P.S.Y., et al., *The metabolism and distribution of docosapentaenoic acid (n−6) in rats and rat hepatocytes.* Lipids, 2000. **35**(1): p. 71-75.

151. Durand, T., et al., *Total synthesis of 4(RS)-F4t-isoprostane methyl ester.* Tetrahedron Letters, 2000. **41**(20): p. 3859-3862.

152. Auvinet, A.-L., et al., *Total synthesis of 4-F3t-neuroprostane and its 4-epimer.* Tetrahedron Letters, 2009. **50**(13): p. 1498-1500.

153. *Magee, K. M. Total synthesis of 20-F4t-Neuroprostane. MS, Boston College, 2011. http://hdl.handle.net/2345/2423.*

154. de la Torre, A., et al., *Total syntheses and in vivo quantitation of novel neurofuran and dihomo-isofuran derived from docosahexaenoic acid and adrenic acid.* Chemistry, 2015. **21**(6): p. 2442-6.

155. Fitzgerald, G.A., J.A. Lawson, and W. Song, *U.S. Patent No. 20150247841. Philadelphia, United States: U.S. Patent & Trademark Office.* 2015.

156. Leung, K.S., et al., *Profiling of Omega-Polyunsaturated Fatty Acids and Their Oxidized Products in Salmon after Different Cooking Methods.* Antioxidants (Basel), 2018. **7**(8).

157. Roy, J., et al., *Non-enzymatic cyclic oxygenated metabolites of omega-3 polyunsaturated fatty acid: Bioactive drugs?* Biochimie, 2016. **120**: p. 56-61.

158. Cuyamendous, C., et al., *The novelty of phytofurans, isofurans, dihomo-isofurans and neurofurans: Discovery, synthesis and potential application.* Biochimie, 2016. **130**: p. 49-62.

159. Navab, M., et al., *Monocyte transmigration induced by modification of low density lipoprotein in cocultures of human aortic wall cells is due to induction of monocyte chemotactic protein 1 synthesis and is abolished by high density lipoprotein.* J Clin Invest, 1991. **88**(6): p. 2039-46.

160. Hara, M.R., et al., *S-nitrosylated GAPDH initiates apoptotic cell death by nuclear translocation following Siah1 binding.* Nat Cell Biol, 2005. **7**(7): p. 665-74.

161. AppliedBiosystems, *Guide to Performing Relative Quantitation of Gene Expression Using Real-Time Quantitative PCR.* 2008: p. 70.

162. Taylor, J.R., *An Introduction to Error Analysis: The Study of Uncertainties in Physical Measurements Second Edition.* University Science Book, 1997. **ISBN-10: 093570275X**.

163. Montgomery, D.C. and C.R. George, *"Chapter 1: The Role of Statistics in Engineering." Applied Statistics and Probability for Engineers. 5th ed.* Hoboken, NJ; John Wiley and Sons, 2010. ISBN-13:978-0-470-05304-1.

164. Wójciak-Stothard, B., L. Williams, and A.J. Ridley, *Monocyte Adhesion and Spreading on Human Endothelial Cells Is Dependent on Rho-regulated Receptor Clustering.* The Journal of Cell Biology, 1999. **145**(6): p. 1293-1307.

165. Martin, K.R., *Both common and specialty mushrooms inhibit adhesion molecule expression and in vitro binding of monocytes to human aortic endothelial cells in a pro-inflammatory environment.* Nutr J, 2010. **9**: p. 29.

166. ATCC, *THP-1 (ATCC TIB-202).* 2018: p. Retrieved from https://www.atcc.org/~/ps/TIB-202.ashx.

167. Sato, Y., et al., *Influence of length on cytotoxicity of multi-walled carbon nanotubes against human acute monocytic leukemia cell line THP-1 in vitro and subcutaneous tissue of rats in vivo.* Mol Biosyst, 2005. **1**(2): p. 176-82.

168. Shu, H., et al., *Activation of PPARalpha or gamma reduces secretion of matrix metalloproteinase 9 but not interleukin 8 from human monocytic THP-1 cells.* Biochem Biophys Res Commun, 2000. **267**(1): p. 345-9.

169. Daigneault, M., et al., *The identification of markers of macrophage differentiation in PMA-stimulated THP-1 cells and monocyte-derived macrophages.* PLoS One, 2010. **5**(1): p. e8668.

170. Craig, M.L., A.J. Bankovich, and R.P. Taylor, *Visualization of the transfer reaction: Tracking immune complexes from erythrocyte complement receptor 1 to macrophages.* Clinical Immunology, 2002. **105**(1): p. 36-47.

171. Strober, W., *Trypan blue exclusion test of cell viability.* Curr Protoc Immunol, 2001. **Appendix 3**: p. Appendix 3B.

172. Watson, A.D., et al., *Structural identification of a novel pro-inflammatory epoxyisoprostane phospholipid in mildly oxidized low density lipoprotein.* J Biol Chem, 1999. **274**(35): p. 24787-98.

173. Sielaff, M., et al., *Evaluation of FASP, SP3, and iST Protocols for Proteomic Sample Preparation in the Low Microgram Range.* J Proteome Res, 2017. **16**(11): p. 4060-4072.